AERODYNAMIC INTERFERENCE INDUCED BY REACTION CONTROLS

F. W. Spaid, et al

Advisory Group for Aerospace Research and Development
Paris, France

December 1973

NORTH ATLANTIC TREATY ORGANIZATION

ADVISORY GROUP FOR AEROSPACE RESEARCH AND DEVELOPMENT

(ORGANISATION DU TRAITE DE L'ATLANTIQUE NORD)

AGARDograph No.173

AERODYNAMIC INTERFERENCE INDUCED BY REACTION CONTROLS

by

F.W.Spaid

and

L.A.Cassel

McDonnell Douglas Corporation
5301 Bolsa Avenue, Huntington Beach, California 92647, USA

Edited by

R.E.Wilson

US Naval Ordnance Laboratory
White Oak, Silver Spring, Maryland 20910, USA

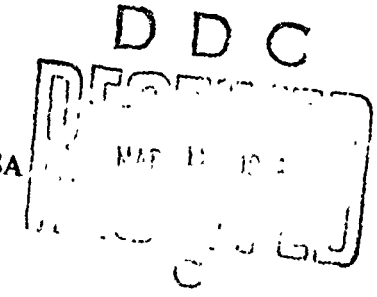

This AGARDograph was prepared at the request of the Fluid Dynamics Panel of AGARD.

THE MISSION OF AGARD

The mission of AGARD is to bring together the leading personalities of the NATO nations in the fields of science and technology relating to aerospace for the following purposes:

- Exchanging of scientific and technical information;
- Continuously stimulating advances in the aerospace sciences relevant to strengthening the common defence posture;
- Improving the co-operation among member nations in aerospace research and development;
- Providing scientific and technical advice and assistance to the North Atlantic Military Committee in the field of aerospace research and development;
- Rendering scientific and technical assistance, as requested, to other NATO bodies and to member nations in connection with research and development problems in the aerospace field;
- Providing assistance to member nations for the purpose of increasing their scientific and technical potential;
- Recommending effective ways for the member nations to use their research and development capabilities for the common benefit of the NATO community.

The highest authority within AGARD is the National Delegates Board consisting of officially appointed senior representatives from each member nation. The mission of AGARD is carried out through the Panels which are composed of experts appointed by the National Delegates, the Consultant and Exchange Program and the Aerospace Applications Studies Program. The results of AGARD work are reported to the member nations and the NATO Authorities through the AGARD series of publications of which this is one.

Participation in AGARD activities is by invitation only and is normally limited to citizens of the NATO nations.

Published December 1973

533.695.7:533.694.6

Printed by Technical Editing and Reproduction Ltd
Harford House, 7-9 Charlotte St, London, W1P 1HD

CONTENTS

AERODYNAMIC INTERFERENCE INDUCED BY REACTION CONTROLS

by

F. W. Spaid
L. A. Cassel

McDonnell Douglas Corporation

SUMMARY

The literature pertaining to the interaction of a sonic or supersonic gaseous jet with a transverse external flow has been reviewed. The flowfields associated with these interactions are complex, and knowledge of them is based largely on results of experiments. Numerous examples of data from flat-plate experiments are presented. These include static pressure distribution, induced forces, flowfield survey, and flow visualization results. Analyses and correlation techniques for jet interaction flows are discussed. The region upstream of a jet in two-dimensional flow is similar to the flow upstream of a forward-facing step, and the flow associated with a jet from a circular nozzle on a flat plate resembles the flow past a blunt-nosed slender body. The single most important variable in determining the scale of these interactions is the ratio of jet momentum flux to the external-flow dynamic pressure. When the external flow is subsonic, the interaction is sensitive to external-flow Mach number in the high subsonic Mach number range and to the ratio between jet and external flow velocity in the low Mach number range. The characteristic dimension of the flowfield in subsonic flow is approximately proportional to the square root of the pressure ratio. A few examples of data for jets exhausting from bodies of revolution show that interference forces can be sensitive to the geometry of the body.

SYMBOLS

a	Speed of sound; also $1 + \left[(\gamma_1 - 1)/2\right] M_1^2 / \left[(\gamma_1 - 1) M_1^2\right]$ in Equations (15) (17) and (18)
A_b	Vehicle or wind tunnel model reference area
A_t	Jet nozzle throat area
b	Nozzle span, also plate span, Figure 55
c	Nozzle discharge coefficient
C_p	Pressure coefficient, $(P - P_1)/q_1$ or $(P - P_\infty)/q_\infty$
C_{p_∞}	Perturbation pressure ratio, $\Delta P/P_\infty = (P - P_1)/P_\infty$
C_p^*	Stagnation point pressure coefficient
d	Slot width or circular nozzle diameter
d_j	Equivalent jet exit diameter, d_j = jet exit area/$(2.0\pi r_j)$, Equations (5-8)
F_i	Interaction force induced by the presence of the jet
g	$\left[\gamma_1(\gamma_1 - 1)M_1^2\right]^{-1}$, Equation (18)
h	Calculated jet penetration height
h_s	Distance measured normal to the wall from the wall to the strong shock in the jet
K	Amplification factor, $(F_i + T)/T_{sv}$, or mass fraction of injectant species
K_3	Amplification factor for jet from a finite span slot with F_i evaluated as the total interaction force upstream of the slot
K_3'	Amplification factor for a finite-span slot in which F_i is evaluated by integrating the pressure distribution over unit span upstream along the x-axis and values of T and T_{sv} per unit span are used
k_4	Empirical constant defined by Equation (4)
L	Distance along the x-axis from the plate leading edge or origin of the boundary layer to the nozzle centerline, $L = L_s + X_s$
L_s	Distance along the x-axis from the plate leading edge or origin of the boundary layer to the separation line
M	Mach number
$\mathcal{M}$	Molecular weight
$\dot{m}_j$	Jet mass flow rate
P	Pressure

P_2'	Second peak static pressure, immediately upstream of the jet, see Figure 2
$P_{\psi b}$	Effective back pressure, two thirds of the stagnation pressure downstream of a normal shock in the external flow, see Equation (22)
$\bar{P}_f$	Average value of pressure at the upstream interface between a jet and the external flow, Equation (12)
$P_{o_{d_2}}$	Stagnation pressure of the dividing streamline of the shear layer upstream of the jet
Q	Dynamic pressure ratio, q_j^*/q_∞
q	Dynamic pressure, $1/2\ \rho V^2$
R	Distance from cone axis normalized by r_j, also radius of ogive-cylinder, Figure 64a
Re	Reynolds number
r	Bow shock radius, see Figure 54, also radial distance from jet nozzle centerline, see Figure 59
$\bar{r}$	Normalized r, $\bar{r} = r/(d\sqrt{P_{o_j}/P_\infty})$
r_j	Radius of cone surface at the jet upstream edge, Equations (5-8)
r_n	Sphere-cylinder radius, see Figure 54
S	Arc length on ogive-cylinder, see Figure 64a, $S = R_\psi$
T	Temperature; thrust
T_{sv}	Vacuum thrust of a sonic jet
V	Velocity
X	Distance along the cone surface from the upstream edge of the jet, normalized, by d_j, Equations (5-8)
x	Coordinate in streamwise direction in plane of jet nozzle exit, also distance from vertex, see Figure 54
X_s	Distance along x-axis from nozzle centerline to upstream separation line
X_{ss}	Distance along x-axis from nozzle centerline to initial pressure rise due to separation
Y_e	Distance from the cone surface to the edge of the mixing layer
Y_ψ	Distance from the cone surface to the dividing streamline, measured normal to the cone axis, normalized by d_j
y	Lateral coordinate, normal to streamwise direction, in plane of jet nozzle exit
y_o	Distance between two circular nozzles, see Figure 49
z	Coordinate normal to x-y plane
α	Polar coordinate angle, see Figure 59
β	Function defined by Equation (12), also $(M_\infty^2 - 1)^{1/2}$, Figure 54
Γ	Jet vortex strength, see Equation 26
γ	Specific heat ratio, c_p/c_v
δ	Boundary layer thickness
Δ	Distance along x-axis from circular nozzle centerline to plate trailing edge, see Figure 55
ΔP	Difference between jet-on and jet-off static pressure
ΔX_s	X-coordinate measured from the point where $P - P_1 = 0.6\ (P_2 - P_1)$, see Figure 9
θ	Angle between jet direction and local surface, $\theta = 0°$ is a jet aligned with the external flow direction, also local shock angle, Figure 54

ϕ	Angle between jet direction and normal to local surface, positive for upstream injection, $\phi = \theta - 90°$
X_j	Mol fraction of injectant species
τ	Stagnation temperature–molecular weight ratio $(T_{0_j}\mathcal{M}_1)/(T_{0_1}\mathcal{M}_j)$

Subscripts

0	Stagnation conditions
1	Region just upstream of separation outside of boundary layer
2	Region downstream of separation shock
3	Conditions in the separation region immediately downstream of the nozzle or pertaining to a jet from a finite-span slot
4	Conditions in region corresponding to the peak downstream pressure after the reattachment shock
∞	Undisturbed freestream conditions
j	Jet flow property
s	Pertaining to separation
e	Nozzle exit conditions

Superscripts

*	Sonic conditions

1 INTRODUCTION

Engineering interest in the flowfields created by sonic or supersonic gaseous jets exhausting approximately normal to an external flow dates from the late 1950's. At about that time secondary fluid injection was proposed as a technique for thrust vector control of rocket motors, and it became apparent that reaction control systems employed on spacecraft would be used within the atmosphere during reentry. The objective of this report is to review the literature pertaining to these flowfields. The report is intended to provide information in sufficient quantity and detail so that it can be used as a reference as well as a guide to those who wish to refer to the original sources.

The complexity of flowfields created by jets interacting with external crossflows is such that the present understanding of them relies heavily on experimental data. In recognition of this situation, a considerable portion of this review has been devoted to presentation and discussion of experimental results. The data which have been included are believed to be representative of the complete body of data contained in the cited sources. Most examples have been chosen to illustrate specific features of the interactions. Efforts have been made to include data which cover a wide range of flow conditions. In instances where roughly equivalent sets of data were available, the data most readily available and familiar to the authors have been used. Types of data include flowfield surveys, flow visualization data, static pressure measurements, and force measurements.

The two-dimensional problem concerning the interaction between a jet from an effectively infinite-span slot and an external flow which is supersonic or hypersonic is reviewed in detail in Section 2.0. Interactions produced by jets from finite-span slots are discussed in Section 3.0. Section 4.0 treats the interference between a circular, underexpanded jet and a supersonic external flow. Both laminar and turbulent boundary layers are considered. Section 5.0 is devoted to the interaction of circular, underexpanded jets from flat plates and ogive-cylinders with subsonic external flows. Some results for jets from finite-span slots are also presented. Conclusions concerning the state of the art are included in Section 6.0.

2 TWO-DIMENSIONAL INTERACTION IN SUPERSONIC FLOW

2.1 Description of the Flowfield

Data obtained from a large number of experimental investigations have made it possible to provide a qualitative description of the two-dimensional jet interaction flowfield when the external flow is supersonic. Mitchell (1) has presented one example of a detailed description of such a flowfield, based upon data obtained by Romeo and Sterrett (2). Some of the important features of the flowfield are shown in Figure 1, a shadowgraph photograph obtained from the investigation of Reference 3. Figure 2 provides a schematic diagram of the flowfield shown in the shadowgraph with the associated static pressure distribution. In this example, the jet is sonic, underexpanded, and normal to the wall. The boundary layer is turbulent upstream of the interaction region, and the effective obstruction to the external flow formed by the jet is larger than the undisturbed boundary-layer thickness. End plates, with glass inserts, mounted at each end of the slot are visible in the photograph.

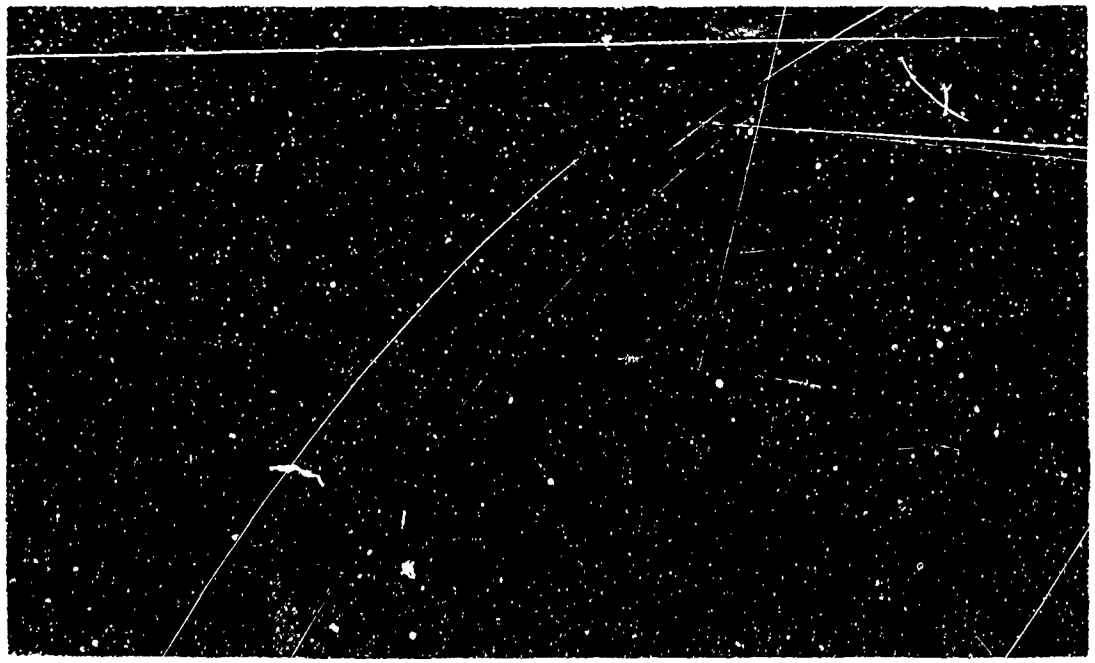

Figure 1. Shadowgraph Photograph of a Typical Jet Interaction Flowfield, Turbulent Boundary Layer, $M_1 = 2.81$

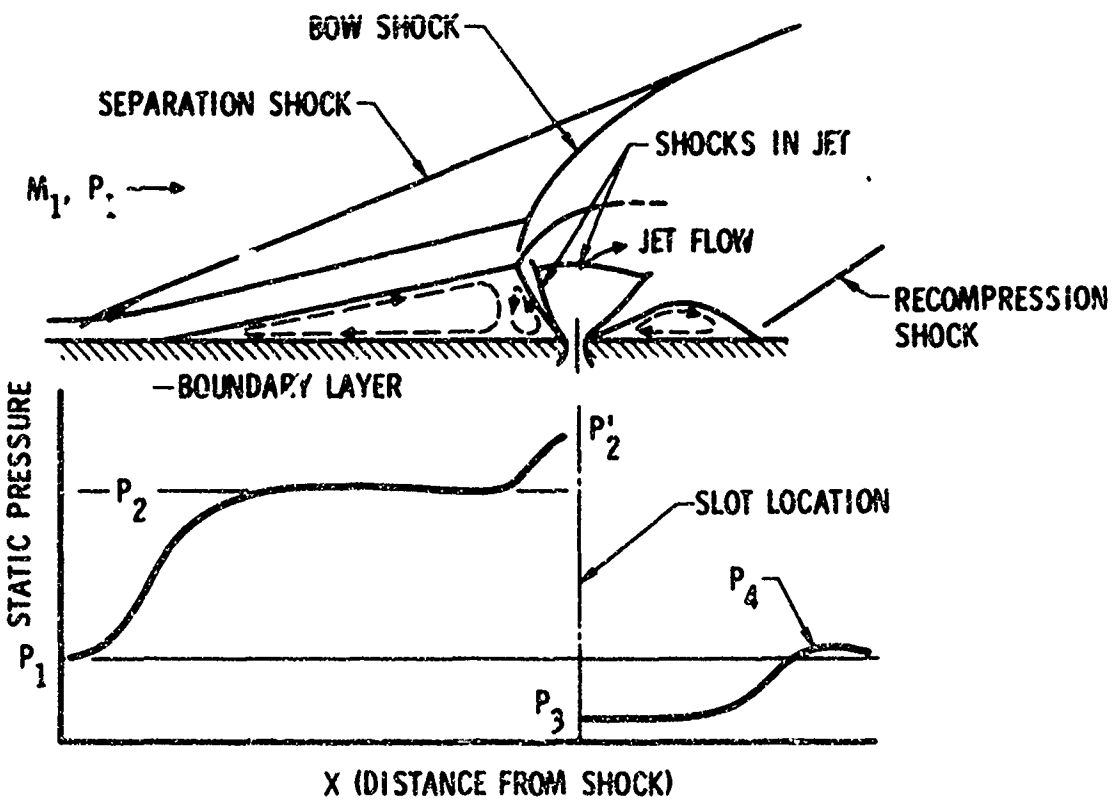

Figure 2. Sketches of Flowfield and Static Pressure Distribution

In the flowfield shown in Figure 1, the boundary layer is separated upstream of the jet location and a shock wave, labeled "separation shock," originates near the separation line. The static pressure rises in the vicinity of separation, reaches a plateau (data from some experiments show a first peak), and rises again in the immediate vicinity of the jet. Static pressure and flow visualization data obtained from many sources including jet interaction experiments imply that the behavior of the flow in the vicinity of separation depends only upon the upstream conditions and is almost independent of the mechanism by which separation is produced. However, in order to satisfy the boundary conditions when separation is caused by a jet, at least two counterrotating vortices are required within the upstream separated region.

The shock structure within an underexpanded jet which interacts with an external flow is quite similar to the shock structure within an underexpanded jet exhausting into a quiescent medium for at least a few exit diameters from the exit plane. When the jet is highly underexpanded, most of the jet flow passes through a normal shock before it is turned to the external-flow direction. A shear layer surrounds the jet at the exit.

The separated external-flow boundary layer meets the shear layer at the upstream boundary of the jet to form the mixing layer between the jet and the external flow. A shock wave, labeled "blow shock" in Figure 2, originates in this region. The multiple images which can be seen for the separation shock, the bow shock, and the recompression shock in Figure 1 indicate that the flow is somewhat unsteady, and that the distance through which the shock waves move is much smaller than the separation distance. Studies of supersonic and hypersonic turbulent boundary-layer flow over solid spoilers and ramps, including measurements of static pressure fluctuations (4, 5), have shown a significant degree of flow unsteadiness in the separated region.

A second separated region exists downstream of the jet. This region has some of the characteristics of the separated region found in flow over a rearward-facing step. When the external flow is supersonic, the static pressure immediately downstream of the jet is less than the static pressure of the undisturbed flow, P_1, as illustrated in Figure 2. In hypersonic flow, downstream pressure distributions in which the ratio P/P_1 is always greater than unity are often observed (6). The geometry of the downstream separated region sketched in Figure 2 implies a component of velocity normal to the wall upstream of reattachment, at least near the dividing streamline. The recompression shock is required to turn the flow parallel to the wall.

Although the example shown in Figures 1 and 2 is believed to exhibit most of the important characteristics of flowfields created by jets from slot-type nozzles, some variations from this pattern are observed. If the jet is not highly underexpanded, or if the exit Mach number is supersonic, the system of shock waves in the jet will be altered. Studies of two-dimensional, supersonic jets exhausting into a quiescent medium reported by Driftmyer (7) did not show normal shock waves in the jet. For a converging jet nozzle, as the jet-to-free-stream pressure ratio is reduced, the normal shock will occur at a lower upstream Mach number until, at a sufficiently low pressure ratio, a system of oblique shocks will take the place of a normal shock. If the pressure ratio is reduced still further, the jet may be entirely subsonic as it is turned.

If the boundary layer of the undisturbed flow is laminar, the separation angle is much smaller than that shown in Figure 1. The laminar boundary layer separation angle is of the order of a few degrees and the associated pressure rise is also much smaller. A shadowgraph photograph of such a flow obtained from the investigation of Reference 6 is presented in Figure 3. Separation tends to promote transition in the shear layer, so that a flow which was entirely laminar in the absence of the jet may become transitional when the jet is introduced. If transition occurs between the separation line and the jet, the static pressure usually rises to a plateau just downstream of separation, and then rises again near the jet location to a final pressure which is comparable to the plateau pressure characteristic of turbulent separation. The location of transition is sensitive to small changes in the external flow and the jet flow, so that a change in the static pressure distribution can be observed for a small variation in nominal flow conditions. Little is known about the details of the region dividing the jet and the external flow. However, because of the inherent instability of free shear layers, it is unlikely that many experimental flowfields remain laminar through reattachment.

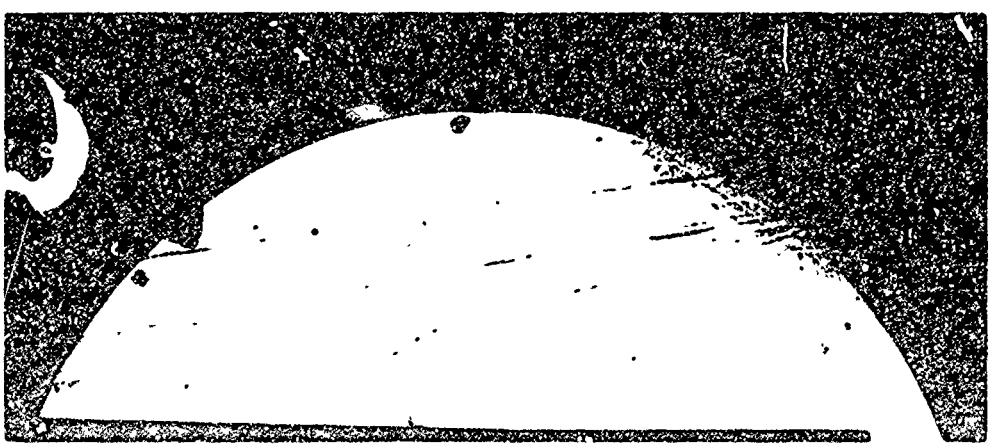

Figure 3. Shadowgraph Photograph of a Typical Jet Interaction Flowfield, Laminar Boundary Layer, $M_1 = 7.9$

2.2 Simulation of the Jet Interaction Flowfield

There are several examples in the literature of different perspectives concerning the formulation of similarity parameters for the jet interaction flowfield. These include application of dimensional analysis, the formulation of simplified analytical models, and the choice of a set of parameters based upon engineering judgment. In any approach, some simplifying assumptions are necessary if the number and complexity of similarity parameters is to be kept within reasonable limits. Consequently, the validity of a set of similarity parameters is limited by the assumptions made in its formulation and by the range of experimental data employed to verify it. In most of the literature cited in the references, the assumptions made in the selection of similarity parameters are essentially the same, but are not always explicitly stated. The requirements for jet interaction flowfield simulation are discussed in detail in the following section in an attempt to identify the assumptions which are implied by a particular set of similarity parameters. Aerodynamic simulation requirements in the absence of jet flow are reviewed briefly, and then extended to include two interacting fluid streams.

Similarity between two flowfields implies that properly normalized dependent variables—the velocity vector and the thermodynamic state—are the same at corresponding stations, i.e., at the same values of the normalized independent variables. Similarity will be achieved if the equations and boundary

conditions governing the fluid motion are identical, when they are nondimensionalized in a consistent manner. If the fluid in question behaves as a perfect gas, the requirements for dynamic and thermal similarity between two flowfields about solid bodies can be stated as follows (8):

1. The bodies must be geometrically similar.

2. Values of Mach number, Reynolds number, Prandtl number, and specific heat ratio must be the same.

3. The dimensionless wall temperature distribution must be the same.

These well-known results are often derived by dimensional analysis, in which a list is made of relevant physical variables such as density, temperature, viscosity, etc., that are then used to form the minimum number of dimensionless groups. This method is simple and is useful when the physical situation is already rather well understood. The difficulty with this approach is that it gives no information about the initial choice of physical variables. A similarity analysis based on the equations of motion eliminates this difficulty and gives additional information. For example, if the preceding simulation requirements are fulfilled for flows about two bodies, then it can be shown that any two consistently defined Reynolds numbers will be matched. There is therefore no need for concern about the proper choice of reference length, reference velocity, etc. Parameters derived from a similarity analysis are coefficients of terms in the equations of motion, and thus have specific physical significance. On the other hand, considerable judgment and intuition is usually required in the process of giving correct physical interpretations to dimensionless groups which are the result of dimensional analysis.

Using either method of analysis, it is possible to define a number of similarity parameters which must be matched to scale the flowfield consisting of a jet exhausting from a body in a uniform flow. The undisturbed uniform flow is selected as a freestream reference state and the overall length of the body, L, is selected as the reference length. The partial list of parameters required for similarity is then written.

$$M_\infty = \frac{V_\infty}{\sqrt{\gamma_\infty R_\infty T_\infty}}, \quad R_{e_{L,\infty}} = \frac{\rho_\infty V_\infty L}{\mu_\infty}, \quad Pr_\infty = \frac{\mu_\infty c_{p_\infty}}{k_\infty}, \quad \gamma_\infty$$

$$\frac{T_w}{T_\infty} = \frac{T_w}{T_\infty}\left(\frac{x}{L}, \frac{y}{L}, \frac{z}{L}\right)$$

If the jet flow is considered to be independent of the external flow, the additional set of parameters

$$M_j = \frac{V_j}{\sqrt{\gamma_j R_j T_j}}, \quad R_{e_{d,j}} = \frac{\rho_j V_j d}{\mu_j}, \quad Pr_j = \frac{\mu_j c_{p_j}}{k_j}, \quad \gamma_j$$

$$\frac{T_w}{T_j} = \frac{T_w}{T_j}\left(\frac{x}{d}, \frac{y}{d}, \frac{z}{d}\right)$$

must be added to assure similarity.

In these parameter definitions, d is a characteristic nozzle dimension and the subscript j refers to a specific location within the jet flow (for instance, at the nozzle exit). The governing equations for the combined flowfield now contain diffusion terms that generate an additional independent dimensionless group, one form of which is the Schmidt number, $\mu/\rho D$, where D is the diffusion coefficient. Similarity of the entire flowfield requires that the same reference quantities be used throughout. This can be achieved if it is required that ratios of corresponding reference quantities for the two streams be matched. If this is done, the previous set of requirements pertaining to the jet alone will be satisfied automatically when those pertaining to the freestream are satisfied. Specifically, it is possible to replace the previous group of jet-related variables by

$$\frac{V_j}{V_\infty}, \quad \frac{R_j T_j}{R_\infty T_\infty}, \quad \frac{\rho_j}{\rho_\infty}, \quad \frac{c_{p_j}}{c_{p_\infty}}, \quad \frac{k_j}{k_\infty}, \quad \gamma_j, \quad \frac{\mu_j}{\mu_\infty}$$

This set of simulation requirements is highly restrictive, but considerable simplification is usually permissible in scaling wind tunnel tests. If the external flow is always air, Pr_∞ and γ_∞ will be nearly matched automatically. The requirement for simulating the wall temperature distribution is only important when higher-order viscous interaction effects are important or when it is necessary to simulate skin friction precisely. Wall temperature effects are sometimes significant in determining the exact extent of the separated regions. Another problem encountered in the design of precise experiments is that simulation of the Mach and Reynolds numbers and dimensionless temperature distribution will not necessarily lead to simulation of the location of boundary layer transition. This is partly because surface roughness effects will not be simulated, but primarily because of wind tunnel boundary layer noise. As a result, the problem of simulating transition location must usually be considered separately from other scaling requirements.

Since free shear layers are nearly always turbulent at Reynolds numbers of practical interest, transport by molecular diffusion and conduction at the shear layer may be neglected, and the only molecular transport properties that must be included are those that influence the vehicle boundary layer

These approximations lead to a simplified set of simulation requirements, one form of which is,

1. Geometric similarity of both the body and the nozzle
2. Duplication of M_∞ and $Re_{L,\infty}$
3. Duplication of γ_j, $(T_{o_j}/\mathcal{M}_j)/(T_{o_\infty}/\mathcal{M}_\infty)$, P_{o_j}/P_{o_∞}

where $\mathcal{M}$ is the molecular weight and the subscript o refers to stagnation conditions. It is clear that the group in Item 3 is not unique. Other discussions of this subject may be found in the literature (9, 10, 11).

Various idealizations of the interaction region have been proposed, from which even simpler sets of scaling requirements can be derived. The range of applicability of each simplified method must be determined by testing it against experimental results. One key idea, variations of which are contained in several proposed analyses, is that the jet can be characterized by its momentum flux vector at the nozzle exit. This assumption leads to the normalization of jet interaction force data by a reference value of jet thrust, rather than by a reference geometric area and the dynamic pressure of the external flow. The following data presentation will illustrate some of the advantages and limitations of this procedure.

2.3 Results of Experiments

Representative examples of jet interaction data will be presented in the following sections. Initially, results from experiments which simulate two dimensional flow as nearly as possible will be presented. The criteria for selection of two-dimensional flow exclude those experiments in which end plates large enough to enclose the separated regions were not used and those in which the distance from the jet to the separation line did not greatly exceed the slot span (see Werle 12 for a discussion of these criteria). End plates are mounted at each end of the slot, aligned with the external flow, and normal to the plane containing the slot.

Experiments conducted for the purpose of creating a flowfield which is very nearly two-dimensional include jets from high aspect ratio slot nozzles in a flat plate, similar experiments in which end plates are used, and axisymmetric experiments. In principle, axisymmetric experiments are preferable. They are seldom conducted, however, probably because the requirement for a model with a very large radius of curvature relative to the jet penetration height causes this type of experiment to be relatively costly. Results from flat plate experiments without end plates are influenced by transverse outflow from the subsonic recirculation regions. End plates do not eliminate end effects, but their use should prevent this outflow. This phenomenon will be discussed in more detail in Section 3.0.

2.3.1 Static Pressure Data

An example of wall static pressure data obtained in supersonic flow with a turbulent boundary layer is presented in Figure 4. Pressures normalized by P_1 are plotted versus X, the distance from the slot. The upstream plateau in the pressure distribution begins to appear at separation distances of roughly 2 inches or more; the pressure immediately upstream of the slot did not reach a limiting value.

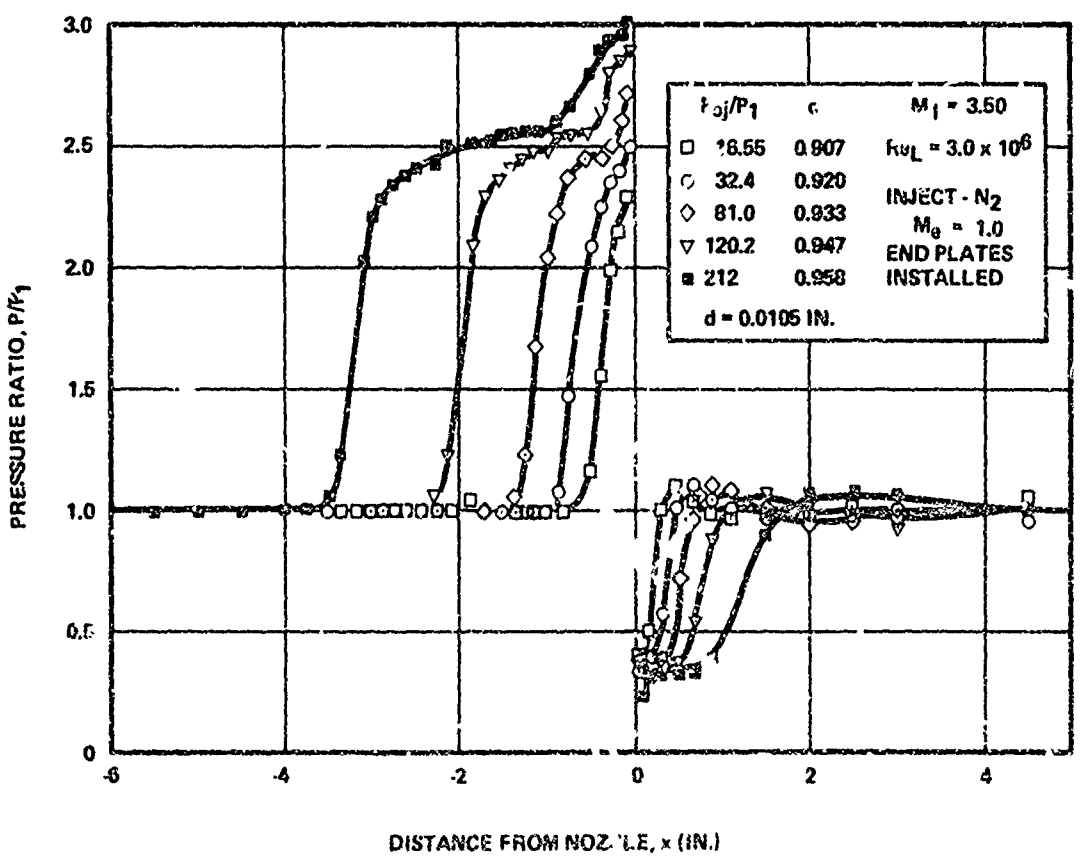

Figure 4. Static Pressure Distributions, Turbulent Boundary Layer $M_1 = 3.50$, Reference 3

Some similar sets of data obtained from experiments with forward-facing steps show that a well-defined plateau is exhibited by the upstream static pressure distribution only when the step height is at least equal to the undisturbed boundary layer thickness ($h/\delta \geq 1$). A notable exception is the data of Driftmyer (13), obtained at $M_1 = 4.9$, in which a plateau was present when $h/\delta_1 \geq 0.3$. In the results shown in Figure 4, the minimum pressure downstream of the slot was nearly constant, independent of jet strength Following the minimum, each of the pressure distributions in the downstream region shows an overshoot of P_1, followed by a decay to P_1.

A similar set of data obtained from experiments on a wind tunnel nozzle wall at a much higher Reynolds number is shown in Figure 5. The test setup for these experiments included a 21-inch slot enclosed between end plates which were 10.0 inches high. The end plates extended 40 inches upstream of the slot and 13.0 inches downstream. The test section was approximately 4 by 4 feet Boundary layer data were obtained on the test section wall opposite the jet. The boundary layer thickness for the test conditions shown here was approximately 2.6 inches. Reynolds numbers based upon an effective flat plate length were computed from Reynolds numbers based on boundary layer momentum thicknesses. A complete description of these experiments can be found in Reference 14. A comparison of Figures 4 and 5 shows that the static pressure distributions have the same general characteristics.

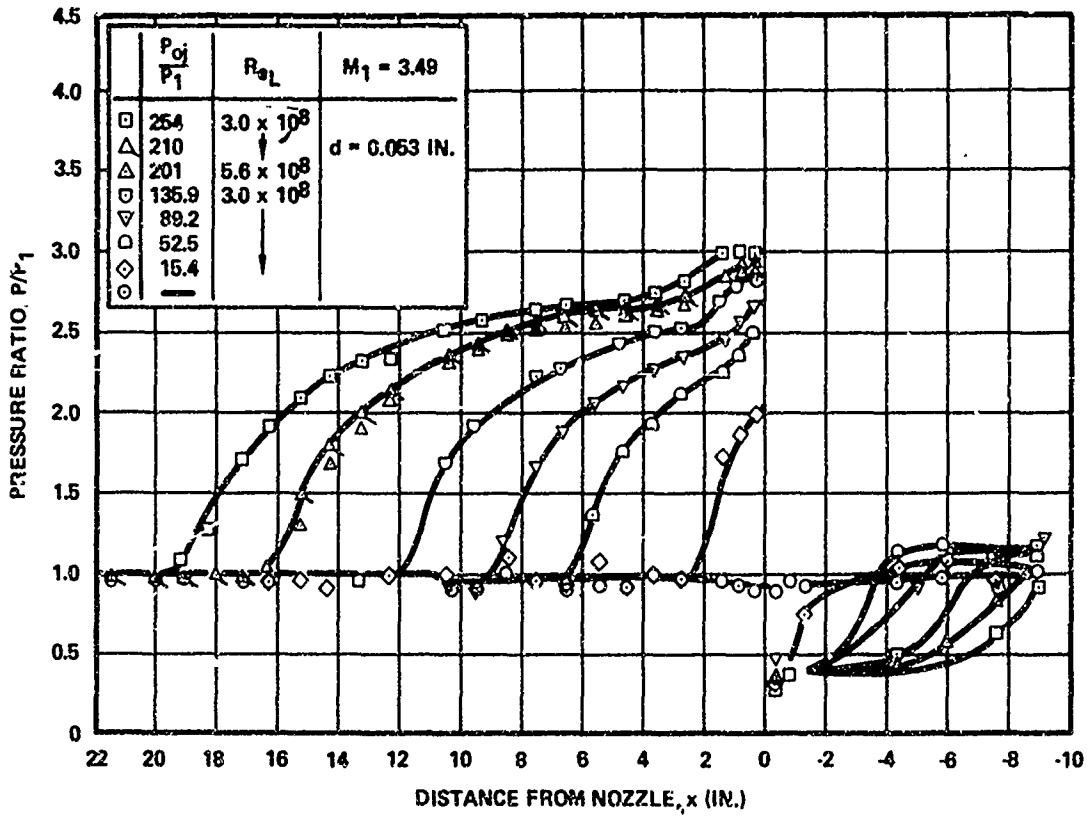

Figure 5. Static Pressure Distributions, $M_1 = 3.49$, High Reynolds Number, Reference 14

Figure 6 gives an example of similar data reported by Barnes, et al (6) obtained from a flat plate experiment at $M_\infty = 6$. The plate measured 27.6 inches by 15 inches and had a 9-inch span slot nozzle located 19.9 inches down-stream of the leading edge. End plates 4 inches high were mounted at either end of the slot, and extended nearly the entire length of the plate. The data labeled "turbulent" in Figure 6 were obtained with a boundary layer trip consisting of a row of 0.078-inch-diameter steel balls located 2.24 inches from the plate leading edge. Viscous interaction and a slight misalignment of the model with the tunnel flow are responsible for differences between P_∞ and the static pressure distribution on the plate in the absence of jet flow. The value of M_1 for these experiments was approximately 7.8. When a boundary-layer trip was used, both static pressure distributions and Schlieren photographs indicated that transition occurred well upstream of the interaction region. The general features of the upstream pressure distributions obtained with a turbulent boundary layer are the same as in the preceding two figures, except that the pressure ratios are higher. Downstream of the slot, the pressure ratios are always greater than unity, in contrast to the lower Mach number results where downstream minimums were less than unity The maximum pressure ratio in the downstream region is seen to depend upon the jet stagnation pressure or mass flow rate Data obtained without the trip show features which are typical of transitional separation, a much longer separation distance, and a lower initial plateau, followed by a region of moderate pressure gradient. These general features have been observed in numerous other experiments in transitional flows at lower Mach numbers, for example, see Strike, et al (15). Note that the pressure distribution in the region downstream of the jet is altered only slightly by the presence of the boundary-layer trip.

Data reported by Barnes, et al, obtained at a lower Reynolds number and without a boundary-layer trip are presented in Figure 7. The character of the static pressure distributions and Schlieren photographs indicate the flow was laminar upstream of the jet. In this case, as in all other nominally laminar jet interaction experiments, no attempt was made to measure fluctuations in flow properties, so that transitional effects cannot be ruled out. These data show much lower plateau pressure ratios than are observed in turbulent interactions at the same Mach number, except when the flow was separated to the leading edge of the plate The average pressure ratios in the downstream region are also lower than comparable turbulent boundary layer values illustrated in the previous figure

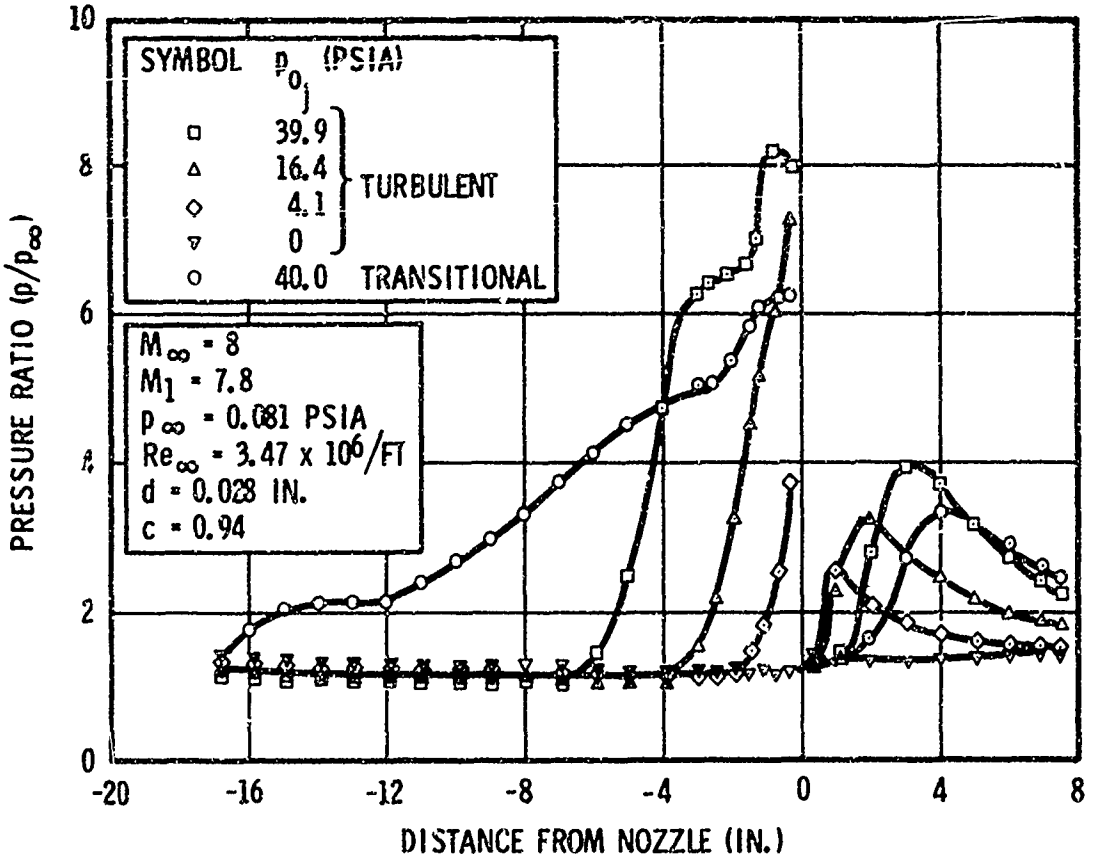

Figure 6. Static Pressure Distributions, M_∞ = 8, Turbulent and Transitional Boundary Layers, Reference 6

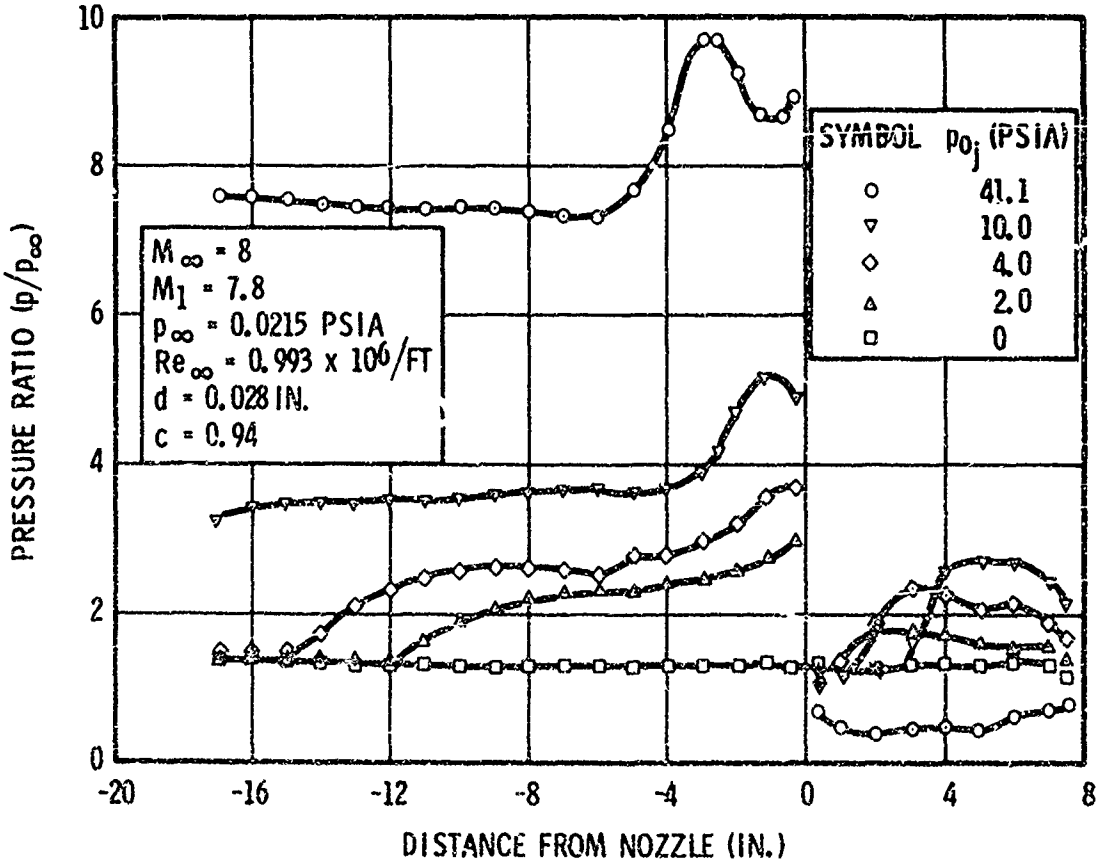

Figure 7. Static Pressure Distributions, M_∞ = 8, Laminar and Transitional Boundary Layers, Reference 6

A summary of plateau pressure data for turbulent interaction with both jets and steps is presented in Figure 8. The data are restricted to those pressure distributions in which a well-defined plateau was formed. The empirical equation proposed for plateau pressure by Zukoski (23)

$$P_2/P_1 = 1 + \frac{M_1}{2} \tag{1}$$

is also shown. The results obtained with jets are self-consistent and agree well with the data in which separation was induced by steps, ramps, and impinging shocks. The supersonic mainstream data ($M_1 \lesssim 6$) show considerably less scatter and systematic variation in these coordinates than the hypersonic data ($M_1 \gtrsim 6$). For supersonic turbulent boundary-layer separation, the variation in P_2/P_1 with Re_L is small, except possibly near the minimum Reynolds numbers at which turbulent boundary layers are observed (10, 23, 24). A significant exception to this conclusion is a set of data presented by Werle, et al (25) with $M_1 = 4$, which show decreasing P_2/P_1 with increasing Reynolds number ($2 \times 10^5 \lesssim Re_L \lesssim 7 \times 10^6$, where L_s is the running length from the effective origin of the turbulent boundary layer to the separation line). Supersonic mainstream data shown in Figure 8 correspond to $10^4 \lesssim Re_{\delta_1} \lesssim 5 \times 10^6$. Considerable scatter and systematic variation is present in the hypersonic mainstream data. Some of the scatter is probably a result of the inherently poorer accuracy and repeatability of shock tunnels and gun tunnels, relative to continuous and blowdown tunnels. In a review of the hypersonic data by Reeves (26), it was concluded that P_2/P_1 becomes increasingly sensitive to the length of the separated shear layer with increasing M_1. This is illustrated by the data of Elfstrom (21), in which separation was induced by a ramp, and P_2/P_1 was observed to depend upon the ramp angle. Only crude estimates of plateau pressures in hypersonic, turbulent flow can be made at the present time.

Werle, et al (25) has suggested that the second peak pressure, P_2', which occurs immediately upstream of the jet, may be approximated by

$$1.2 \leq \frac{P_2' - P_1}{P_2 - P_1} \leq 1.3 \tag{2}$$

The examples of data presented here and other two-dimensional flow data indicate that this is a reasonable estimate.

Only a rather small body of two-dimensional, laminar jet interaction data have been obtained. A limited number of comparisons indicate that the plateau pressure levels agree with data obtained from step- or ramp-induced separated flows. An empirical equation which agrees well with data from laminar flows is (27)

$$C_{P_2} = \frac{1.6}{\left[Re_{L_s}\left(M_1^2 - 1\right)\right]^{1/4}} \tag{3}$$

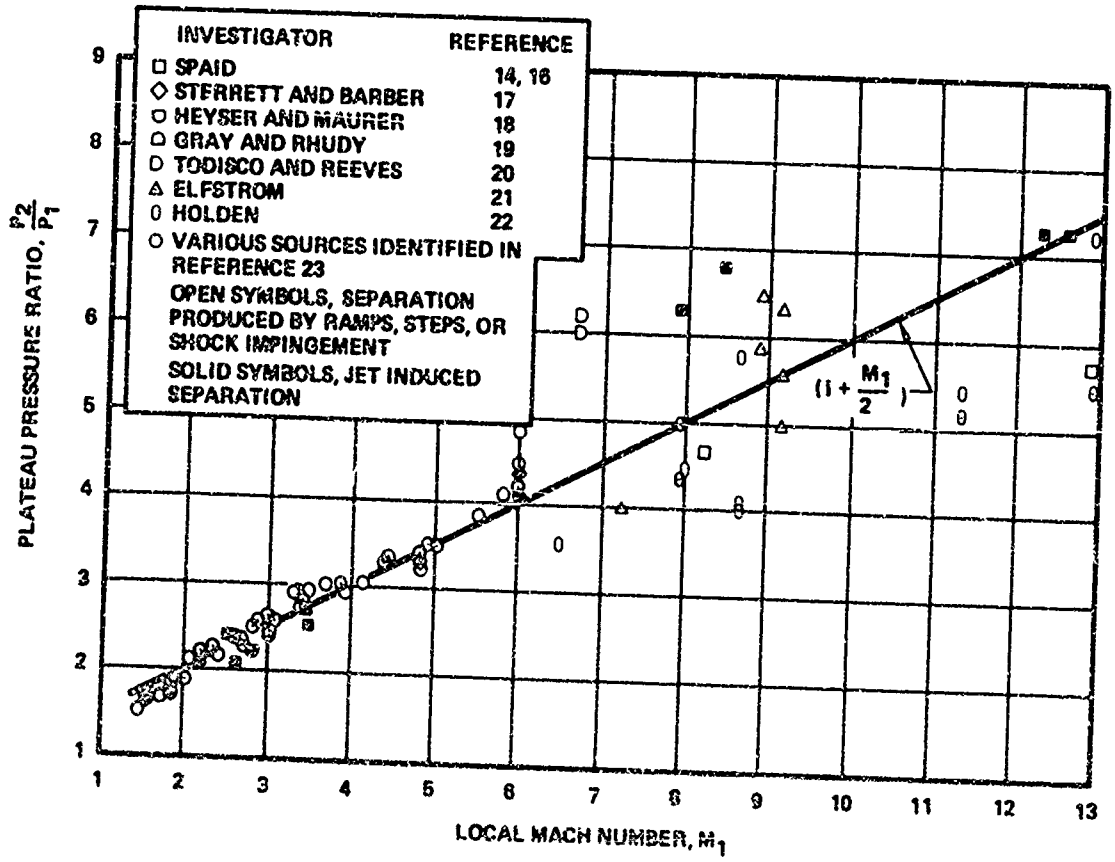

Figure 8. Correlation of Plateau Pressure Data for Two-Dimensional Turbulent Boundary Layer Separation

Results of studies reported by Zukoski (23), Werle, et al (25), and Driftmyer (13) agree concerning the length scales for pressure distributions resulting from two-dimensional turbulent separation caused by jets or solid obstructions. They indicate that δ_1 is the appropriate length scale for the static pressure distribution in the region beginning with the initial pressure rise and extending somewhat downstream of the location of maximum pressure gradient. Farther downstream, the dominant length scale changes to the separation distance, step height, or effective jet penetration height. Jet interaction data obtained at high Mach numbers and Reynolds numbers are in agreement with these results, at least in the region scaled by δ_1, as shown in Figure 9. Data in that figure cover wide ranges in flow conditions including $2.5 \leq M_1 \leq 12.4$, 0.71 in. $\leq \delta_1 \leq 4.0$ in., and $3 \times 10^4 \leq Re_{\delta_1} \leq 5 \times 10^6$. In this case, the origin has been located at the point $P - P_1 = 0.6\,(P_2 - P_1)$. The separation line would have been a more physically meaningful choice for the origin of coordinates; however, experimental separation locations were available in only a few instances. It is clear that any choice of origin which would cause superposition of the regions of maximum dP/dX would show the same result.

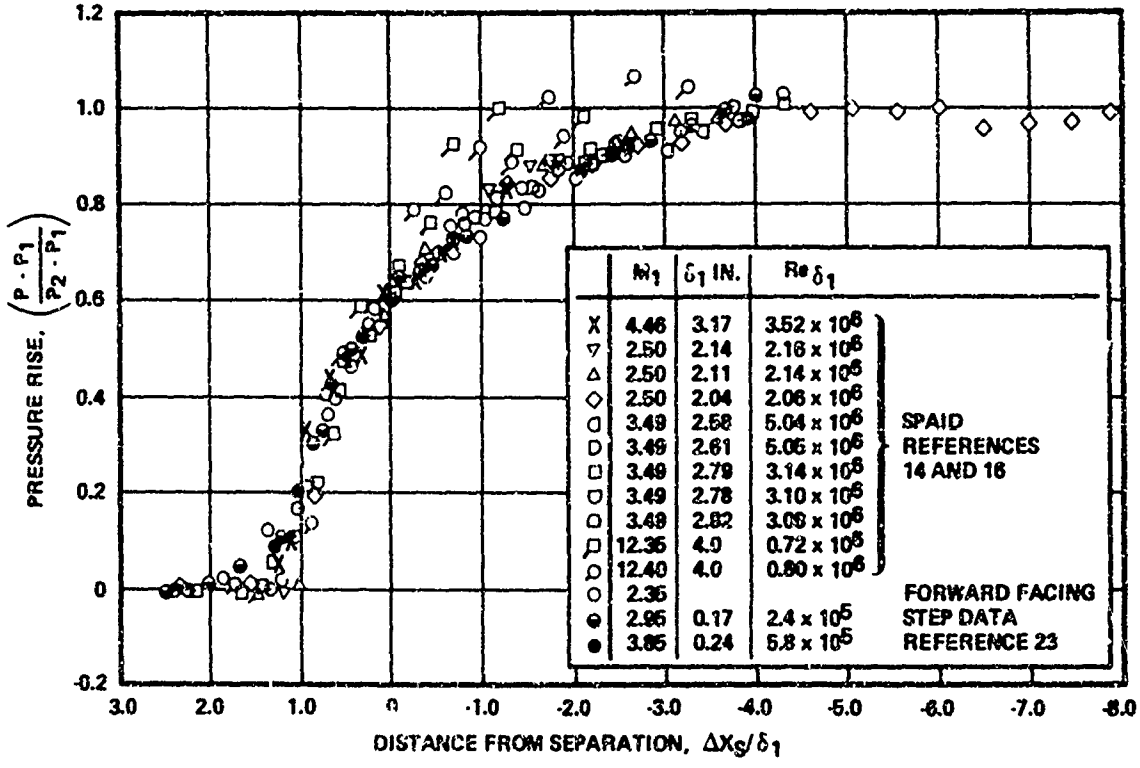

Figure 9. Correlation of Static Pressure Distribution for Turbulent Boundary Layer Separation

Much less information is available about the region downstream of the jet than about the upstream region. The studies presented by Barnes, et al, (6) and by Kaufman and Koch (28) are the most comprehensive. An analysis and limited comparison with data is presented by Tang, et al, (29). A correlation of data obtained at $M_1 = 4.0$ is presented by Werle, et al, (25).

A compilation of data pertaining to the minimum pressure, P_3, downstream of the jet is plotted versus M_1 in Figure 10. Included are turbulent flow data covering a wide Reynolds number range, data where the boundary layer was laminar in the absence of the jet, a wide range of values of P_{0j}/P_1, and experiments with air, nitrogen, and helium jets. Some of these data were obtained either with rather small end plates (31) or without end plates (32). Some evidence (3, 6) indicates that the value of P_3/P_1 may not be sensitive to the presence or absence of end plates. The range of values obtained from a single set of experiments at a single Mach number and Reynolds number are shown as a vertical line with a single symbol. Little variation with P_{0j}/P_1 was observed in the supersonic range. Pressure ratios obtained with helium as injectant were higher than those obtained from experiments with air or nitrogen jets. The large variation shown by the hypersonic data is partly a result of the large pressure gradients in this region (see Figure 6) which depend on jet flow rate or P_{0j}/P_1. As the steeper gradients change location with fixed pressure tap locations, resolution of the pressure distribution changes for a given experiment. Other sources of variation include scatter resulting from low absolute pressure levels in this region or from a variety of sources in the shock tunnel data. Systematic variation with jet flow conditions is probably present also. In spite of these difficulties, a reasonably clear trend of increasing P_3/P_1 is present. The nominally laminar data agree with the turbulent data for $M_1 < 7$. It is possible that the shear layers downstream of the jets were actually turbulent in these experiments. The data of Kaufman (33) for $M_1 > 9$ have not been included because of the large variation in pressure ratio measured at the first downstream pressure tap location.

Also included in Figure 10 is a curve for laminar flow obtained from a jet-mixing analysis presented in Reference 6. The theory predicts the observed trend with Mach number. Since the theory depends upon Re_L and $(P_{0j}d)/(P_1 L)$ where L is the distance from the plate leading edge to the slot and d is the slot width, the theoretical prediction is actually a two-parameter family of curves in these coordinates.

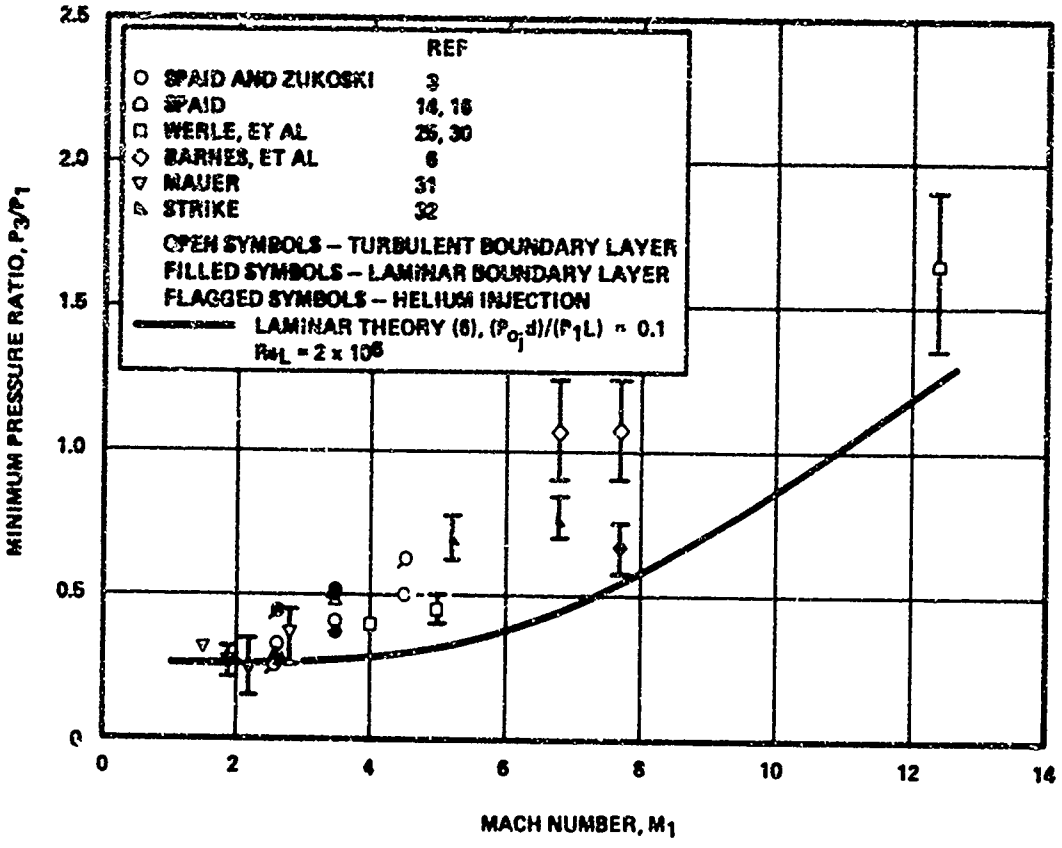

Figure 10. Minimum Pressure Downstream of a Transverse Jet

Figure 11 includes data and semi-empirical predictions for the peak pressure P_4/P_1, in the downstream region, for turbulent interactions. In the analysis of Barnes, et al (6), it is assumed that P_4 is proportional to the static pressure in the jet, just after it has passed through the normal shock. The resulting expression for both laminar and turbulent interactions is

$$\frac{P_4}{P_1} = k_4 \frac{P_{o_j}/P_1}{h/d} \tag{4}$$

where: $k_4 = 0.2$ for $\gamma_j = 1.4$; $k_4 = 0.22$ for $\gamma_j = 1.67$; and h is the predicted penetration height of the jet, which depends upon $(P_{o_j}/P_1)/(d/L)$, γ_1, M_1 and Re_L for normal sonic injection. The method of Kaufman and Koch (28) is derived from the method of Barnes, et al. Both the data and analyses show a trend of increasing P_4/P_1 with increasing P_{o_j}/P_1 or jet mass flow rate.

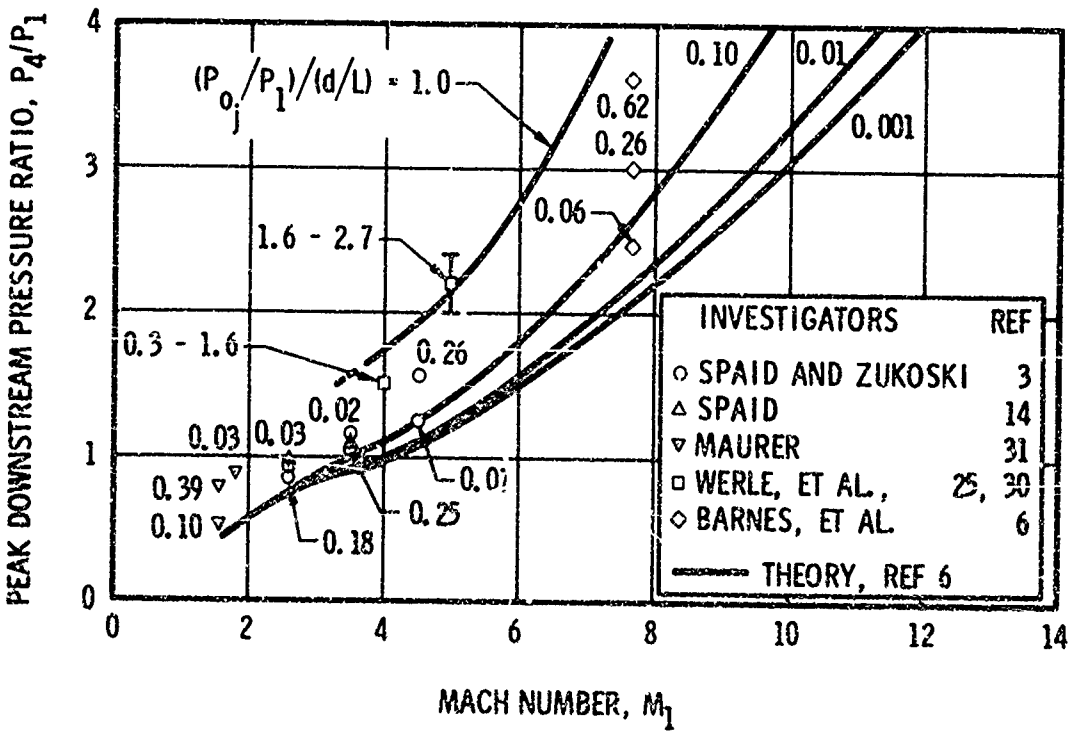

Figure 11. Peak Pressure Downstream of a Transverse Jet, Turbulent Boundary Layer

The range of measured values of P_4/P_1 for nominally laminar flows is shown in Figure 12. The range of values obtained from a single set of experiments at a single Mach number is shown as a vertical line with a single symbol. The data of Barnes, et al, and Strike (32) show increasing P_4/P_1 with increasing jet pressure ratio or mass flow rate. Comparisons between data and the analyses of Barnes, et al, and Kaufman and Koch (28) show fair agreement. However, the data are not sufficient in either quantity or quality to permit definite conclusions to be reached.

Barnes, et al, Kaufman and Koch, and Werle, et al, (25) have suggested that the length scale of the downstream flow field is proportional to the effective penetration height of the jet Werle, et al, present a good correlation of data for a single value of M_1 by utilizing this idea. A review of data which cover a wide range of flow conditions (28) indicates that this assumption is reasonable.

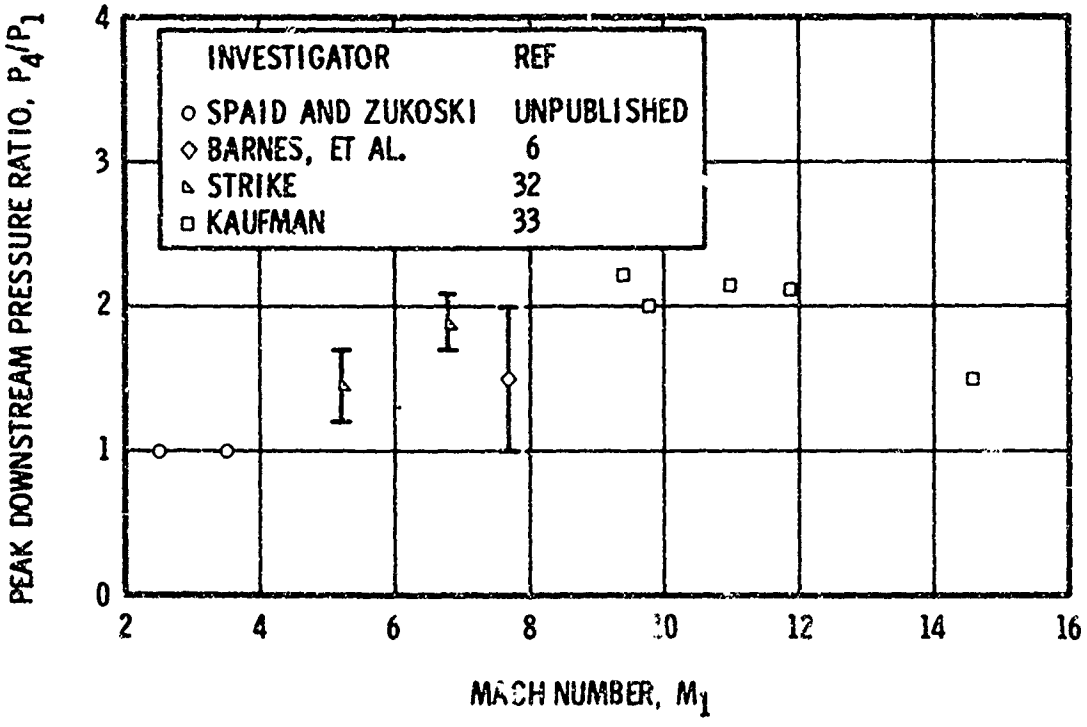

Figure 12. Peak Pressure Downstream of a Transverse Jet, Laminar Boundary Layer

2.3.2 Flow Surveys and Concentration Measurements

A small number of flow survey and concentration measurement experiments have been made for two-dimensional jet interaction flows. Pitot pressure and concentration data for argon and helium injection have been reported by Spaid (34). End plates were not used and significant three-dimensional effects were probably present Buffum, et al, (35) present concentration data for helium injection into an expanding two-dimensional nozzle.

Detailed flowfield surveys downstream of a two-dimensional normal, sonic air jet have been conducted by Werle, et al, (30) at $M_1 = 5$, with a turbulent boundary layer upstream of the interaction region. Data included shadowgraph photographs, pitot pressures, stagnation temperatures, and static pressures measured using a 10-degree half-angle conical probe Streamlines were mapped by computing integrals of mass flow rate in the direction normal to the plate at various X-locations. An example of data obtained from this investigation is presented in Figure 13 The Z-coordinate is measured from the plate surface, normal to the plate. Similar flow survey data obtained from experiments without end plates have been reported by Strike (32).

Shreeve (11) has conducted an experimental study of the flow produced by a circumferential jet from the surface of a 5-degree half-angle cone model at $M_\infty = 6$ A sketch of Shreeves's model installed in the tunnel is shown in Figure 14 The boundary layer upstream of the interaction region was turbulent, and the angle, θ, between the jet direction and the cone surface was varied from 5 to 120 degrees The jet exit Mach number was 1.4. Data included shadowgraph and Schlieren photographs, static pressure distributions downstream of the jet, pitot pressure surveys, and stagnation temperature surveys This experimental arrangement was chosen in order to eliminate end effects, but significant transverse curvature effects were present Transformed coordinates were used in an attempt to remove these effects

Values of the downstream peak pressure, P_4/P_j were shown by Shreeve to depend upon θ and P_{o_j}/P_1 In his experiments, $1.5 \leq P_4/P_1 \leq 2.3$, which is consistent with the results shown in Figure 11. The flow survey measurements were used to determine the location of the dividing streamline between the jet and the external flow. It was shown that profiles of mass flux could be obtained with sufficient accuracy from the pitot pressure and stagnation temperature measurements The displacement of the dividing streamline was found to be insensitive to jet inclination angle for $5 \leq \theta \leq 20$ degrees Within this range, the following correlation equation represents the data

$$RY_\psi = 0.563 \left(\theta^{0.06} \frac{P_{o_j}}{P_1}\right)^{0.361} X^{0.121} \qquad (5)$$

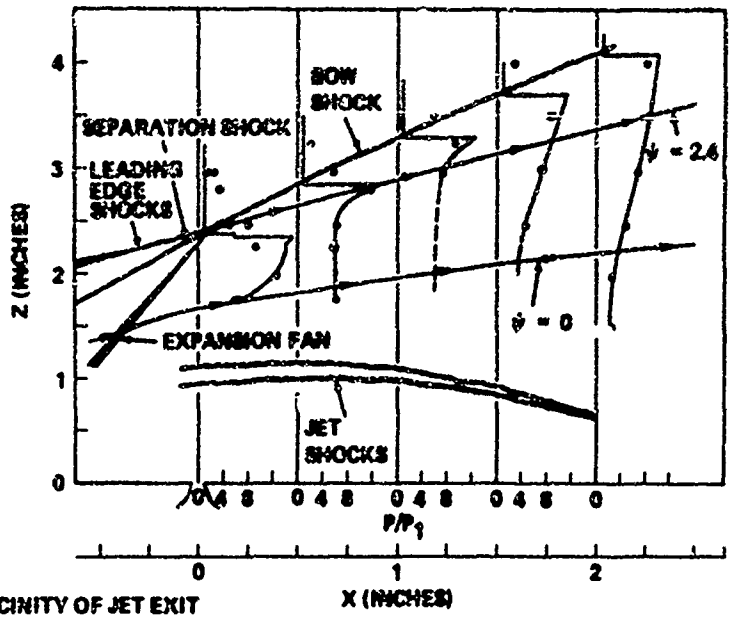

(a) VICINITY OF JET EXIT

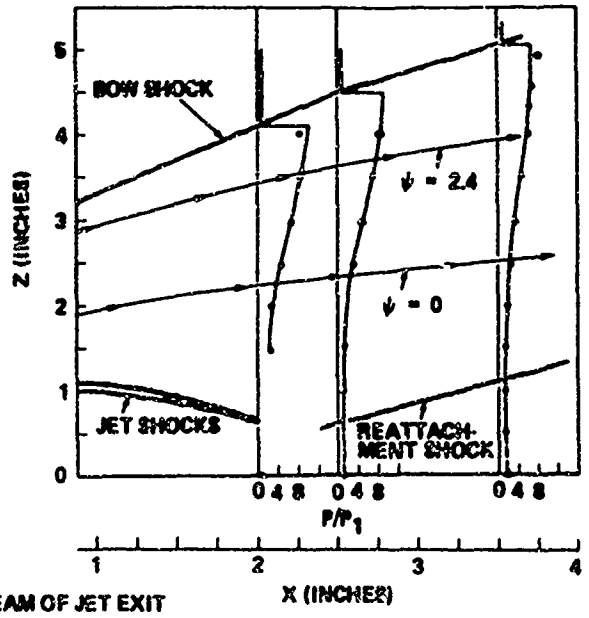

(b) DOWNSTREAM OF JET EXIT

Figure 13. Flowfield Survey Data From Reference 30 $M_\infty = 5$, $P_{0_j}/P_1 = 550$, Turbulent Boundary Layer

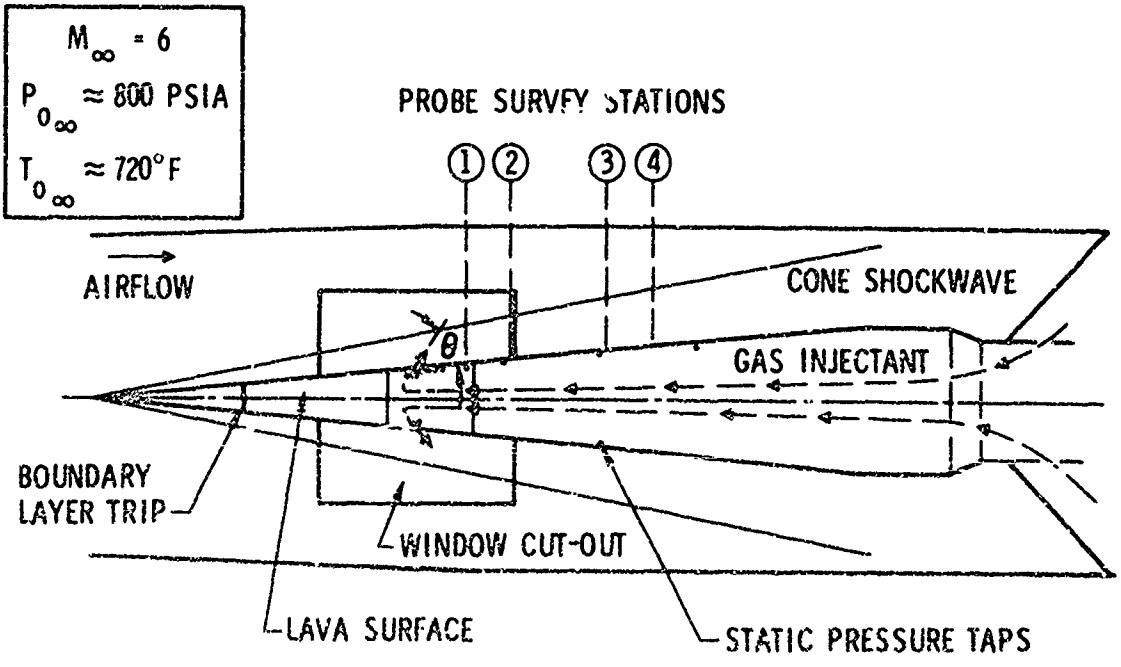

Figure 14 Schematic of Shreeve's Experiment, Reference 11

where

R = distance from cone axis normalized by r_j, the radius of the cone surface at the jet upstream edge

Y_ψ = distance from the cone surface to the dividing streamline, measured normal to the cone axis, normalized by d_j

d_j = equivalent jet exit diameter, d_j = jet exit area/$(2\pi r_j)$

X = distance along the cone surface from the upstream edge of the jet, normalized by d_j.

For θ = 45 degrees, the dividing streamline was correlated by,

$$RY_\psi = 0.231 \left(X^{0.275} P_{o_j}/P_1 \right)^{0.650} \tag{6}$$

and for near-normal jets, the following approximate correlation equations were obtained:

$$RY_\psi = 0.197 \left(X^{0.125} P_{o_j}/P_1 \right)^{0.818} : \quad \theta = 90 \text{ degrees} \tag{7}$$

$$RY_\psi = 0.226 \left(X^{0.111} P_{o_j}/P_1 \right)^{0.818} : \quad \theta = 120 \text{ degrees} \tag{8}$$

The edge of the mixing layer, Y_e, was also located. A plot of Y_ψ/Y_e versus P_{o_j}/P_1 for various angles shows that $0.4 \leq Y_\psi/Y_e \leq 0.7$. The total displacement effect of the jet on the outer flow was evaluated, including the contribution from turbulent shear in the mixing layer. Analysis of the data showed that for $P_{o_j}/P_1 \sim 20$ at $\theta \leq 45$ degrees, the total displacement of the outer flow by the jet is not more than 18 percent greater than the dividing streamline displacement. The influence of turbulent shear was to increase the total displacement effect, relative to Y_ψ with increasing θ. In general, the rate of mass entrainment into the mixing region was found to increase with increasing θ.

Results of a series of two-dimensional experiments conducted at Mach 2.5 with variations in T_{o_∞}, T_{o_j}, and injectant composition have been reported by Thayer (10) and by Thayer and Corlett (36). The boundary layer upstream of the interaction region was turbulent. Data included injectant concentration measurements in the upstream separated region. An example of these data is given in Figure 15, in which X, the injectant mol fraction, is plotted versus X/X_{ss}, where X_{ss} is the distance from the slot to the location of the initial pressure rise upstream of separation. These data show that a major fraction of the gas in the upstream recirculation region comes from the jet. The concentration distributions show some of the characteristics of the static pressure distribution, including a concentration plateau. Plateau mass fractions were correlated by the parameter $(T_{o_j}/M_j)/(T_1/M_1)$ as shown in Figure 16.

Concentration data such as those shown in Figures 15 and 16 were used to estimate the rates of mass transfer across the shear layers. The total mass within the recirculation region is constant, so that as injectant material and air are transported across the shear layers, an equal mass flux of mixture is transported across the shear layers in the opposite direction. The presence of a large region where the injectant concentration is nearly constant implies that the air and injectant mix within this region in a time which is short compared with the average time which a mass of fluid remains within this region. It follows that the ratio of injectant mass to air in the recirculation region is directly proportional to the ratio of mass transfer rates. This result can be written

$$K_{jr} = \frac{\dot{m}_{j_r}}{\dot{m}_{j_r} + \dot{m}_{a_r}} \tag{9}$$

or

$$\frac{\dot{m}_{a_r}}{\dot{m}_{j_r}} = \frac{1}{K_{j_r}} - 1$$

where K_{j_r} is the plateau mass fraction of injectant gas, $\dot{m}_{j_r}$ is the mass flux of injectant gas into the recirculation region, and $\dot{m}_{a_r}$ is the corresponding air mass flux. This principle was applied to results of experiments in which a known mass flux of a tracer gas was bled into the recirculation region upstream of a forward-facing step, and measurements of tracer gas concentration were made upstream of the step. Equation (9) was then used to determine $\dot{m}_{a_r}$ with the known tracer gas mass flow rate replacing $\dot{m}_{j_r}$. It was further assumed that the average mass flux of air transported across the shear layer upstream of a jet is equal to the corresponding mass flux when the flow is separated by a forward-facing step, if the separation distances and external flow conditions are the same. Values of $\dot{m}_{a_r}$ determined from the forward-facing step experiments were used with values of K_{j_r} determined from the jet interaction experiments to determine $\dot{m}_{j_r}$. It was found that the normalized air mass flux was

$$W_{a_r} = \frac{\dot{m}_{a_r}}{\rho_1 U_1 X_{ss} b} = 0.023 \tag{10}$$

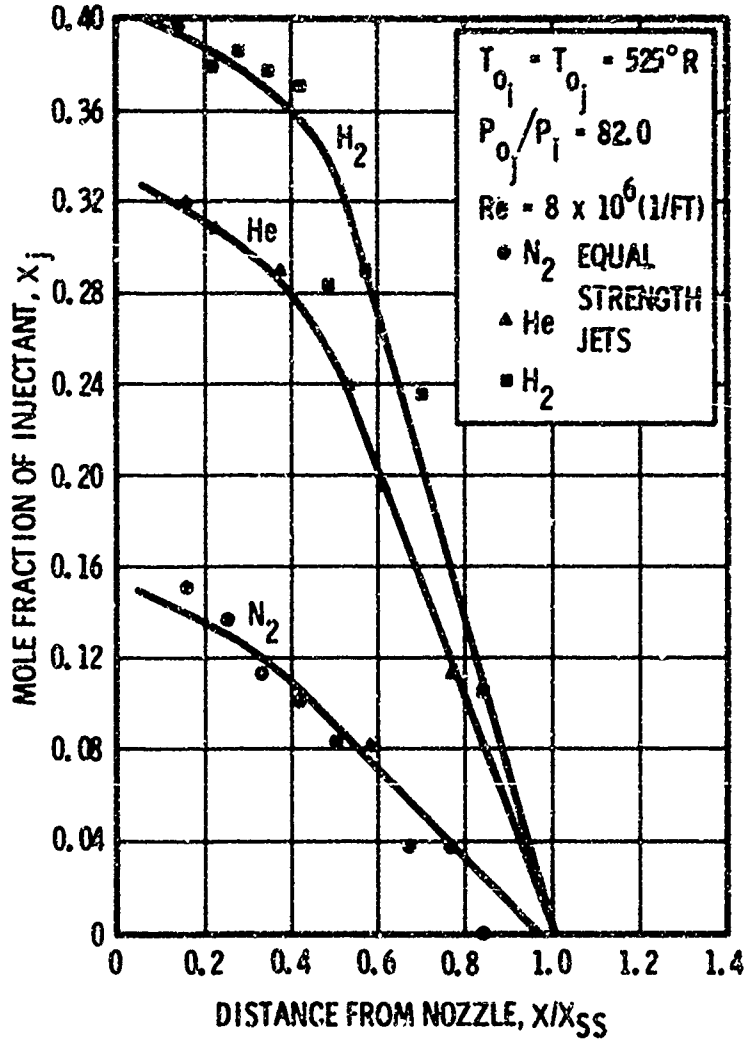

Figure 15. Injectant Concentration in the Upstream Recirculation Region, Reference 10

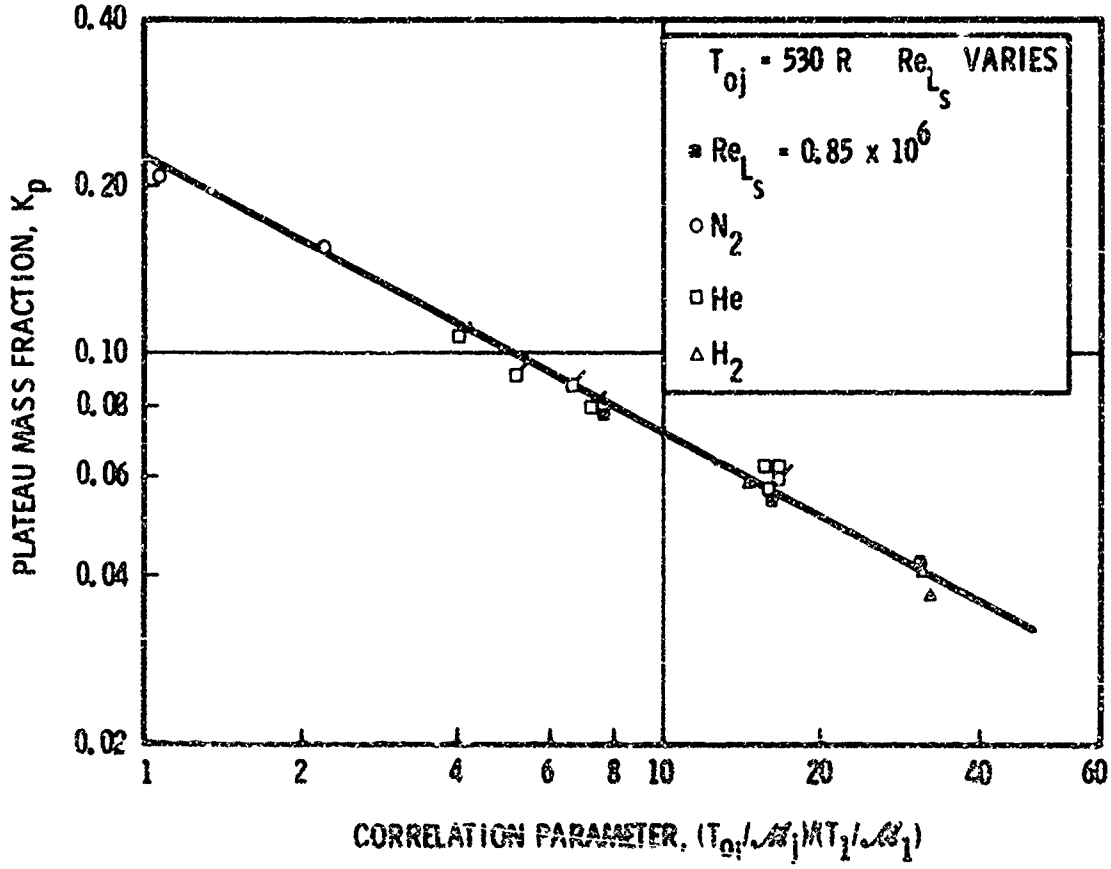

Figure 16. Correlation of the Plateau Mass Fraction, Reference 10

for the entire range of flow conditions covered by this investigation. Roughly 5 percent of the total jet mass flow, $\dot{m}_j$, rate passed through the upstream recirculation region. Figure 17 shows $\dot{m}_{j_r}/\dot{m}_j$ as a function of T_{o_1}/T_{o_j} for various injectant gases.

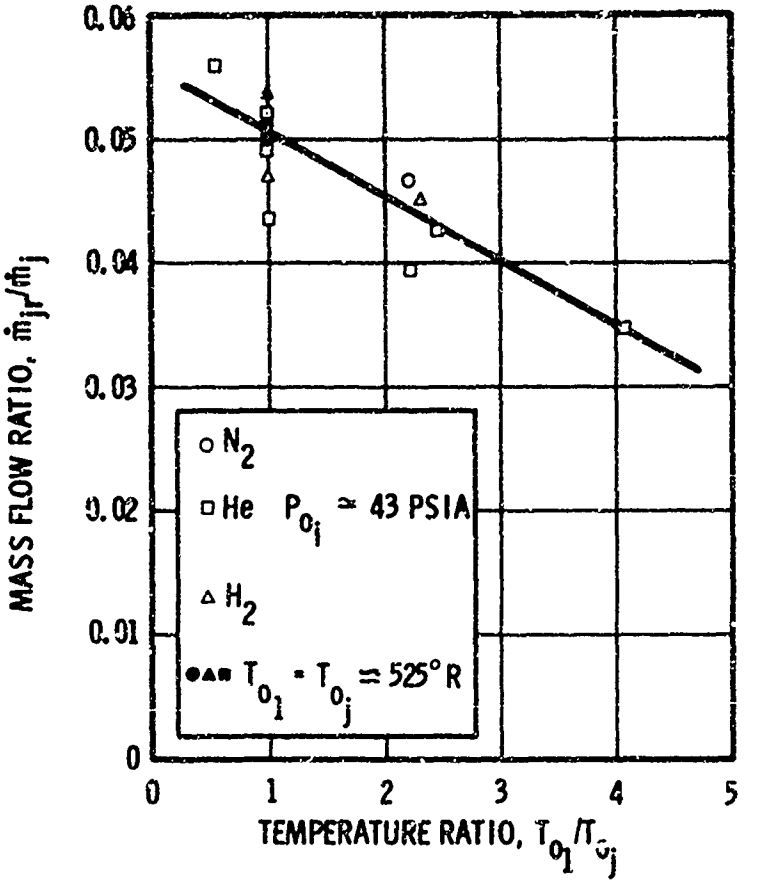

Figure 17. Estimated Injectant Mass Flow Rates Through the Upstream Recirculation Region, Reference 10

2.3.3 Force Data

The interaction force developed upstream of a two-dimensional, normal, sonic jet in turbulent flow has been the subject of many investigations. Figure 18 summarizes the data known to the present authors in the form of amplification factor, K, versus M_1 for air or nitrogen jets. Amplification factor is defined as

$$K = \frac{F_i + T}{T_{SV}} \tag{11}$$

where

F_i = interaction force, in this case including only the region upstream of the jet, force/unit jet span

T = jet thrust

T_{SV} = vacuum thrust of a sonic jet having the same stagnation conditions and mass flow rate as the actual jet

To calculate the amplification factors in all but one case shown in Figure 18, interaction forces were determined by integrating static pressure distributions upstream of the slot along the X-axis. The exceptional case is the data of Hawk and Amick (37) which were obtained by direct measurement of forces.

Many of the sets of data were obtained from flat plate experiments at constant external flow conditions, fixed slot width, and varying P_{o_j}/P_1. As a result, variations in pressure ratio also correspond to variations in jet mass flow rate, size of the effective obstruction produced by the jet, Reynolds number at separation, distance between transition and separation, aspect ratio of the separated region, etc. Data taken in this manner always show a decrease in amplification factor with increasing P_{o_j}/P_1. Series of data of this type are indicated in Figure 18 by symbols connected by a vertical line. Although substantial variation in the data is present at a fixed Mach number, the data indicate that the influence of M_1 on K is quite small. The data of References 3, 14, and 16 are the only sets of data obtained with large end plates which include measurements made at several values of M_1 in the same facility and with the same model and instrumentation. Examination of these data separately also supports the conclusion that the influence of M_1 on K is small.

The data presented in Figure 18 cover a very wide range of effective flat plate Reynolds numbers, ranging from 2.0×10^6 to 6.5×10^8. The extremes in this Reynolds number range are represented by

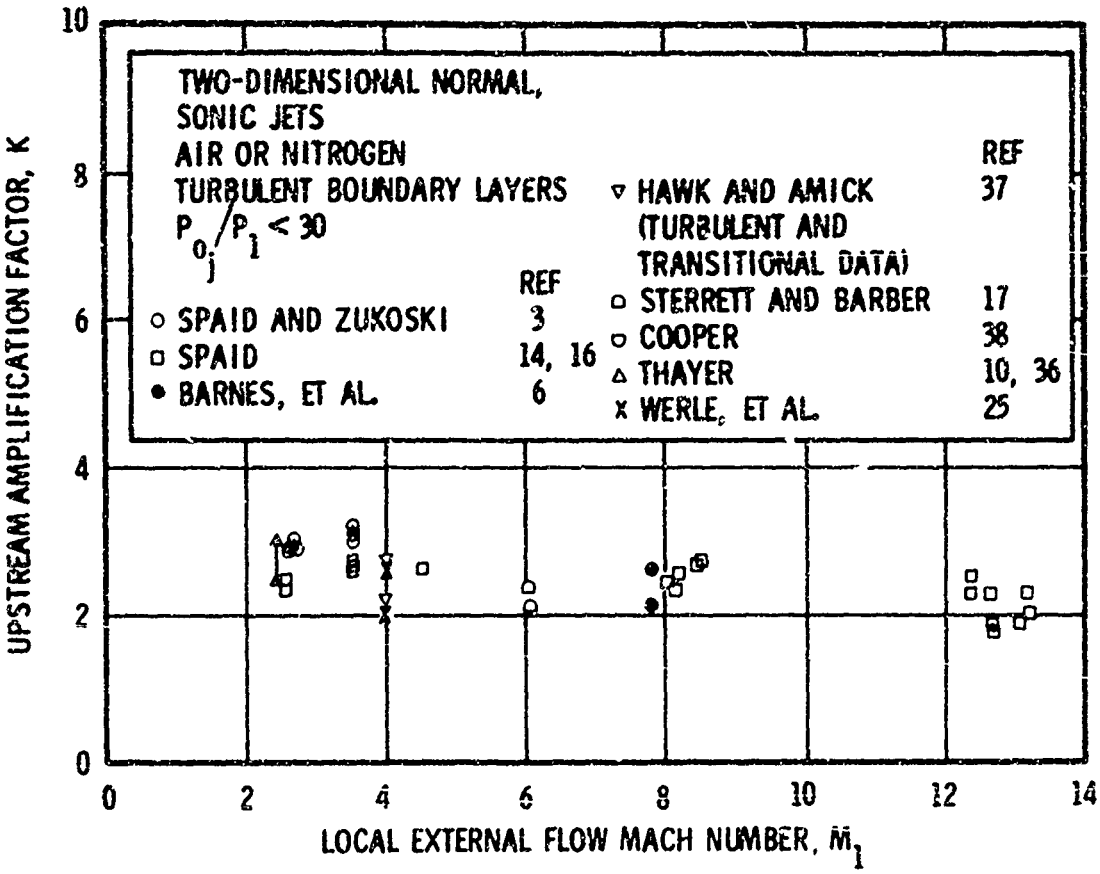

Figure 18 Effect of External Flow Mach Number on Jet Interaction Performance

data from different facilities. Data from a given test series in which P_{0_j} are varied corresponds to variation in Re_{L_s}; however, corresponding variations in K cannot definitely be attributed to a Reynolds number effect for reasons which have already been discussed. Although some differences exist between sets of data obtained from different facilities at the same Mach number and at different Reynolds numbers, no consistent performance trend with Reynolds number has been found. A change of more than 5:1 in Reynolds number at a nominal Mach number of 8 in data obtained from a shock tunnel experiment (16) did not produce a significant effect on the normalized interaction force. In this case, X_s/L was always very small, so that the distinction between L and L_s was unimportant. Data presented by Thayer (10) in the form of K versus Re_{L_s} ($0.4 \times 10^6 < Re_{L_s} < 2.5 \times 10^6$) show the effect of Reynolds number to be very small with nitrogen or hellum as injectant, but data obtained with hydrogen as injectant show an 11 percent increase with increasing Re_{L_s} within the same range. A similar set of data obtained at $M_1 = 4$ by Werle, et al, (25) in which the freestream unit Reynolds number was changed by a factor of 3:1 did not show a significant effect of Reynolds number.

The decrease in K with increasing P_{0_j}/P_1 for a fixed slot width and a fixed external flow has often been interpreted as an effect of pressure ratio, but the independent effect of pressure ratio can only be determined with confidence from experiments in which effects of other variables can be evaluated, i.e., experiments in which the slot width is changed. A plot of F_i/T_{SV} versus $(P_{0_j}dc/P_1\delta_1)$ is shown in Figure 19, using data from Reference 14. The quantity c is the discharge coefficient for the slot and δ_1 is the boundary-layer thickness of the undisturbed flow, essentially constant in this case. The boundary-layer thickness was chosen for purposes of normalization because it is a characteristic length corresponding to the external flow. The usefulness of this method of normalization for situations in which δ_1 varies has not been demonstrated conclusively. These data have been used for the purpose of this comparison, because they include a large variation in slot width and accurate measurements of jet mass flow rate. Jet mass flow rate measurements independent of those computed from the slot area and jet stagnation conditions are highly desirable. First, the slot area is seldom known to the required accuracy even in the absence of jet flow effects. Second, slot geometries and Reynolds numbers are usually in a range such that the discharge coefficients are significantly different from unity and dependent upon Reynolds number. Third, slots have been known to deform enough at high values of jet stagnation pressure to cause large changes in nozzle area (39). The data of Figure 19 are almost completely independent of pressure ratio or slot width for $3.26 \leq P_{0_j}/P_1 \leq 254$. These data span the range of subsonic to highly underexpanded jet flow at the nozzle exit. Data reported by Werle, et al, (25) show similar results. These experiments were conducted in turbulent boundary layer flow at $M = 4$ and with slot widths of 0.005 to 0.030 inch. Jet mass flow rate was determined by a metering system built to ASME specifications. The upstream interaction force was shown to be independent of slot width or pressure ratio at constant jet mass flow rate.

The effect of jet exit Mach number, M_e, is probably best illustrated by results reported by Sterett, et al, (40), in which experiments were conducted at $M_\infty = 6$ with a flat plate having several interchangeable jet nozzles. Interaction forces were determined by integrating static pressure distributions along the X-axis. Figure 20 presents data from that investigation. No end plates were used, but relative performance of jets with various exit Mach numbers may not be significantly affected by the presence or absence of end plates. The ordinate of Figure 20 is the interaction force plus the jet thrust (per unit span) converted to conventional aerodynamic coefficient form, with the plate length used as the reference length. The solid lines are calculated jet thrust, normalized in the same manner. The data

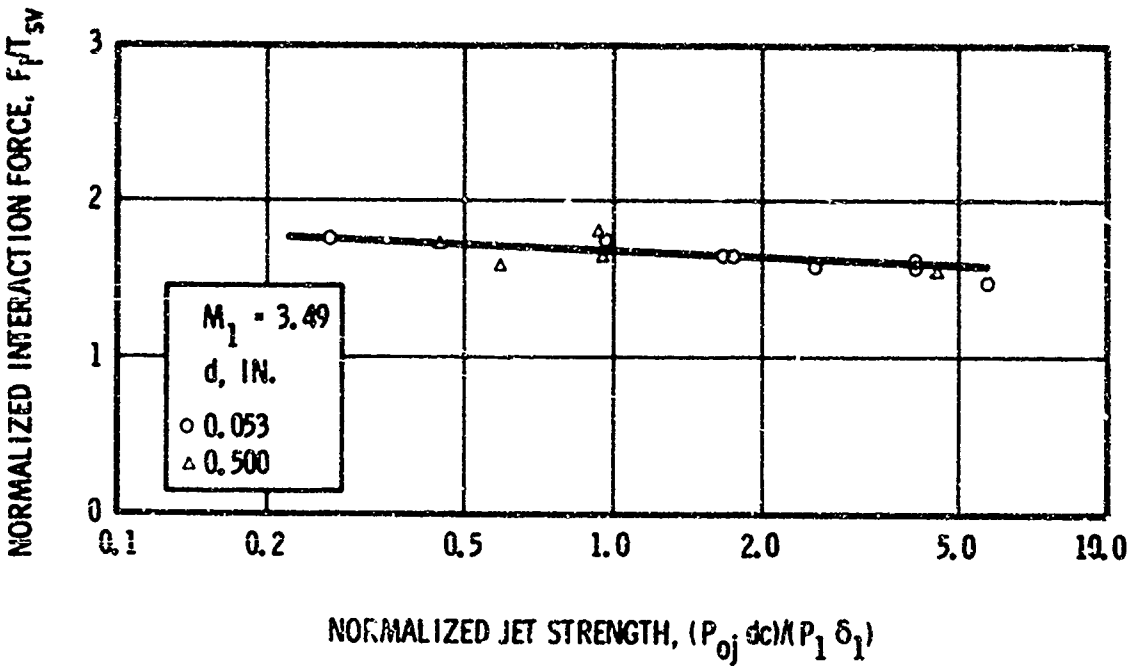

Figure 19. Effect of Pressure Ratio and Slot Width on Interaction Force, Reference 14

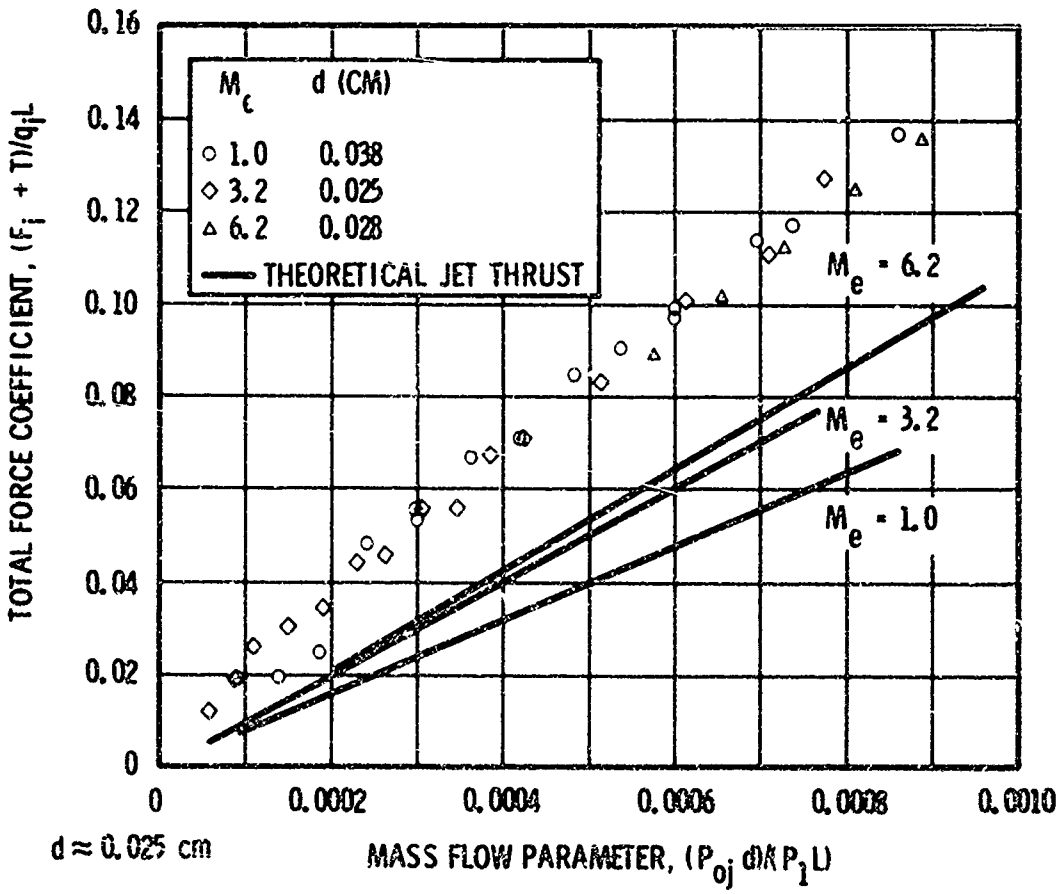

Figure 20. Effect of Jet Exit Mach Number on Jet Interaction Performance, Reference 32

show that the total force, interaction plus jet thrust, is essentially independent of jet exit Mach number; an increase in jet thrust produced by increasing the nozzle expansion ratio is almost precisely compensated by a reduction in interaction force. Static pressure data showed that this reduction in interaction force was associated with a reduction in the separation distance, rather than a change in the pressure levels.

Some of the most direct evidence concerning the influence of γ_1 and γ_j on the jet interaction flowfield comes from the investigation by Thayer (10). The freestream specific heat ratio was changed from 1.4 to 1.32 by changing T_{o_1}. Other parameters were adjusted to duplicate the Reynolds number and pressure ratio. The decrease in γ_1 was associated with a 2 percent increase in P_2/P_1 and an

unchanging separation distance. A change in injectant specific heat ratio from 1.4 to 1.67, corresponding to a change in injectant gas from hydrogen to helium, resulted in essentially no change in the upstream static pressure distribution, when all other similarity parameters were held constant.

The influence of the state of the boundary layer on force amplification is illustrated in Figure 21 by data from Reference 6, taken at $M_\infty = 8$. These results show that all of the laminar and most of the transitional test conditions exhibit substantially larger amplification factors than those obtained from experiments in turbulent flow. The results of experiments by Hawk and Amick (37) at $M_1 = 4$ show the same trend as the data of Figure 21. References 6 and 37 contain the only data pertaining to interaction forces produced in the region upstream of a jet in two-dimensional, laminar flow known to the authors.

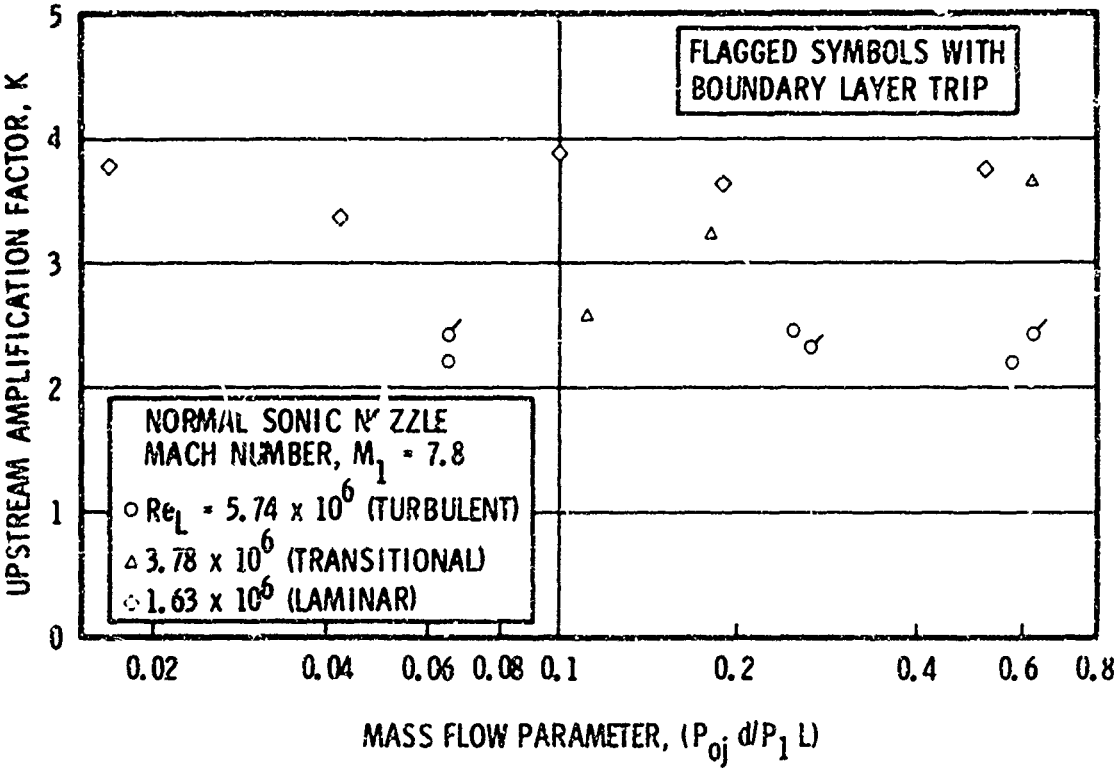

Figure 21. Jet Interaction Performance for Laminar, Transitional, and Turbulent Boundary Layers, $M_1 = 7.8$, Reference 6

Little attention has been given to the contribution to the interaction force of the region downstream of the jet in two-dimensional flow. Data obtained at moderately low supersonic Mach numbers (such as that presented in Figure 4) show that the contribution of the downstream region is in the direction opposite to the thrust. Data reported in Reference 3 which were obtained in turbulent flow at Mach 4.54 showed essentially zero net interaction force contribution from the downstream region. The summaries of downstream static pressure data presented in Figures 10, 11, and 12 tend to imply that the contribution to the total interaction force increases with increasing M_1. Two-dimensional turbulent flow data from the investigation of Barnes, et al. (6) for $M_\infty = 8$ are shown in Figure 22. These data show rather large positive contributions from the downstream region, which decrease relative to the upstream contribution with increasing jet mass flow rate. Comparable data for laminar flow, on the other hand, show a relatively small negative contribution from the downstream region at low flow rates, changing to a small positive contribution with increasing flow rate. Results obtained by Kaufman (33) from shock tunnel experiments in laminar flow at high Mach numbers ($7.2 < M_1 < 15.8$) and low Reynolds numbers ($4.5 \times 10^4 \leq Re_L < 5 \times 10^5$) showed rather large amplification factors at low values of P_{0_j}/P_1. The larger portion of the interaction force was always associated with the downstream region. Many of the pressure distributions showed significant overpressures at the pressure tap location nearest the aft end of the plate, thus raising the possibility that the measured interaction force would have been larger had the tests been conducted with a longer plate, or that the interaction may have been influenced by the sting or by a high pressure region underneath the plate. End plates were used during a few of these experiments.

Jet gases other than air or nitrogen have been used in several sets of experiments. Data obtained by Barnes, et al, (6) allow a comparison of nitrogen, argon, and helium jets with $M_\infty = 8$ and a laminar boundary layer. The variation in total amplification factor, including both the upstream and downstream regions, was within the data scatter, when comparisons were made between data obtained with the same nozzle at the same value of P_{0_j}/P_1. Data with helium and nitrogen jets in turbulent flow at $M_1 = 2.61$ and 3.50 were reported by Spaid and Zukoski (3). The amplification factors for the upstream region were 6 to 7 percent higher with helium as injectant than with nitrogen. Pressure levels downstream were higher for helium jets than for nitrogen jets, but the downstream forces were not determined. Strike (32) has presented data obtained in laminar flow without end plates at $M_1 = 6.8$, with jets of nitrogen, helium, argon, and carbon dioxide. Data were taken by direct measurement of forces. No effect of jet gas properties upon the amplification factor was found.

Thayer and Corlett (10, 36) presented results of experiments with $M_1 = 2.5$ in turbulent flow. In these experiments both freestream and jet stagnation temperatures were varied. Nitrogen, helium, and hydrogen were used as the jet gas. Amplification factors were determined in the upstream region by

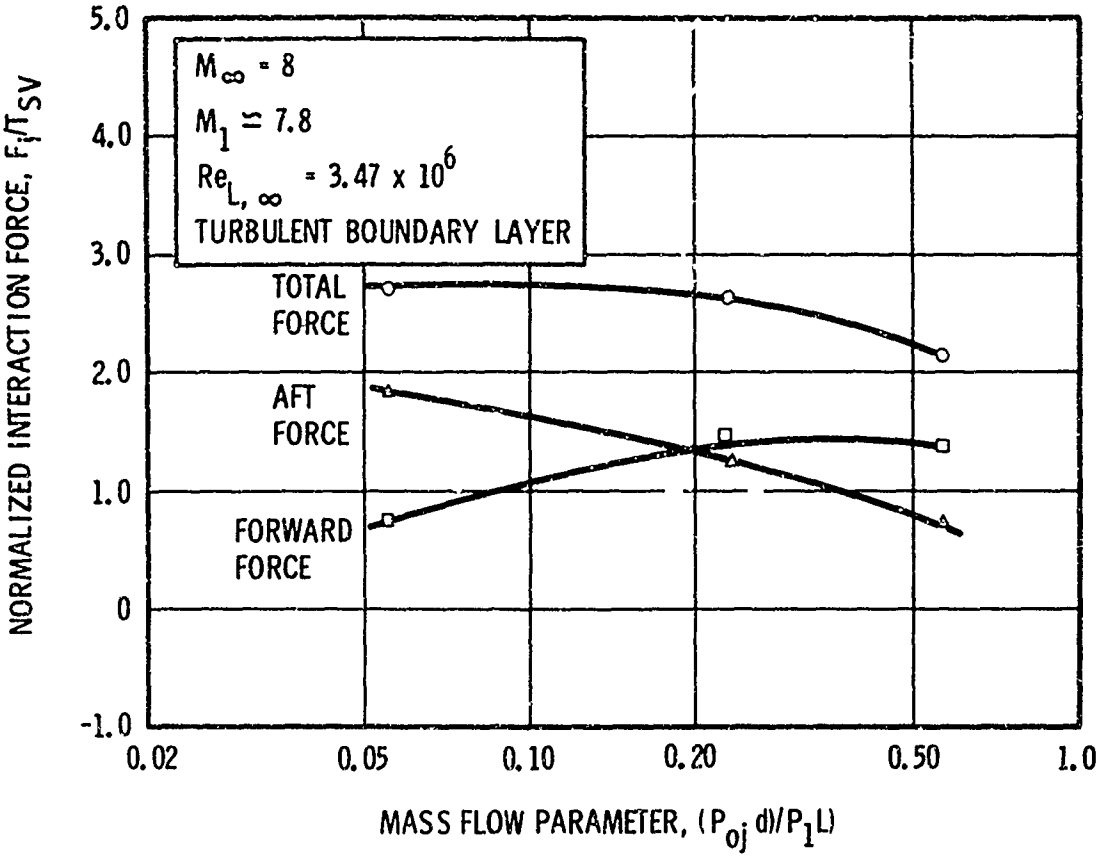

Figure 22. Contributions of Upstream and Downstream Region to Interaction Force in Hypersonic Flow, Data from Reference 6

integration of static pressure distributions. These data have been correlated by the parameter $(T_{oj}/\mathcal{M}_j)/(T_1/\mathcal{M}_1)$ as shown in Figure 23. The amplification factor increases with increasing values of this parameter, for $(T_{oj}/\mathcal{M}_j)/(T_1/\mathcal{M}_1) \leq 7$. These results do not contradict those of References 3, 6, and 32, if it is assumed that the relevant reference temperature for the external flow is the stagnation temperature, rather than T_1. Data obtained at other values of M_1 which are directly comparable to those of Figure 23 will be needed in order to evaluate such an assumption. Shadowgraph photographs were obtained for some of the test conditions, which indicated that the shock structure in the jet was essentially independent of temperature and molecular weight.

2.4 Analyses and Correlation Techniques

Approaches to analysis of the jet interaction flowfield can be separated into two categories. One category includes those which are intended to provide direct numerical or analytical solutions to equations of motion. In the second category are flowfield models which are primarily intended to provide parameters for correlation of experimental data. The latter category can be further separated into analyses which allow mixing between the jet and mainstream and those which assume that a slip line divides the two flows.

2.4.1 Applications of Numerical Methods

Because of the complexity of the jet interaction flowfield, solutions of the equations of motion incorporating realistic assumptions have not been obtained. Most theoretical studies have used either a high degree of empiricism or gross simplifications, or both, in order to obtain solutions. Two attempts to achieve solutions to equations which closely approximate the governing equations are known.

Zakkay (41) applied the method of numerical solution of the inviscid, time-dependent equations of motion to the problems of flow over a forward-facing step and flow of an underexpanded jet into still air, apparently with the ultimate objective of combining the two flowfields into a jet interaction solution. Such a combination would involve an analogy by which the forward-facing step would replace the blockage or displacement effect which the jet imposes on the mainstream. The separation point was specified a priori in the forward-facing step flowfield computations. Although the results obtained for the two separate flowfields were promising, computations for the more difficult jet interaction case have not been published.

Lee and Barfield (42) have carried out computations for a two-dimensional inviscid model of the flowfield, in which a blunt-body calculation is matched to a method-of-characteristics calculation for a normal, slightly supersonic jet. The method of characteristics provides the shape of the jet boundary, which is modeled as a solid obstacle in the inviscid external flow. Since separation is excluded, the model is not realistic, but it is possible that trends with variations in jet flow parameters may be correctly predicted by such a model.

Several investigators, including Broadwell (43) and Dahm (44), have used blast wave theory to represent the external flow. This theory is inviscid, and is limited to strong bow shocks (large M_1). The solutions are functions of the energy addition which created the blast wave. When the blast wave analogy is applied to hypersonic flow past blunt-nosed solid bodies, the energy addition is identified with

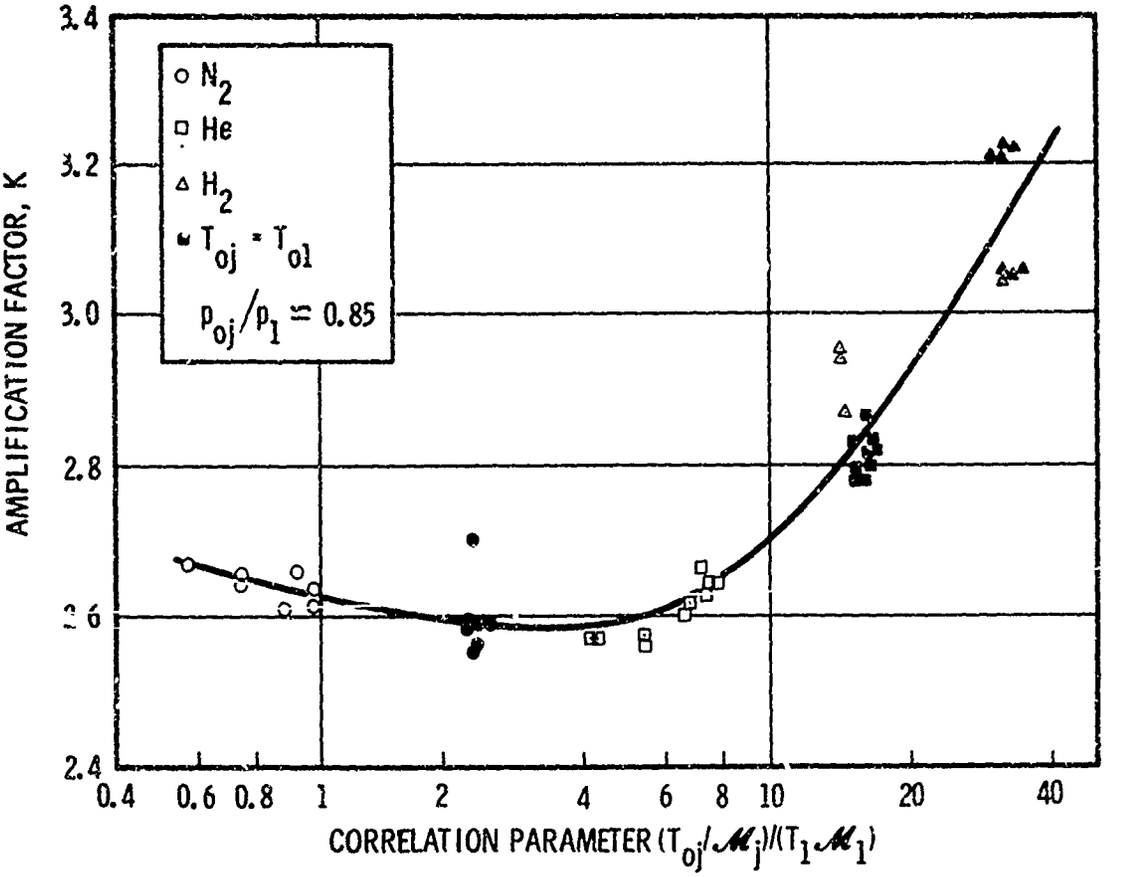

Figure 23. Dependence of the Amplification Factor on Molecular Weight and Temperature, Reference 10

the drag of the body. Such solutions are not valid near the nose. The use of blast wave theory in a jet interaction analysis requires that the jet be represented as an equivalent energy addition. Discussions of jet interaction theories employing blast wave theory are provided by Cassel, et al (45). Strike (32) has proposed a jet interaction analysis employing blast wave theory in which an estimate of the effect of boundary-layer separation is added. All of these investigators applied blast wave theory almost exclusively to three-dimensional flows. It is probably not useful as a representation of the observed two-dimensional flowfield illustrated in Figures 1 and 2 because: (a) it is inviscid; (b) it fails near the nose of a blunt body, so that it cannot give a good representation of the flow upstream of the jet near the wall; and (c) the analogy between the jet and an equivalent energy addition is not a good representation of the physical phenomena in that portion of the actual flow which is dominated by the jet, i.e., the flow near the wall downstream of the nozzle exit, since explicit description of the jet flow is not included.

Most other analyses of the two-dimensional flowfield (3, 6, 25, 28, 31, 32, 45 to 51) are based on a more detailed representation of the physical phenomena including the separated boundary layer upstream of the jet. However, most of these models ignore mixing between the two streams during the jet turning process, or rely upon an assumption comparable to ignoring mixing, such as the assumption that the height of a shock in the jet is proportional to the jet penetration height. Since mixing is not accounted for in these analyses, it is possible to discuss separately the models which are assumed to represent the external flow and the jet flow.

2.4.2 Analyses of the External Flow

For many purposes, the flow upstream of a jet can be regarded as being identical to the flow upstream of an equivalent forward-facing step, i.e., a step at the jet nozzle location which would produce the same value of X_s. Data from many investigations indicate that this analogy can be used to predict details of the flowfield if the region immediately upstream of the jet or step is excluded, whenever sufficient data from experiments with steps are available. If the height of an equivalent step can be found, correlations such as those given in Figures 8 and 9 can be used to represent the upstream static pressure distribution. Additional information pertaining to step-induced separation can be found in References 13, 23, and 52.

The early model due to Vinson, et al, (48) assumed isentropic compression of the external flow by a ramp formed by the separated region. This approach is probably quite realistic for laminar separation, where the separation angles are small, but it is known to be significantly in error for the more abrupt separation angles characteristic of turbulent flow. Vinson (48) correlated data from jet-induced and step-induced turbulent boundary-layer separation. His correlations depend upon the ratio h/δ_1. The predicted dependence of various flowfield parameters upon h/δ_1 is particularly strong when $h/\delta_1 < 1$. Werle (12) compared predictions of Vinson's model with data from several investigations and found that the predicted effects of h/δ_1 tend to be too strong.

Strike, et al, (15) proposed a model for the external flow in which the interaction force was computed in two parts. One part resulted from the pressure rise computed from an empirical equation for separation plateau pressure and the other resulted from the pressure rise associated with a normal shock in the external flow. The size of each region was assumed to be proportional to the calculated jet

penetration height. The pressure levels measured on a wall upstream of a jet in either two- or three-dimensional flow are always substantially lower than those which are predicted by the normal shock equations, so that this model is not believed to be realistic. It has been superseded by the more recent work of Strike (32).

Young and Barfield (50) have presented an analysis of the external flow in which Mager's free, shock-separated turbulent boundary layer model (53) and the method of Reshotko and Tucker were used to determine property changes across the separation region. The mixing theory of Korst (54) was then used to follow the development of the shear layer up to the region in the immediate vicinity of the jet.

An important aspect of the external flow model concerns the manner in which the external flow is matched to the jet flow, since this matching process is important in determining the influence of M_1 on the analytical predictions. In most models of the flow, a control volume representing jet flow and mixing region is employed.

Spaid and Zukoski (3) analyzed a control volume in the region immediately upstream of the jet, for the purpose of obtaining an estimate of P_f, which is an average value of pressure at the upstream interface between the jet and the external flow. The result is

$$\frac{P_f}{P_2} = 1 + 0.124 \frac{\gamma_1 M_2^2}{1 + \frac{\gamma_1 - 1}{2} M_2^2} = 1 + \beta \tag{12}$$

where M_2 is the Mach number at the edge of the shear layer in Region 2, which was estimated from the empirical expression (23) $M_2 = 3/4\ M_1$, and P_2/P_1 was obtained from Equation (1). The quantity β is proportional to the momentum of the recirculating flow. The estimate of P_f/P_2 given by Equation (12) decreases slowly from 1.19 to 1.07 as M_1 increases from 2 to 12 for $\gamma_1 = 1.4$. Werle (12) has shown that this estimate is in reasonable agreement with data from the drag of forward-facing steps.

In the model proposed by Barnes, et al, (6) for turbulent flow, the drag coefficient of the effective obstruction presented by the jet to the external flow, C_X, was assumed to be of the form

$$C_X = a \frac{P_2 - P_1}{q_1} + b \frac{P_{o_{d_2}} - P_1}{q_1} \tag{13}$$

where $P_{o_{d_2}}$ is the stagnation pressure of the dividing streamline of the shear layer upstream of the jet. The value of $P_{o_{d_2}}$ was computed from the jet-mixing theory of Korst (54), as extended by Tang, et al, (29). It depends primarily on M_1 and on the properties of the boundary layer upstream of separation. Parametric calculations from this analysis show that the predicted trends of upstream amplification factor with $(P_{o_j} d)/P_1 L$) actually arise from the influence of h/δ_1 on $P_{o_{d_2}}$. Calculated values of K are independent of both Re_L and P_{o_j}/P_1, but decrease slightly with $(P_{o_j} d)/(P_1 L)$ at fixed Re_L. These calculations are therefore in agreement with observations that the upstream amplification factor is independent of P_{o_j}/P_1 when $P_{o_j} d$ and L are constant, and that it decreases slightly with increasing P_{o_j}/P_1 when d and L are constant.

Many other investigators have either assumed that the average pressure acting on the upstream boundary of the jet is proportional to P_2, or have made approximately equivalent assumptions. In most of the latter, the effective back pressure which determines the jet shock location is related to P_2. This class of assumptions gives results which are in reasonable agreement with experiment, and is consistent with the flow geometry as determined from Schlieren or shadowgraph photographs.

2.4.3 Analyses of the Jet Flow

In most analytical models of jet interaction, it has been assumed that mixing between the two streams does not play an important role during the jet turning process. These analyses tend to group into three categories in terms of how the jet flow is modeled:

1. Isentropic expansion models
2. Nonisentropic models, utilizing a control volume near the jet nozzle exit.
3. Jet-shock models.

The simplest version of Category 1 is the assumption that the jet expands isentropically from P_{o_j} to P_1 and is attached to the wall downstream, so that h/d is determined by the governing equation for one-dimensional isentropic flow with area change (12, 38). This assumption leads to the predictions that, (a) h/d is independent of the external flow dynamic pressure for fixed P_{o_j}/P_1, and, (b) that the influence of γ_j is very strong at large P_{o_j}/P_1. Both of these predictions are at odds with experimental observation. A more sophisticated model employing the isentropic flow assumption has been proposed by Maurer (31). In this model, the pressure to which the flow expands is determined as part of the solution. Maurer's analysis is aimed primarily at the flowfield associated with a jet from a finite-span slot. Good agreement is shown between predictions of this analysis and results of experiments at low supersonic Mach numbers (31).

Analyses of the second category do not use the assumption of isentropic jet flow. Instead, conservation equations are applied to a control volume in the vicinity of the jet nozzle exit, and a sufficient number of additional assumptions are made to enable a solution to be obtained. Since the nature of these assumptions is limited only by the imagination of the investigator, a considerable variety may be found in the literature.

The third category of jet models characterize the jet by its shock structure. Shadowgraph or Schlieren photographs obtained from experiments with underexpanded sonic jets usually show a shock structure in the jet which is similar to that exhibited by an underexpanded jet exhausting into a quiescent medium. One of these shocks has been observed to be roughly parallel to the jet nozzle exit, and similar in appearance to the Mach disk of an axisymmetric underexpanded jet. These observations have prompted several investigators to use information obtained from studies of jets exhausting into still air in the development of models for the jet interaction flowfield (17, 25, 28, 48). In these models, the jet is characterized by the position and strength of the strong shock analogous to the Mach disk.

Amick (49) has proposed a novel approach involving isentropic expansion in which a circle-arc jet trajectory is computed by the method of characteristics. Amick's circle-arc jet analysis assumes that the nozzle is constructed to produce a jet having a radius of curvature at the nozzle exit which provides it dynamic equilibrium with the pressure difference imposed upon it by the external flow. Experiments were conducted with an appropriately designed nozzle to test the validity of this theory. These experiments were two-dimensional and were conducted at relatively low Reynolds number, $10^5 \leq Re_L < 7.5 \times 10^5$ in hypersonic flow, $7.6 < M_1 < 7.9$. A nozzle designed to produce a supersonic circle-arc jet under the range of conditions of the test was installed near the trailing edge of a flat plate model. The nozzle was inclined 45 degrees upstream of the normal to the plate surface. Wedge end plates were used, with the angle chosen so that the upper surface of the wedge approximately matched the surface of the shear layer when the jet was operating. Tests were conducted in which $X_s < L$, referred to as the weak jet regime, and also in which the flow was separated to the leading edge of the plate, described as the strong jet regime. Interaction force data were obtained directly from force measurements. A comparison between theory and experiment is shown in Figure 24. The quantity λ is the angle of intersection between the shear layer and the jet, which is used in computing results from the theory. It is treated here as a free parameter. Predictions of the theory are seen to be rather insensitive to variation in λ, at least in the strong jet regime. The amplification factor is defined as the total normal force increment due to the jet, normalized by the vacuum thrust of a sonic jet having the same reservoir conditions as the actual jet. (In the original reference, a slightly different definition of amplification factor was used.) Good agreement is shown between theory and experiment. Very large amplification factors are achieved in the weak jet regime, which decrease with increasing jet thrust when the flow is separated to the plate leading edge. These results are in marked contrast to those obtained in turbulent flow with normal, sonic jets shown in Figure 18.

Vinson (48) performed two-dimensional calculations for a jet exhausting into a low-pressure environment, using the method of characteristics. The terminal shock was assumed to occur when the pressure downstream of a normal shock at the jet centerline would cause the downstream pressure to match the ambient pressure. The computed terminal shock locations were independent of γ_j when presented in the coordinates, h_s/d_e versus P_e/P_b, where d_e and P_e are evaluated at the jet exit, and P_b is

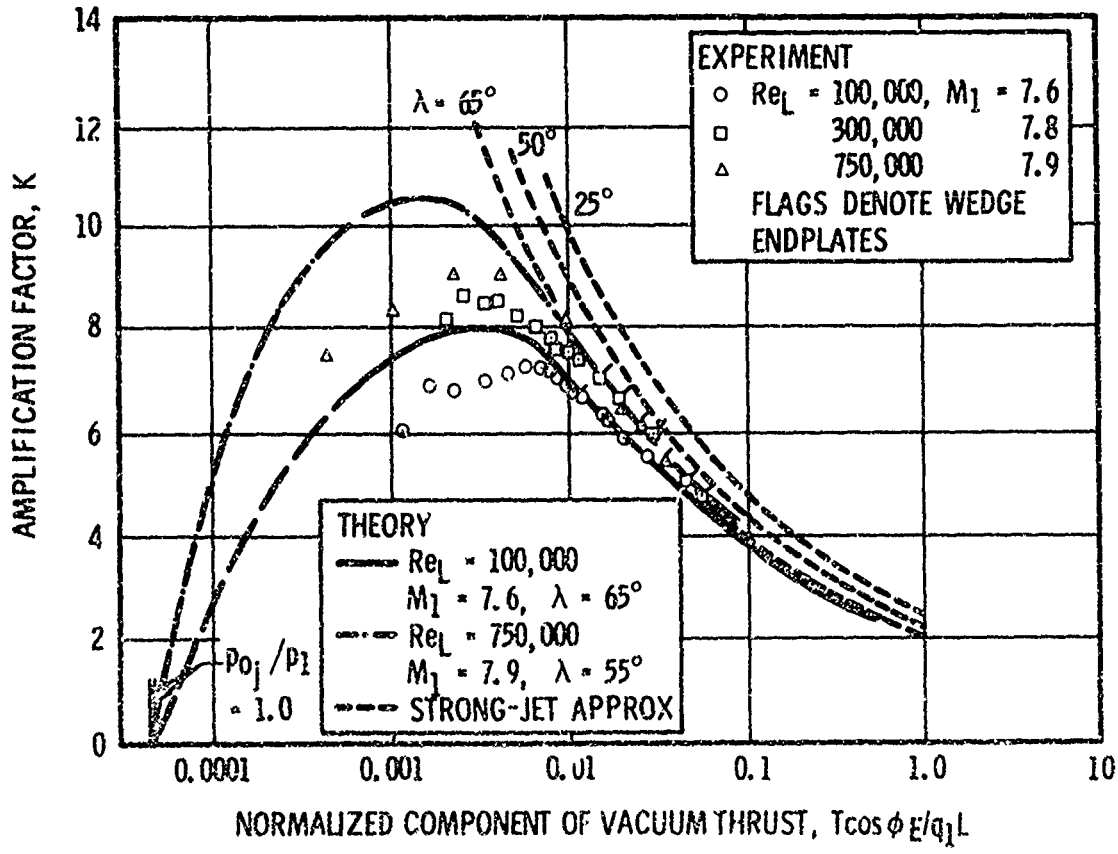

Figure 24. Comparison of Experiment and Theory for Circle-Arc Jet Flap, Reference 49

the back pressure or pressure of the surroundings. Sterrett and Barber (17) have also performed calculations for two-dimensional underexpanded jets by the method of characteristics. They included cases in which the pressures were not the same on both sides of the jet. Both sets of calculations have been compared with experimental data for two-dimensional sonic jets by Werle, et al (39). Results of both sets of calculations were shown to be essentially identical and predicted values of h_s/d_e which were slightly larger than the measured values. This result implies that an additional adjustment in the static pressure takes place downstream of the normal shock. Data for two-dimensional sonic jets and axisymmetric sonic and supersonic jetr were correlated by the empirical equation

$$\frac{h_s}{d_e} = 0.7 \left(\frac{\gamma_j M_e P_e}{P_b} \right)^{\frac{1}{j+1}} \tag{14}$$

where j is 0 in two-dimensional flow and 1 in axisymmetric flow.

Werle, et al, used Equation (14) as part of a two-dimensional jet interaction analysis (25). It was shown that this equation could be used to predict the effective forward facing step height, h, produced by a jet if P_2' were chosen as the effective back pressure, $\bar{P}_b$, and if $h = 1.36\, h_s$. In the investigation by Werle, et al (39), this method of estimating effective step height was then combined with the correlation of Equation (1), and the separation angles implied by that relationship to give a simple expression for upstream amplification factor, K.

$$K = 1 + \left(\frac{1.47\, M_1}{1 + 0.65\, M_1} \right) \left(\frac{\gamma_j M_e^2}{1 + \gamma_j M_e^2} \right) \frac{h}{h_s} \tag{15}$$

Equation (15) predicts a trend of increasing K with increasing M_e which is not in agreement with experiment. This comparison is described below in Section 2.4.4.

Driftmyer (7) conducted flow-visualization studies of two-dimensional jets exhausting into still air for M_e = 1.0, 2.89, and 2.99. The shock heights associated with the sonic jets agreed with previous results. Shock patterns obtained with the supersonic jets were qualitatively different from those produced by sonic jets as illustrated in Figure 25. Calculations by the method of characteristics were carried out for supersonic exit Mach numbers and the results showed the same behavior. The value of h_s was defined for the supersonic jets as shown in Figure 25. Data and calculations for axisymmetric and two-dimensional, sonic and supersonic jets were shown to correlate within ±20 percent with the expression

$$\frac{h_s}{d_e} = \left[\left(\frac{1}{j+1} \right) \left(\frac{\gamma_j M_e^2 P_e}{P_b} \right) \right]^{\frac{1}{j+1}} \left(\gamma_j M_e \right)^{j-1} \tag{16}$$

If Equation (16) is used in place of Equation (14) to derive an expression for upstream amplification factor analogous to Equation (15), a trend of decreasing K with increasing M_e is predicted. This result is not in agreement with the experimental results shown in Figure 20.

Direct observations by Hefner and Sterrett (55) of jet-shock locations for $M_1 = 6$ show $h_s/d \sim (P_{o_j}/P_1)^{0.75}$, implying a variation in effective back pressure with P_{o_j}/P_1. This behavior is consistent with the commonly observed trend of decreasing amplification factor with increasing jet mass flow rate mentioned earlier. It is possible that an analysis utilizing a jet-shock model for the jet flow could show such a trend if it were coupled with a relatively sophisticated model of the external flow, such as that produced by Barnes, et al (6).

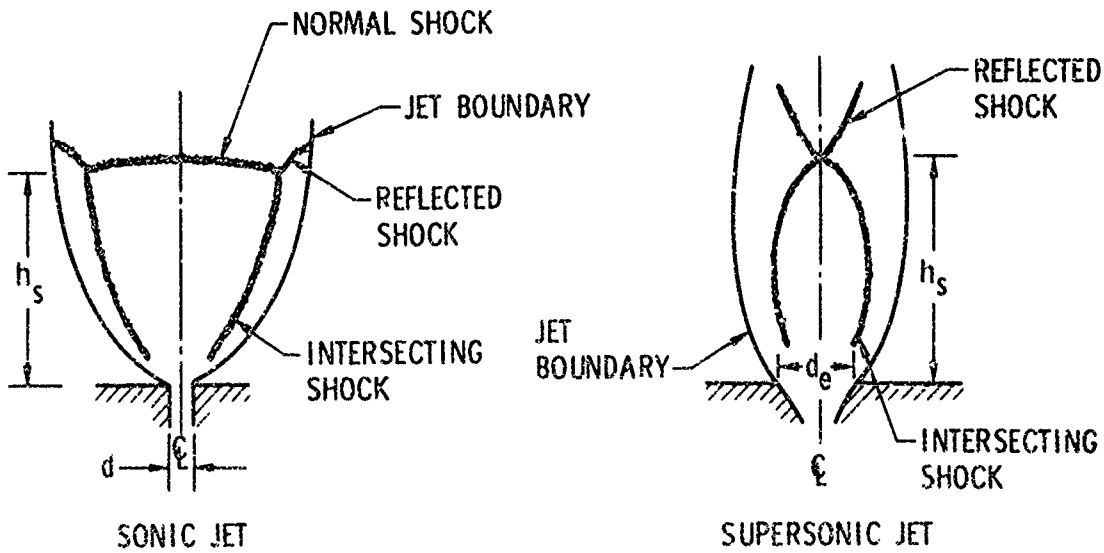

Figure 25 Plume Structures of Two Dimensional, Sonic and Supersonic Jets Exhausting into Still Air, Reference 7

Although the jet shock models are about as successful as the better models of the other two categories in predicting trends exhibited by a range of jet interaction data, they suffer from some deficiencies. First, they are limited to underexpanded jets. Second, the data of Reference 10 indicates that the observed effects of temperature and molecular weight, shown in Figure 23, do not correlate with jet shock height for large values of $(T_{o_j}\mathscr{M}_1/T_{o_1}\mathscr{M}_j)$. This effect will be discussed in the following section.

None of the proposed theories of the preceding three categories give an explicit dependence of h/d upon temperature or molecular weight. Therefore, they are unable to account for Thayer's results (10), which show an explicit dependence upon τ. Except for an empirical correlation of Kaufman and Koch (28), which gives $h/d \sim (P_{o_j}/P_1)^{0.85}$ and the models which utilize the one-dimensional isentropic area-ratio relation, all of the theories predict $h/d \sim (P_{o_j}/P_1)^{0.99}$ (48), at least when ReL_s is constant. The predicted influence of γ_j is generally weak, except for the isentropic flow model.

2.4.4 Influence of Mixing Between the Two Streams

Some major elements of the early direct analysis methods (43, 44) which employed blast wave analogies are useful beyond the limitations of blast wave theory. The blast wave analogy was only employed to provide numerical solutions for the effect of the jet on the mainstream. The central aspects of the analyses by Broadwell (43) and Dahm (44) involved the determination of the volume addition to the mainstream (or displacement of the mainstream) due to energy release from the jet. These analyses provided methods for computing a characteristic dimension of the flowfield. Equations derived to calculate this dimension provide similarity parameters for correlating the effects of variations in jet and mainstream properties on the interaction flowfield.

Broadwell computed the drag of an equivalent obstruction by assuming that the injected flow is accelerated to the velocity of the undisturbed external flow. He also assumed that the effect of the volume added by the jet can be accounted for by adding sufficient heat to a part of the external flow to produce the same volume change which would be produced by the mass addition. Dahm's analysis differs in detail from that of Broadwell, but the final result is nearly the same. If h is the height of the equivalent obstacle, then values of h computed by either method are proportional to the jet mass flow rate. Broadwell's analysis leads to equivalent obstacle height scaling in the form

$$\frac{h}{h_{\tau=1}} = \frac{1}{\tau^{1/2}}\left(\frac{1+a\tau}{1+a}\right) \tag{17}$$

where

$$\tau = \frac{T_{o_j}}{\mathscr{M}_j}\frac{\mathscr{M}_1}{T_{o_1}}$$

T_{o_j} = jet stagnation temperature

T_{o_1} = external flow stagnation temperature

$\mathscr{M}_j$ = jet gas molecular weight

$\mathscr{M}_1$ = external flow molecular weight

$$a = \frac{1+\left(\frac{\gamma_1-1}{2}\right)M_1^2}{\left(\gamma_1-1\right)M_1^2}$$

and the corresponding expression from Dahm's analysis is

$$\frac{h}{h_{\tau=1}} = \frac{1}{\tau^{1/2}}\left(\frac{1/2+a\tau+g}{1/2+a+g}\right) \tag{18}$$

where

$$g = \frac{1}{\gamma_1\left(\gamma_1-1\right)M_1^2}$$

In each case, the factor $1/\tau^{1/2}$ arises from the assumption that the jet flow is accelerated to the external flow velocity, and the term in brackets comes from the influence of volume or mass addition by the jet. In Figure 26, predictions from Equations (17) and (18) are compared with the data reported by Thayer and Corlett (36) and by Strike (32).

In Figure 26, values of $h/h_{\tau=1}$ were computed from the experimental data using the assumption that the interaction force produced by the jet is proportional to h, for a fixed external flow. Some scatter was present in the data, which is not indicated on the figure. The data of Strike were taken at $M_1 = 6.8$ with a flat plate model having a finite span transverse slot. The boundary layer upstream of the interaction region was laminar, and variations in τ were obtained by using different injectant gases, thus changing $\mathscr{M}_j$ only. Interaction forces were obtained from force measurements. The data of Thayer and Corlett are in qualitative agreement with the theories, although the experimental magnitude of variation

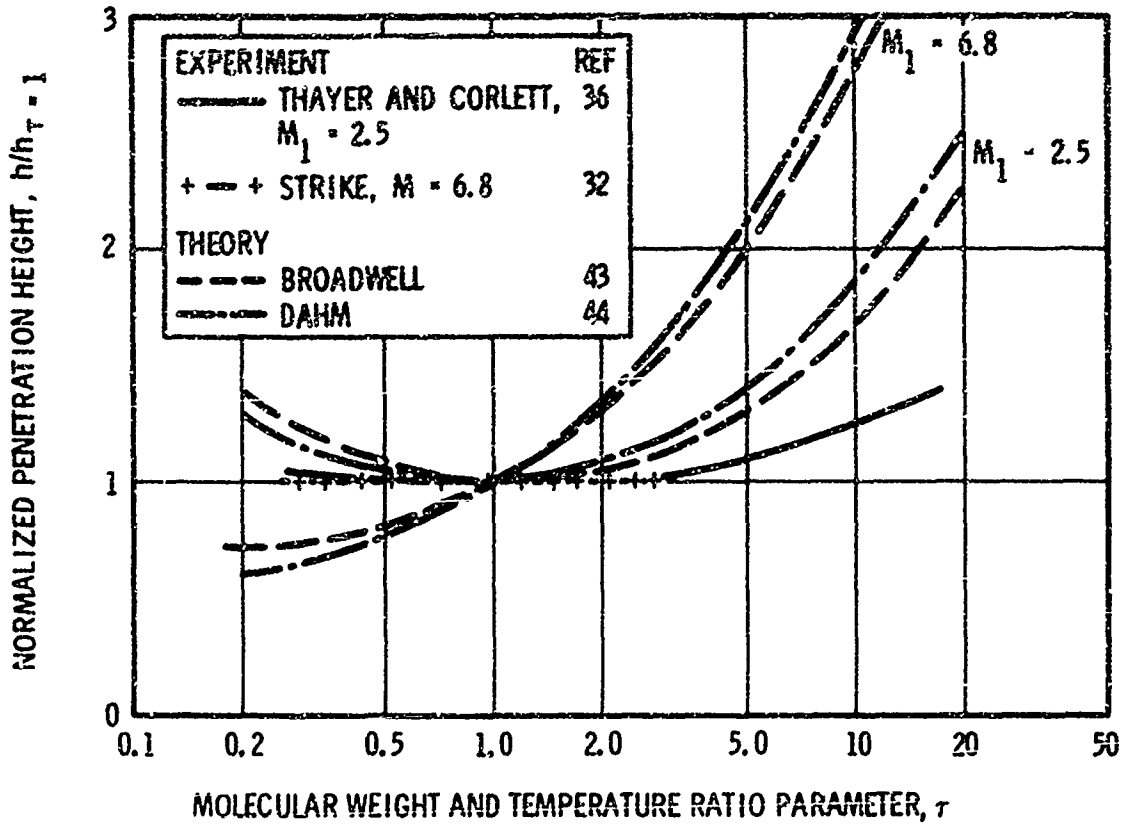

Figure 28. Influence of Jet Gas Temperature and Molecular Weight

in $h/h_{\tau=1}$ is much smaller than the theoretical prediction. On the other hand, the data of Strike at $M_1 = 6.8$ are independent of τ, in contrast to substantial variation predicted by the theories at this Mach number. Most analyses predict no explicit influence of τ on jet interaction performance for all values of M_1, and are thus in good agreement with Strike's data (32) concerning the influence of stagnation temperature and molecular weight. On the other hand, the flowfield models proposed by Broadwell and Dahm are the only ones which show the qualitative behavior of the data of Thayer and Corlett which cover a wider range of τ than is included in any other set of data. It is possible that some combination of the assumptions used by Broadwell or Dahm with flowfield models proposed by others would predict the observed dependence of jet interaction performance on M_1 and τ.

In summary, a fairly wide range of jet flow turning models gives essentially the same predictions, within a constant factor, of the influences of temperature, molecular weight, and pressure ratio on the jet interaction flowfield. The discussion presented in Reference 56 illustrates this point in more detail (see Figure 3 of that paper). Reference 56 is concerned with jets from circular holes. The jet turning models examined in that paper are based upon one-dimensional gasdynamics, so that the results can be applied to two-dimensional flow after relatively minor and obvious modifications.

2.4.5 Influence of Mach Number on Amplification Factor

The predicted and measured influence of M_1 on jet interaction performance in two-dimensional flow is summarized in Figure 27. The ordinate is the amplification factor, K, defined here as the jet thrust plus the interaction force generated upstream of the jet, normalized by the vacuum thrust of a sonic jet. Figure 27 is restricted to turbulent boundary layers upstream of the interaction, and normal, sonic jets with $\gamma_j = 1.4$. Not all of the theories predict a single curve in these coordinates. Computations were made using values of other variables such as P_{o_j}/P_1, $(P_{o_j}d)/(P_1L)$, h/d, and Re_o which are representative of the available experimental data. The trends with M_1 predicted by the theories are, for the most part, not sensitive to variations in these other variables. One exception is the analysis of Lee and Barfield (42) which is sensitive to the quantity

$$M_1^2 \left(1 + \frac{\gamma - 1}{2} M_1^2\right)^{-\frac{\gamma}{\gamma-1}} \frac{P_{o_j} d}{P_1 L}$$

when this term is less than approximately 0.06. A limited Mach number range is shown in Figure 27 for some of the analyses. This is a result of limited information available in the original references, or statements by the respective authors concerning the applicable Mach number range.

The data on amplification factor appear to indicate a trend of decreasing K with increasing M_1. This is at least partially misleading, since more detailed comparisons tend to show significant shifts in K between data obtained from different test setups and facilities at the same Mach number. It is not possible to identify a "best" analysis, purely on the basis of this type of comparison. A rather wide range of Mach number trends are shown by the analysis, in contrast to the greater degree of unanimity concerning the influence of jet fluid properties. The differences in Mach number predictions arise from the details of the differences between the theories. A very lengthy discussion would be necessary to explain these

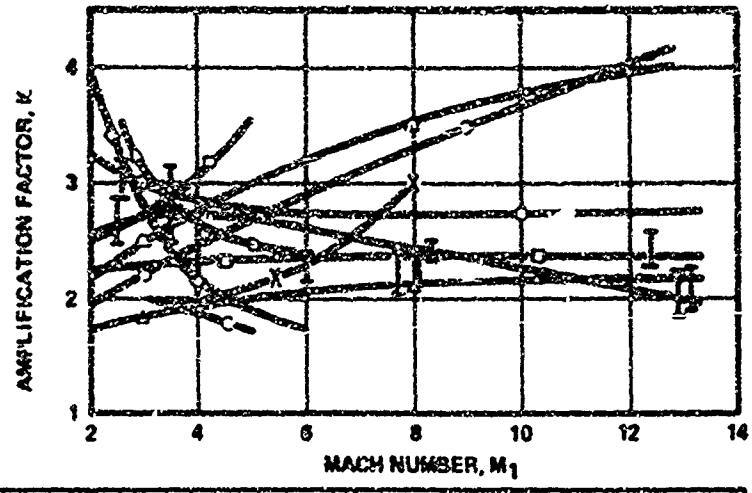

TURBULENT BOUNDARY LAYER
TWO-DIMENSIONAL FLOW, NORMAL, SONIC JET, $\gamma_j = 1.4$

INVESTIGATORS	REF NO.	COMMENTS
○ SPAID AND ZUKOSKI	3	
△ WERLE, ET AL.	25	
□ BARNES, ET AL.	6	$P_{oj}d/P_1L = 0.1$
▽ VINSON	48	$h/\delta_1 = 2$, $Re_\delta = 10^5$
◇ DENNIN	47	$P_{oj}/P_1 = 100$
○ KAUFMAN AND KOCH	28	$P_{oj}/P_1 = 100$
X STRIKE	22	
○ YOUNG AND BARFIELD	50	$P_{oj}d/P_1L = 0.1$
○ LEE AND BARFIELD	42	$P_{oj}/P_1 = 197$
○ AMICK	49	CIRCLE – ARC JET FLAP WEAK JET APPROXIMATION
▷ WU AND AOYAMA	51	

I DATA, VARIOUS SOURCES, SEE FIGURE 18

Figure 27. Upstream Amplification Factor Predictions from Theoretical and Semi-Empirical Analyses

variations satisfactorily. More detailed evaluations of some of the analyses represented on Figure 27 may be found in the review by Werle (12). Those theories which predict the most strongly increasing or decreasing trend of K and M_1 are not in good agreement with the data. In contrast, because of the strongly empirical nature of most of the theories, little importance should be attached to the differences in predictions of absolute levels.

3 JETS FROM FINITE-SPAN SLOTS IN SUPERSONIC FLOW

Numerous data obtained from transverse-slot experiments conducted with and without end plates tend to indicate that the use of end plates is a necessary requirement for obtaining even a fair approximation to two-dimensional flow when the separation distance ahead of the slot is more than 10 or 20 percent of the slot length. Although end plates will introduce spurious effects themselves, the work of Lewis, Kubota, and Lees (57) shows that end plates can be used to achieve an excellent approximation to a two-dimensional flow, for the case of laminar separation induced by a wedge.

Sketches of static pressure distributions obtained in nearly two-dimensional flow and with a finite-span slot are presented in Figure 28. When end plates are removed, the length of the separated region decreases, and the interaction region extends outboard from ends of the slot. If the height of the effective obstruction produced by the jet is sufficiently small relative to the slot span, b, the plateau pressure measured along the X-axis will remain almost unchanged and the static pressure distribution upstream of the slot will be nearly independent of y for $y<b/2$. Strong lateral flows in the upstream separated region were indicated by the oil flow visualization studies of Heyser and Maurer (18), when end plates were not used. Such indications of lateral flow were negligible when end plates were installed. Similar evidence of transverse outflow from the separated region has been reported by Whitehead, et al, (59) who studied separated regions produced by forward-facing steps of finite span.

The influence of lateral flows, which apparently always develop in experiments with finite-span transverse jets, is not understood in detail. However, the following qualitative explanation has been proposed by Spaid and Zukoski (3). In a true two-dimensional flow over a step, the dividing streamline separating the primary flow from the recirculating flow is roughly a straight line extending from the separation point to the top of the step, as shown in the sketch of Figure 29. However, if fluid escapes from the recirculation region in the transverse direction, then the new reattaching streamline, which divides the flow passing over the step from that entering the recirculating zone, must now include a part of the boundary layer flow upstream of the separation point (Figure 29b).

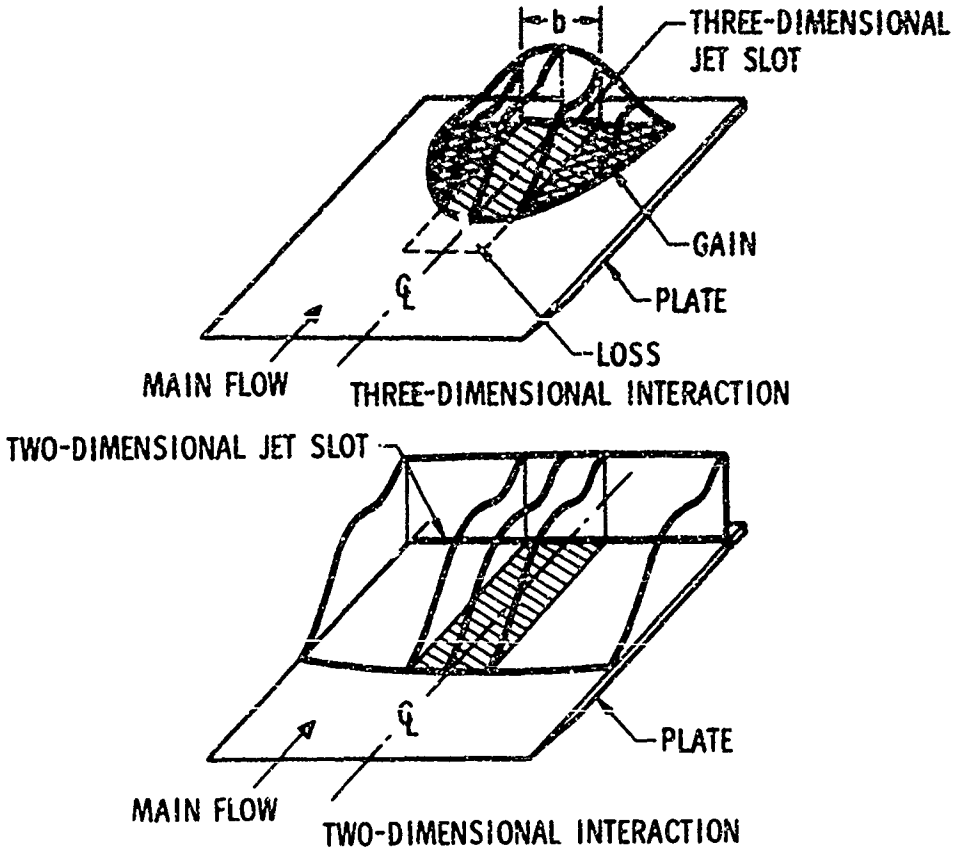

Figure 28. Sketch of the Static Pressure Distribution in the Aerodynamic Interaction Regions for Two- and Three-Dimensional Jet Slot, Reference 58

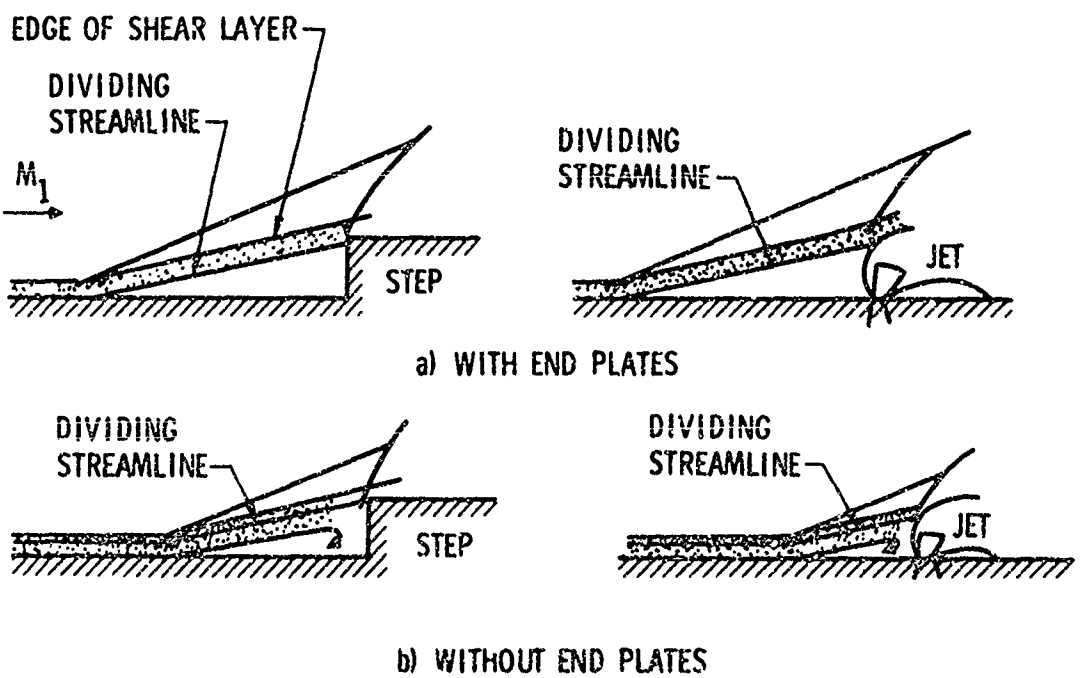

Figure 29. Effect of End Plates on Flows over Forward-Facing Steps and Gaseous Jets

The reattachment pressure will increase as the reattaching streamline moves farther out into the high-velocity region of the shear layer. This effect is shown by the data of Whitehead, et al (59). If the separation distance is not too great relative to slot span b, the turning angle made by the flow at separation remains constant despite the lateral flow. Thus, as the normal coordinate of the reattaching streamline moves away from the wall (near separation) in response to an increasing lateral flow, the separation point must move toward the step so that the reattaching streamline can intersect the top of the step.

If this picture is correct, and if it is applicable to the jet interaction problem, a lateral flow should cause a reduction in the induced force produced in the region directly upstream of the jet by a given jet flow per unit span. This reduction will be caused by two mechanisms. Since the turning angle of the flow is constant, the plateau pressure will also be constant and the only cause for a force reduction is the reduced length of the separated region. First, for the jet interaction case, the length of this separated region is reduced directly by the lateral flow for the same reason that it was in the case of a step. Second, the increase in the drag of the effective obstruction produced by the jet. This increase in drag causes a reduction in the height of the obstacle, producing a further reduction in the length of the separated zone (Figure 29b). Data reported in Reference 59, for flow over steps both with and without end plates, and similar jet interaction data (55) tend to indicate that the reduction in jet penetration may be the dominant mechanism in hypersonic flow. In summary, a lateral flow from the separated region can cause an appreciable reduction in the separation distance, even though the plateau pressure remains unchanged from the two-dimensional case. At the same time, other axial static pressure distributions measured at locations off the axial centerline, but outside of the immediate ends of the slot, agree quite well with the centerline pressure distribution.

Maurer (31) has proposed an analysis of the flowfield associated with jets from finite-span slots in which lateral flow from the separated region is taken into account explicitly. Good agreement is shown between results from Maurer's theory and his experimental data obtained at $1.57 \leq M_1 \leq 2.80$. The data consisted of forces obtained by integrating pressures upstream along the X-axis. Strike (32) proposed a modification of Maurer's analysis concerning the manner of computing the stagnation pressure of the air which flows parallel to the slot within the separated region. This modification resulted in slightly poorer agreement between the theory and Maurer's data, but substantially improved the agreement between the theory and data reported by Strike for $5.2 \leq M_1 \leq 6.8$, which were obtained by direct measurement of forces.

Spaid and Zukoski (3) have proposed h/b as a correlation parameter for flows produced by normal, sonic, finite-span slots. In their model, h is a value of jet penetration height, computed from a two-dimensional, semiempirical analysis given by

$$h = \frac{\dot{m}_j a_j^*}{\left[(1+\beta)(P_2 - P_1) + (\beta - 0.2)P_1\right]} \tag{19}$$

where

m_j = jet mass flow rate per unit

a_j^* = jet velocity where $M_j = 1$

In Equation (19), β and P_2/P_1 are obtained from Equations (12) and (1), respectively. Data from several sources are presented in Figure 30 in the form of K_3' versus h/b. The quantity K_3' is an amplification factor derived from the integral of the static pressure distribution per unit span along the upstream X-axis. Except at the low values of h/b where the data of Maurer do not correlate well, the data show a consistent variation of K_3 with h/b. Of particular interest are the data of Romeo, since b, d, and P_{0j}/P_1 are varied independently. The dotted line in Figure 30 is the mean value of Romeo's data (58) (d = 0.1, 0.05, and 0.02 inch) for an amplification factor K_3 based upon the total interaction force for the entire region upstream of the slot. These data are also correlated (±10 percent) by h/b. The difference between K_3 and K_3' shows a poor measure of the interaction force from centerline pressure integration when a plate large enough to contain the entire separated region is considered.

Static pressure data obtained from experiments with jets from circular holes, to be presented in the next section, show a large contribution to ineraction force coming from the region downstream of the jet. The shock which originates near the jet nozzle exit has a shape that is similar to that produced by a blunt body. This shock intersects the plate and produces regions of increased pressure on either side of the jet which extend downstream for a considerable distance. This mechanism produces regions of increased pressure downstream and to the sides of a jet from a finite-span slot. At low Mach numbers, the large low-pressure region immediately downstream of the slot may cancel the effect of the downstream high-pressure regions. At hypersonic Mach numbers, the net force generated downstream of a finite-span slot should always act in the direction of the jet thrust. Unpublished data obtained from the investigation of Reference 6 at $M_1 = 7.8$ show that this is indeed true. Amplification factors greater than 4 were produced on a large plate by a finite-span normal, sonic slot with a turbulent boundary layer upstream of the interaction.

Data obtained from various nozzles exhausting from a flat plate into a Mach 7.8 external flow with a laminar upstream boundary layer are shown in Figure 31 (6). In this case, most of the force was obtained from the region upstream of the jet. These data show a relatively small influence of nozzle configuration on amplification, when the entire interaction force is measured, both upstream and downstream of the nozzle. This lack of influence of nozzle configuration on the interaction force is particularly interesting, since the nozzle configuration exerts a profound influence on the static pressure distribution.

4 JETS FROM CIRCULAR NOZZLES IN SUPERSONIC FLOW

4.1 Description of the Flowfield

The interaction between an axisymmetric underexpanded jet and flow over a surface from which the jet exhausts is illustrated in Figure 32. The shadowgraph photograph and photograph of an oilflow experiment are from data reported by Street (60). The jet exhausts from a sonic orifice

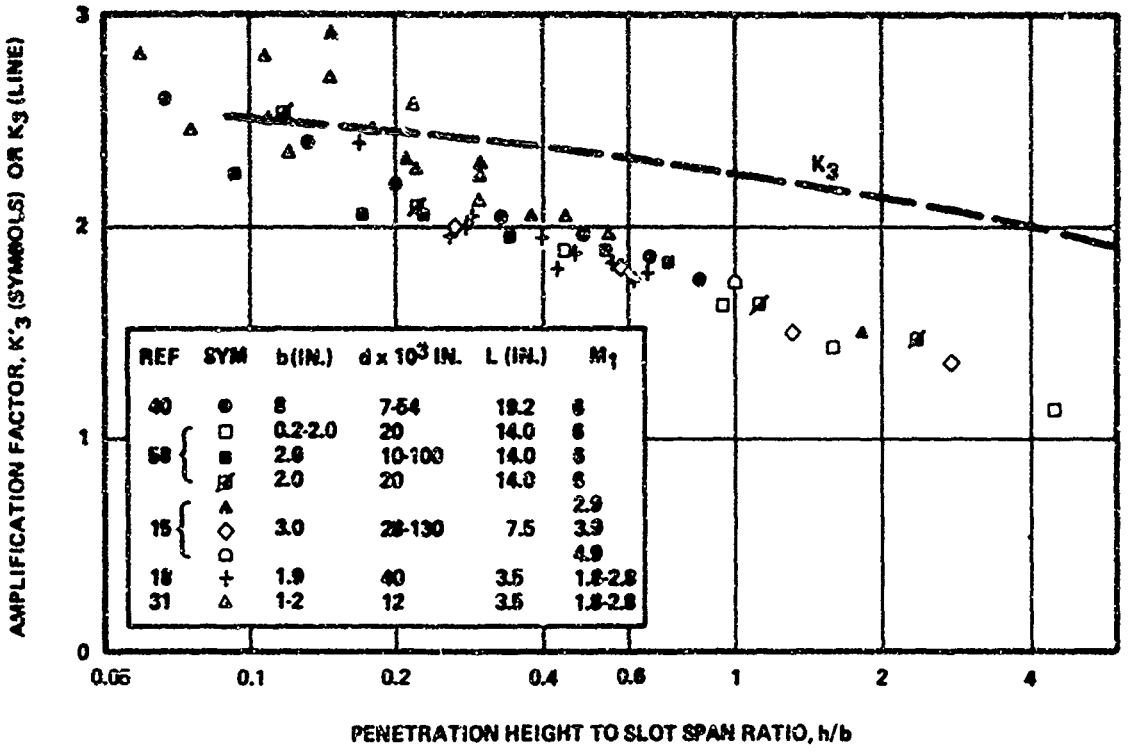

Figure 30. Dependence of K_3 and K'_3 on Ratio of Penetration Height to Slot Span, Reference 3

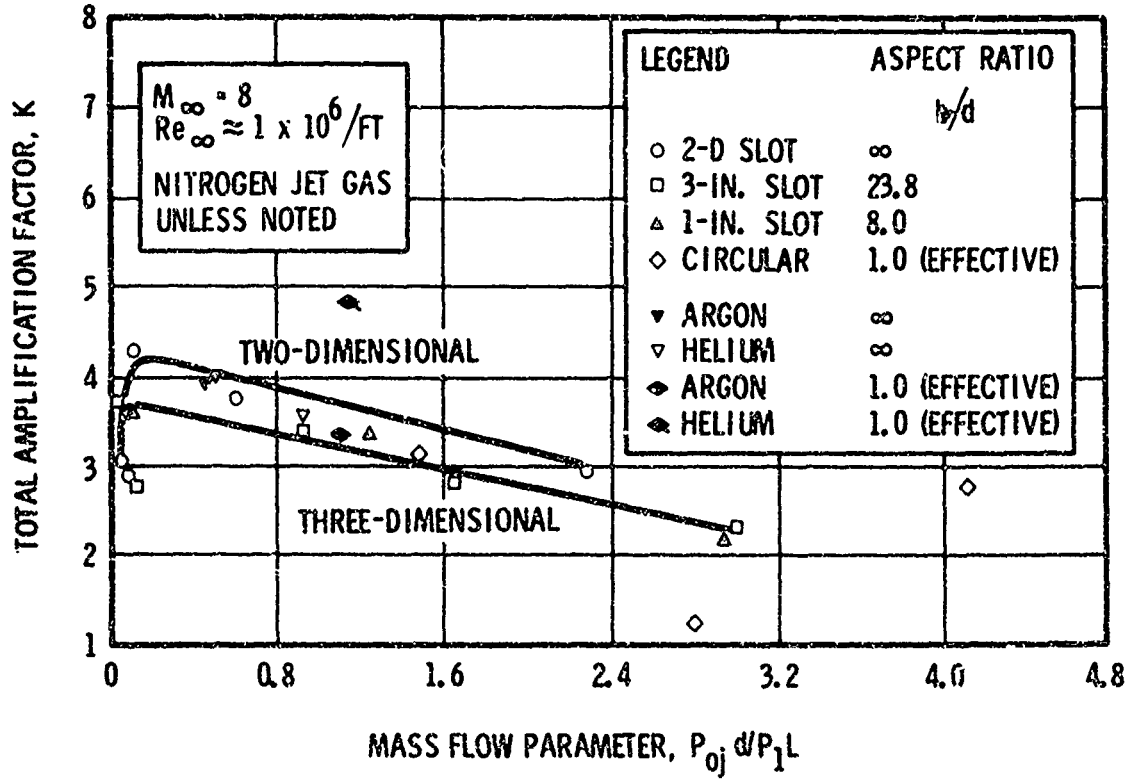

Figure 31. The Effect of Nozzle Geometry on Jet Interaction Effectiveness in Laminar Flows, Reference 6

located on the afterbody of an ogive-cylinder at zero angle of attack. The boundary layer approaching the jet is turbulent. Various interpretations of this flow have been offered (45, 61 to 63).

As shown in Figure 32a, the jet plume presents an obstacle to the external flow, which causes a strong shock and separates the boundary layer upstream of the jet. In contrast to the two-dimensional situation in which the entire external flow must go over the jet-induced obstruction, the flow can go around the three-dimensional jet. The extent of boundary-layer separation for a given jet penetration height is usually much less for a jet from a circular hole than for a two-dimensional flow. As a result of high pressures downstream of the shock and mixing between the two streams, the jet is turned in the direction of the external flow. A three-dimensional shock structure forms in the jet plume as it is turned, bounded by a three-dimensional mixing layer. Strong mixing is evident on the leading edge of the jet plume. The mixing layer surrounds the plume and reattaches

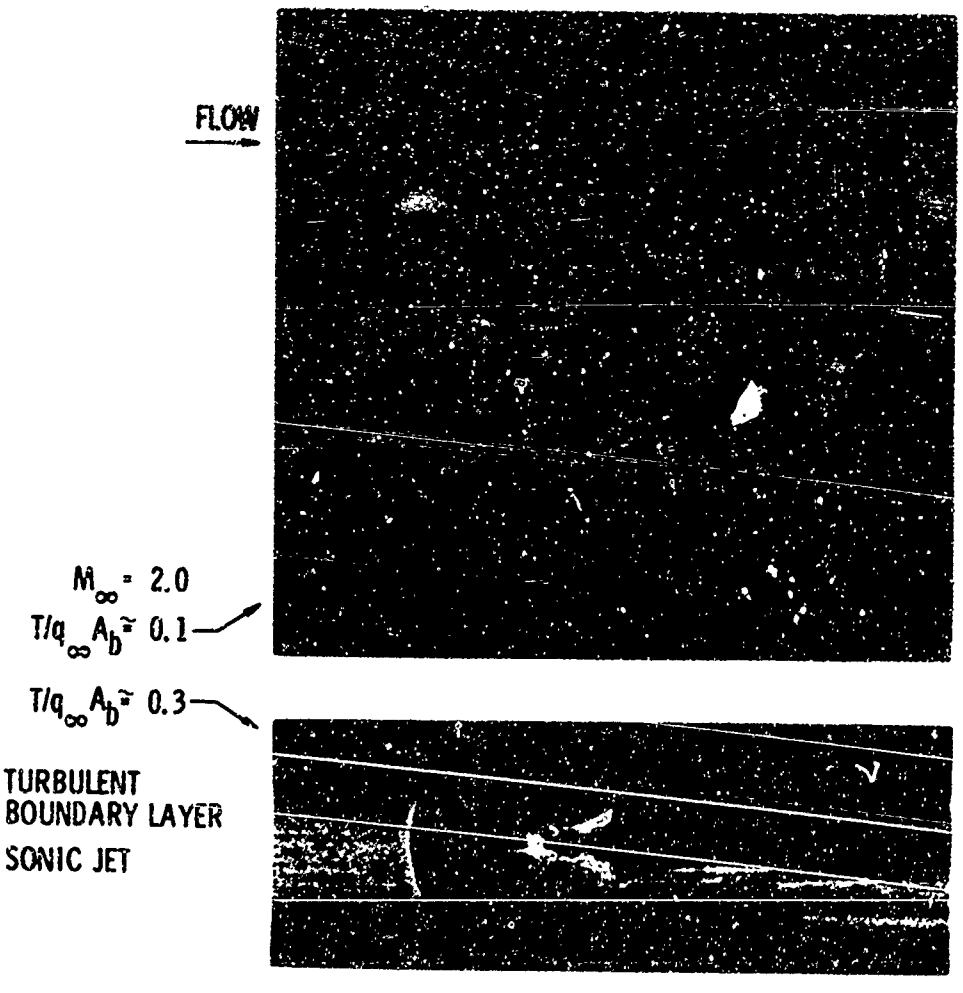

Figure 32. Flow Visualization Data, Jets from Circular Nozzles, Reference 60

to the body downstream (approximately one body diameter downstream of the jet exit in Figure 32). In the region where the mixing layer surrounding the jet reattaches to the body, a set of vortices forms in the jet wake. The patterns in the oilflow on the sides of the jet wake, shown in Figure 32b, are believed to be related to these vortices. A wide range of flow visualization data for jet-induced interference on bodies of revolution is provided by Street (60).

The shock structure in the jet near the nozzle exit has received attention from a group of investigators whose objective has been to define the jet trajectory. One feature of interest is the strong shock, often referred to as the Riemann wave or Mach disk in studies of highly underexpanded axisymmetric jets exhausting into still air. Under these conditions, the Mach disk is dish-shaped and parallel to the exit plane (64). When the jet plume is transverse to a supersonic external flow, there is evidence that the jet is partially turned before the Riemann wave is encountered. Sketches of this shock structure derived from Schlieren photographs of underexpanded jets exhausting into still air and a supersonic external flow are shown in Figure 33. Measurements of jet shock locations are reported by Orth and Funk (65), Schetz, et al (66, 67), and Billig, et al (56). Using the description of Reference 56, the Mach disk in Figure 32a is found skewed approximately 45 degrees from the horizontal and centered approximately one model radius aft of and above the jet exit.

4.2 Results of Circular Jet Experiments

Some of the parameters used in presenting data in this section are based on the assumption that the jet can be characterized by specifying its momentum flux vector at the jet nozzle exit and the jet exit Mach number. This assumption leads to various possible choices for parameters in addition to those needed for simulating flow about the body alone, such as

$$\frac{P_{o_j} A_t}{q_1 A_b} \text{ or } \frac{T}{q_1 A_b}, \gamma_j, M_e, \phi$$

where A_t is the jet nozzle throat area, ϕ is the nozzle inclination angle, and A_b is an appropriate vehicle or model reference area. The length scale of the interaction flowfield will be proportional to $(P_{o_j} A_t / q_1)^{1/2}$. This simplified characterization of the jet is inadequate when the region far downstream of the jet nozzle exit is important (68).

4.2.1 Concentration, Pitot Pressure, and Velocity Surveys

Several sources of data concerning the distribution of pressure, velocity, and injectant jet fluid concentration are available (61 to 63, 65). Typical jet fluid concentration profiles are shown

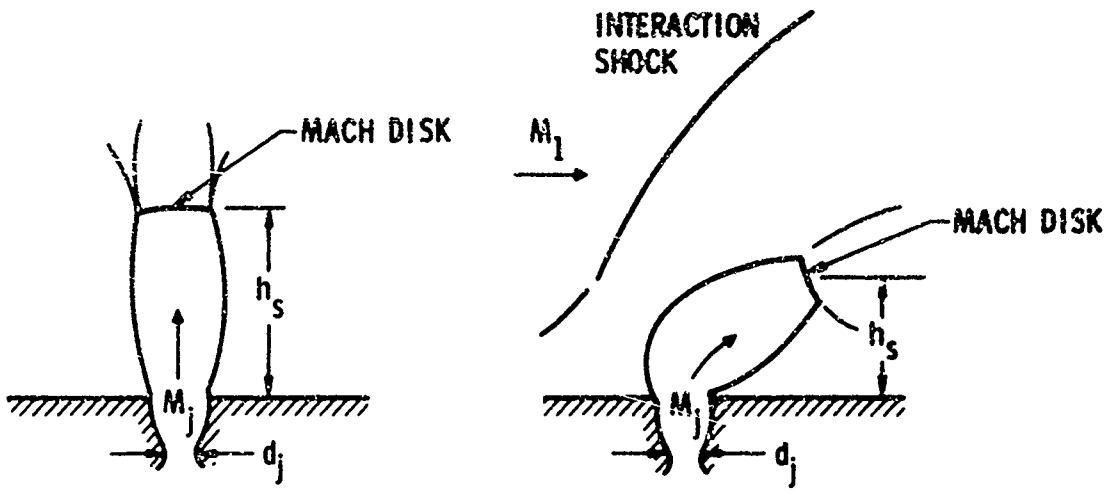

Figure 33. Interpretation of Shock Structure for Underexpanded Gaseous Injection into Still Air and into a Supersonic Crossflow Proposed in Reference 56

in Figure 34 (62). The scale is normalized by a calculated value of penetration height, h, derived from a simple momentum balance (64) as

$$\frac{h}{d} = \frac{1}{M_1}\left(\frac{2\,P_{o_j}\gamma_j}{C_F P_1 \gamma_1}\right)^{1/2}\left\{\frac{2}{\gamma_j-1}\left(\frac{2}{\gamma_j+1}\right)^{\frac{\gamma_j+1}{\gamma_j-1}}\left[1-\frac{P_1}{P_{o_j}}^{\frac{\gamma_j-1}{\gamma_j}}\right]\right\}^{1/4} \tag{20}$$

These data indicate that within a distance of twice the penetration height downstream of the jet exit, the line of maximum jet fluid concentration is turned nearly parallel to the plate.

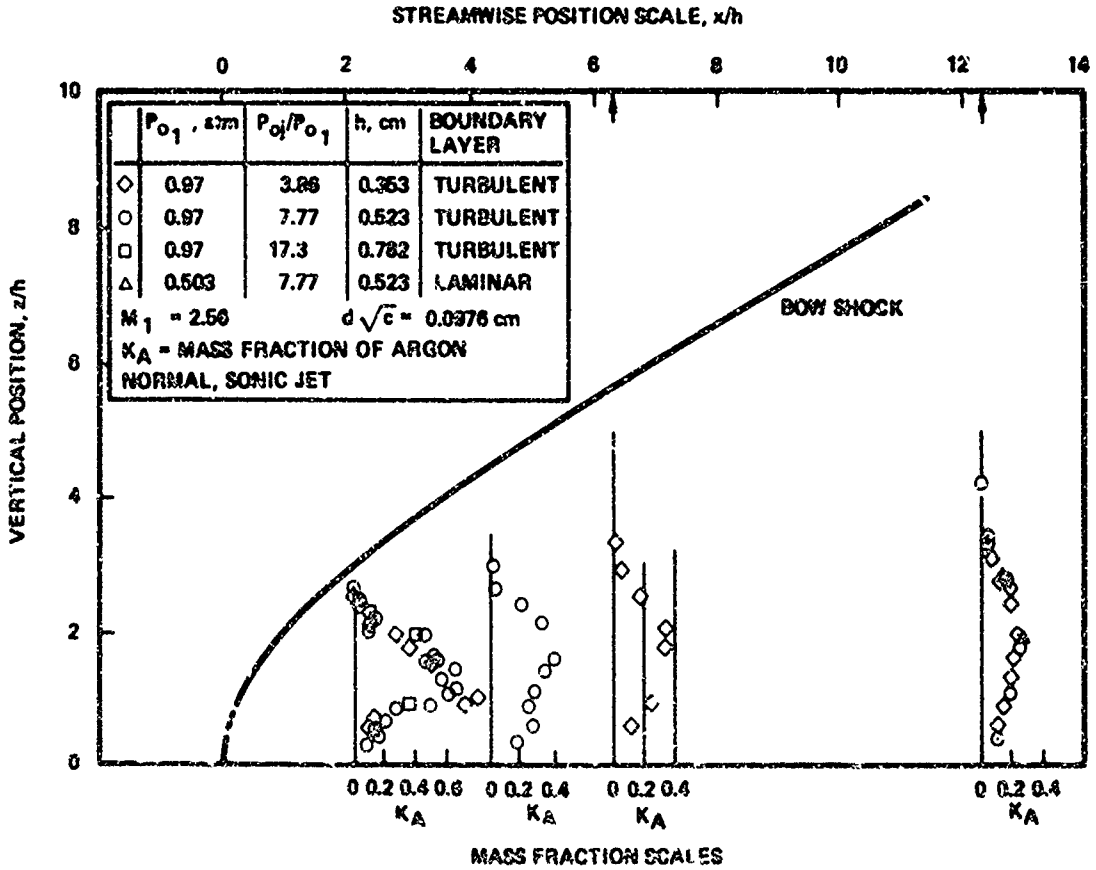

Figure 34. Argon Jet Gas Concentration Profiles in Centerline Plane, Reference 62

Velocity, Mach number, and total pressure profiles in the jet are shown in Figure 35 (62). The data of Figure 35 correspond to three values of the lateral distance of the profile from the jet trajectory meridian plane, y (normalized by h). These data indicate that total pressure and velocity deficits in the jet wake follow the concentration of jet fluid. The large total pressure deficit near the line of maximum jet fluid concentration indicates the presence of strong shocks in the jet turning process.

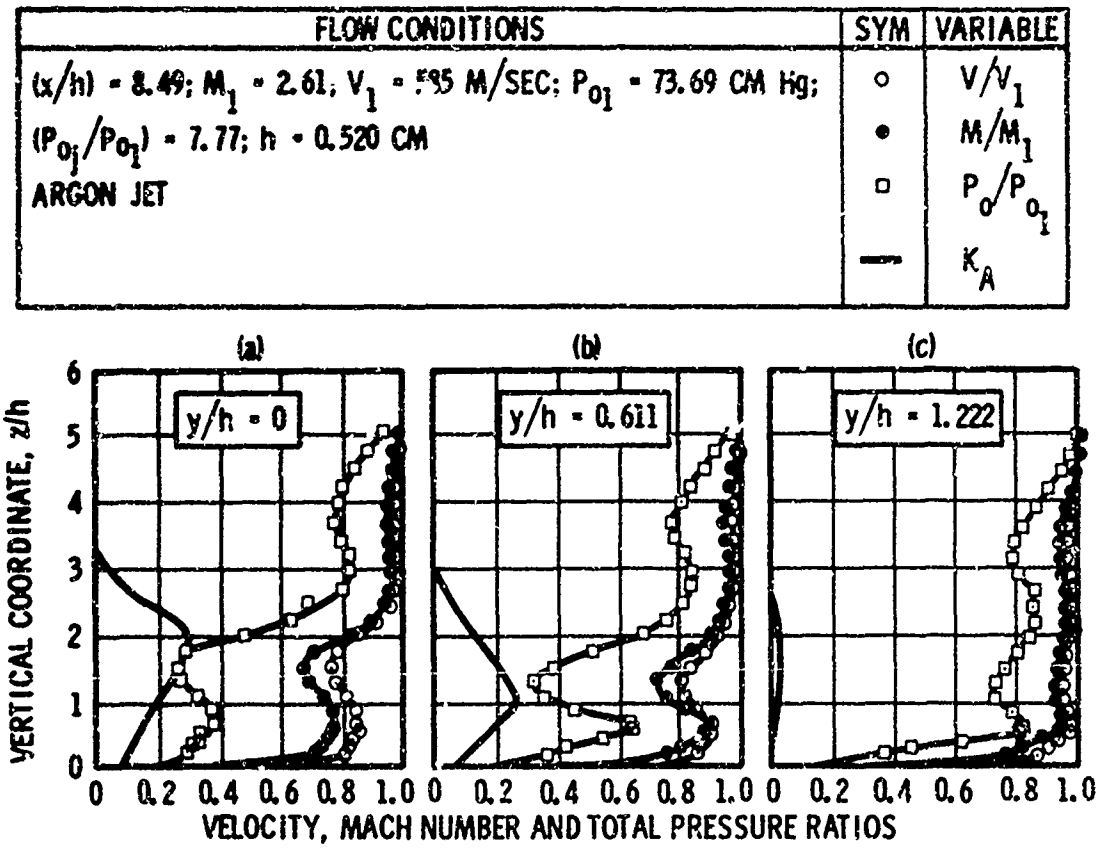

Figure 35. Velocity, Mach Number, and Total Pressure Profiles Downstream of Jet Exit, Reference 62

In Figure 36, cross sections of jet concentration contours are shown at locations which are 2.08 and 12.3 times the penetration height downstream of a point where the extrapolated bow shock would intersect the plate, which is slightly forward of the jet exit (62). The kidney shape of the concentration contours is similar to that of a subsonic jet exhausting transverse to a subsonic mainstream. This shape is evidence of the presence of vortices that transport mainstream fluid into the jet and accelerate the mixing process.

One of the most extensive investigations of the concentration field downstream of a jet has been conducted by Torrence (69, 70). Gases were injected from a circular, sonic orifice 0.123 centimeters in diameter located 24 centimeters downstream of the leading edge of a 23 by 75 centimeter flat plate. Local external-flow properties were $M_1 = 4.03$ and $Re = 7.87 \times 10^7$ per meter. Injectant gases included helium, hydrogen, argon, helium-air, argon-air, and ethylene-air mixtures. The ethylene-air mixtures were 3 percent by volume ethylene, which acted as a tracer. Tests were conducted at a jet-to-freestream dynamic pressure ratio of 1.0, except for some of the air-injection tests. Freestream and injectant stagnation temperature were maintained at approximately 300°K. Concentration profiles similar to those of Figure 34 were obtained at several downstream stations for each test condition. An example of data obtained by Torrence is shown in Figure 37. These data show the axial decay of the maximum value of injectant mass fraction measured at each downstream station for a range of injectant conditions. Extrapolation of straight lines faired through the data to $K_{max} = 1.0$ defines a reference length, X_a, for each test condition, which can be interpreted as the location of the end of the inviscid core of an equivalent coaxial jet. Values of X_a determined in this manner are seen to lie upstream of the nearest survey station, $X/d \simeq 6$. These data are shown to lie on a single line when plotted in the form K_{max} versus X/X_a.

Orth and Funk (65) have presented concentration profiles obtained downstream of hydrogen jets. The external flow Mach number was 2.72 and the jet exit Mach numbers varied from 1.0 to 1.67. Measurements were confined to the X-Z plane. Comparisons were made with jet trajectories predicted by the analysis of Schetz and Billing (71). Reasonable agreement was shown between the data and trends predicted by the analysis.

Povinelli, et al (72) used concentration measurements to define the outer jet boundaries in the meridian plane of normal, circular helium jets injected into a Mach 2 airstream. Jet exit Mach numbers of 1 to 4 were tested. The jet boundary was defined as the location of 1 percent helium concentration. Jet boundary data (75, 72) have been correlated by Povinelli, et al (72), by the empirical expression

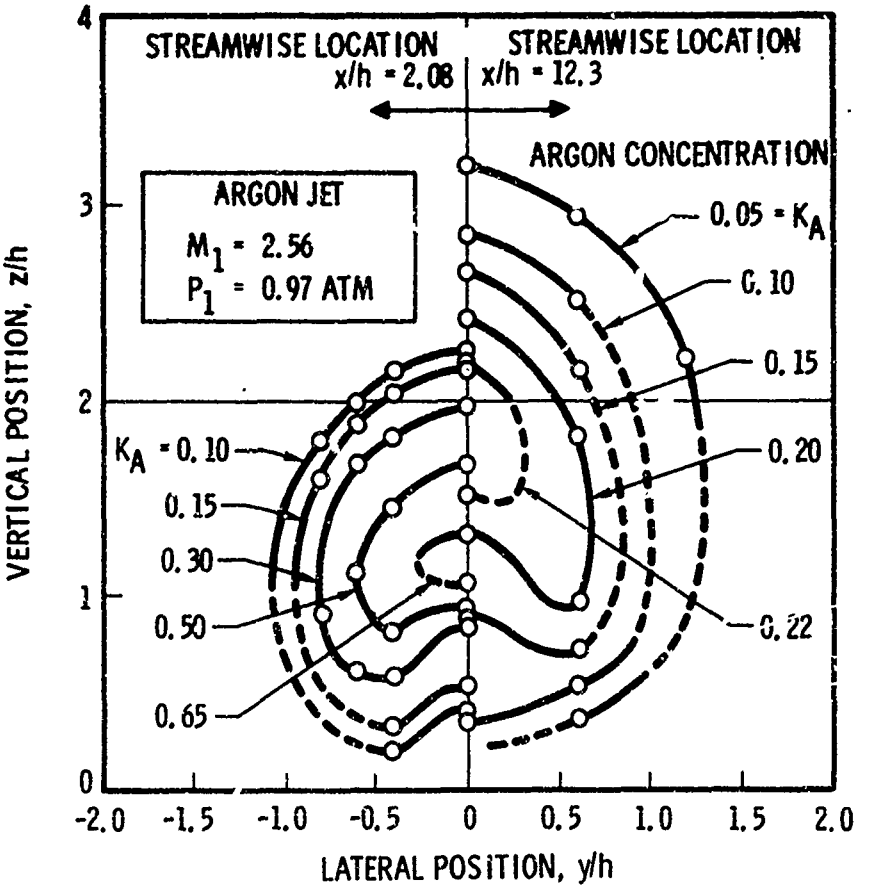

Figure 36. Injectant Concentration Contours in Cross-Sectional Plane Downstream of Jet Exit, Reference 62

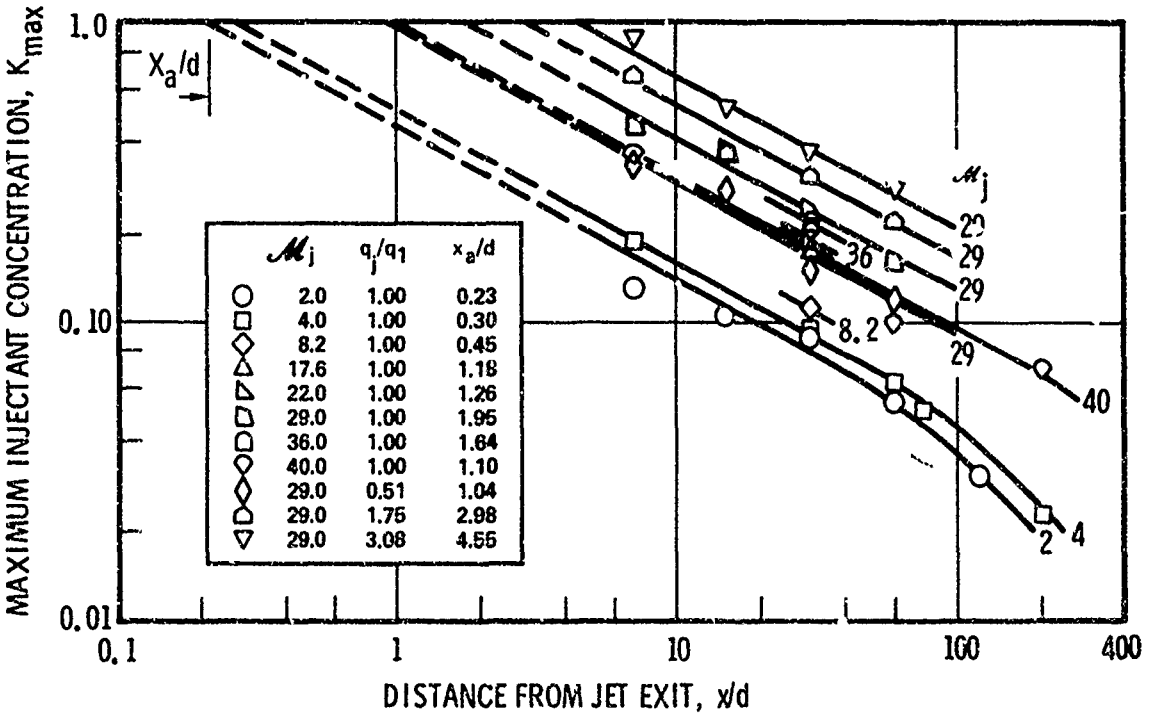

Figure 37. Effect of Injectant Composition and Blowing Rate on Injectant Concentration Downstream of Normal Sonic, Circular Jets, Reference 70

$$\frac{y_j}{d_e} = 1.92\left(\frac{q_j}{q_1}\right)^{0.35}\left(\frac{M_1}{M_e}\right)^{0.094}\left(\frac{X}{d_e}+0.5\right)^{0.277} \qquad (21)$$

where y_j is the jet boundary coordinate measured from the plane of the nozzle exit. The influence of M_e is obscured somewhat by this method of presentation. When M_e is increased from 1 to 4, with fixed external flow conditions and fixed jet mass flow rate, the penetration is increased by approximately 25 percent.

Hersch, et al (73) have shown that helium jet boundary data can be obtained by densitometer analysis of Schlieren photographs, if the method is calibrated by comparison with concentration measurements.

The magnitudes of lateral velocity components in the jet vortices have been reported by Dahlke (74). An example of measurements made by Dahlke is shown in Figure 38. The velocities were measured with a calibrated multiorifice pressure probe in the cross section plane 8.63 body diameters downstream of a sonic jet exhausting normal to the surface of an ogive cylinder at zero angle of attack. The jet exit is three calibers from the origin of a four caliber ogive nose. Some correlations of these data have been used by Durando to model the variation of strength and position of these vortices (75, 76, 77).

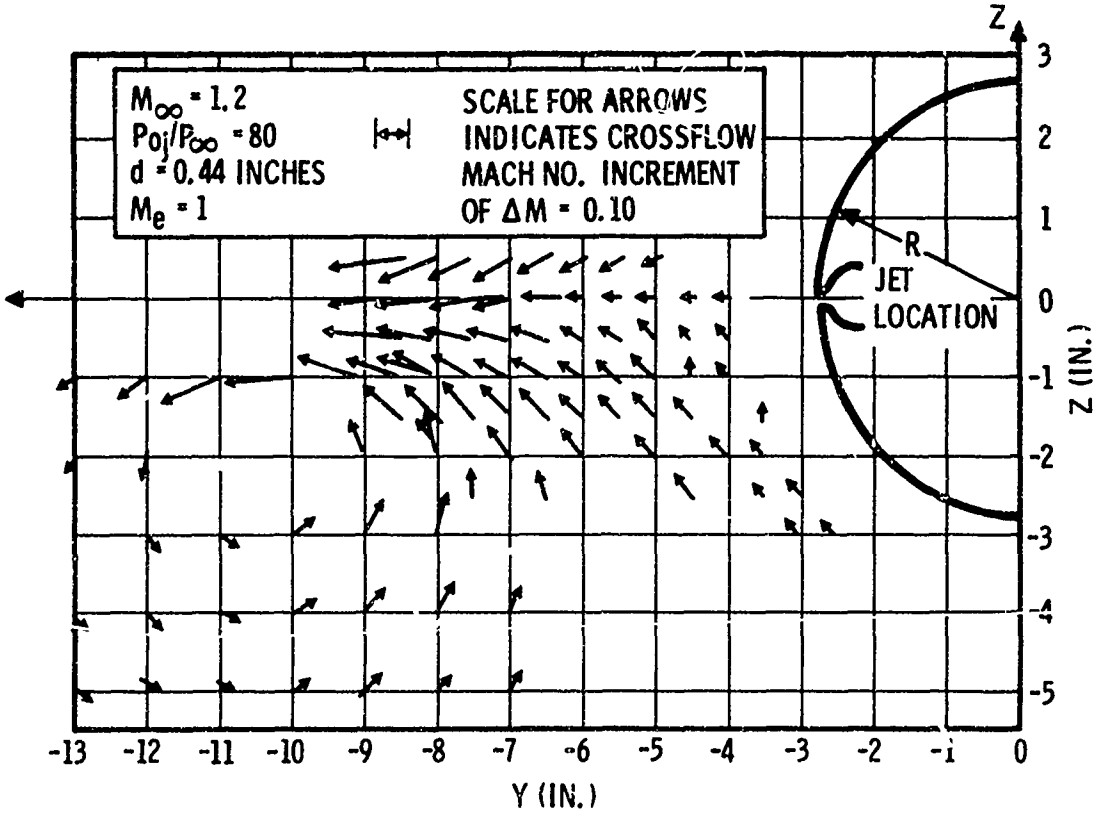

Figure 38. Crossflow Components of Mach Number Far Downstream of Jet Nozzle, Reference 91

4.2.2 Interference Pressures and Forces

In predicting aerodynamic forces induced by the jet plume, the principal subject of analysis is usually the pressure distribution near the jet in the plane of the jet exit (or a contour including the jet exit). As illustrated in Figure 32, the primary interference shock structure and flow disturbance occur in this region. When jet thrust is high compared with the interference forces induced in this region, forces induced by downstream interference become more important. In the latter case, the jet wake can affect downstream surfaces that have either large lift efficiency, large moment arms, or out-of-plane moment capability.

A typical representation of the disturbance-induced pressure distribution near the jet is shown in Figure 39 (62). This figure shows constant-pressure contours in the vicinity of a circular sonic jet exhausting from a flat plate into a Mach .5 external flow. The jet is normal to the plate surface, and the boundary layer on the plate is turbulent upstream of separation induced by the jet plume. The length scale is normalized by the penetration height, h, given in Equation (20). The parameter P/P_∞ on the contours is the ratio of the pressure induced by the jet to the pressure on the plate with the jet off. The interference causes increases in pressure both upstream and downstream of the jet except in the region directly behind the jet nozzle exit, where the pressures are decreased. The pressure contour map of Figure 40 is similar to that of the previous figure, except that in this case the boundary layer is laminar upstream of the interaction region. The general features of the distributions are qualitatively similar, except that in laminar flow the pressure ratios tend to be smaller and the region of influence is larger.

Centerline static pressure data for sonic and supersonic jets exhausting into a hypersonic external flow, $M_1 = 7.8$, with a laminar boundary layer, are presented in Figure 41. These data are qualitatively similar to those of the previous figure. Note that the effect of increasing M_e results in a decreased extent of separation upstream of the jet.

A significant effect that is particularly difficult to correlate is the independent effect of mainstream Mach number in the supersonic range. Typical data for the effect of Mach number are shown in Figure 42 for both laminar and turbulent boundary layers (62). The length scales are normalized by the penetration height, h, computed from Equation (20). As shown in this figure, the gross scale of the disturbance is fairly well correlated, although systematic variation with M_1 is still

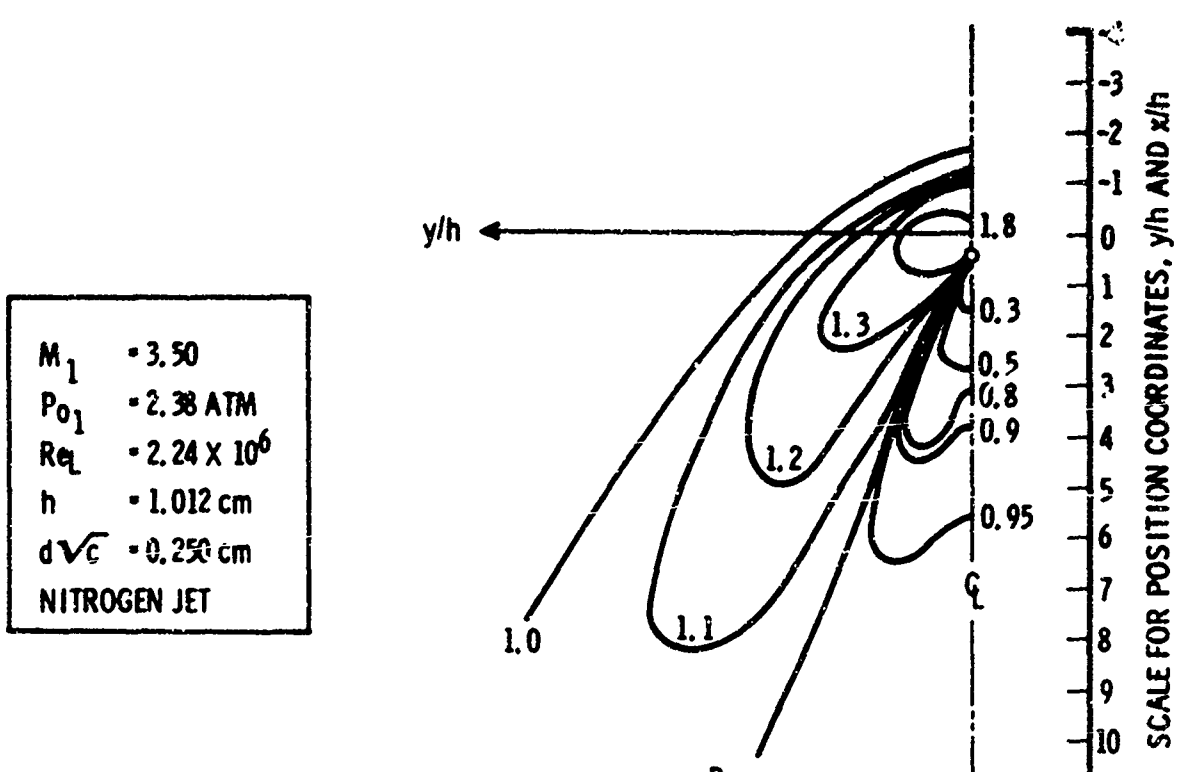

Figure 39. Typical Interference Pressure Contours for Circular Jet and Turbulent Boundary Layer, Reference 62

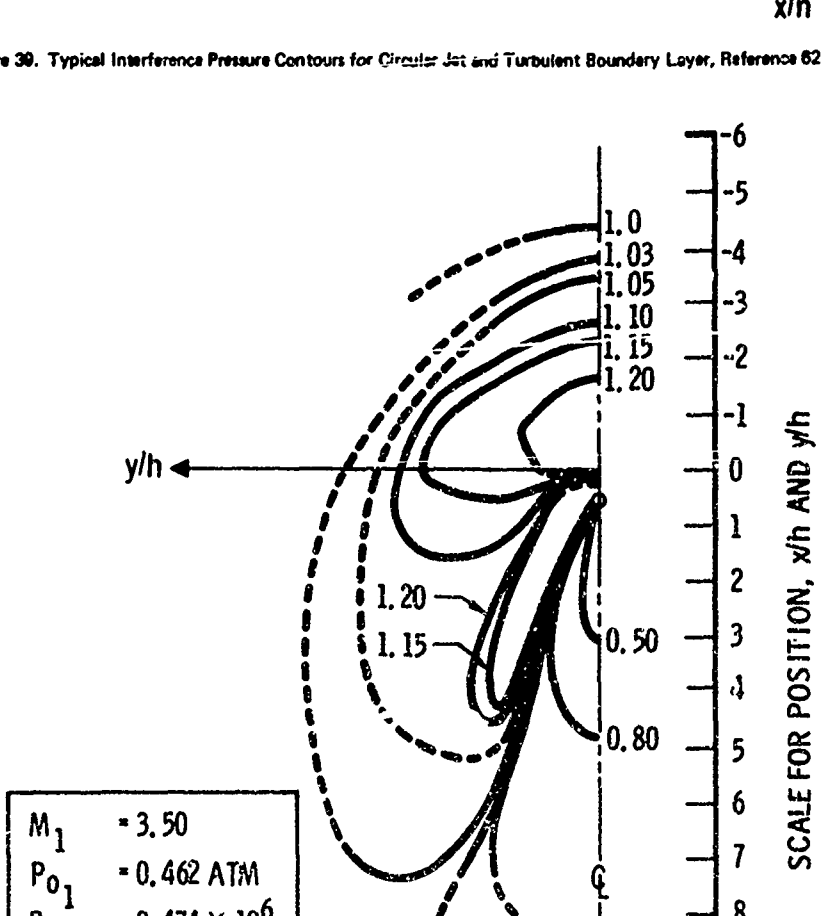

Figure 40. Typical Interference Pressure Contours for Circular Jet and Laminar Boundary Layer, Reference 62

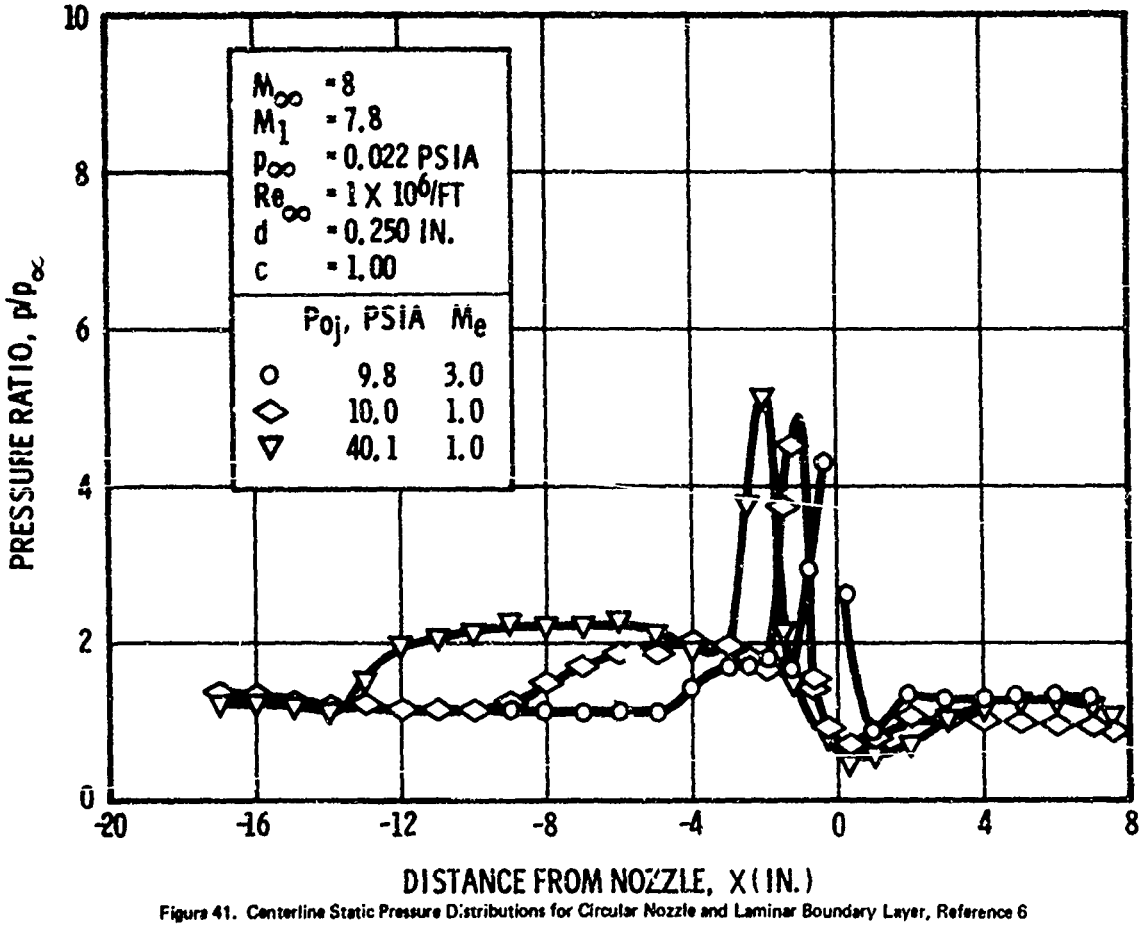

Figure 41. Centerline Static Pressure Distributions for Circular Nozzle and Laminar Boundary Layer, Reference 6

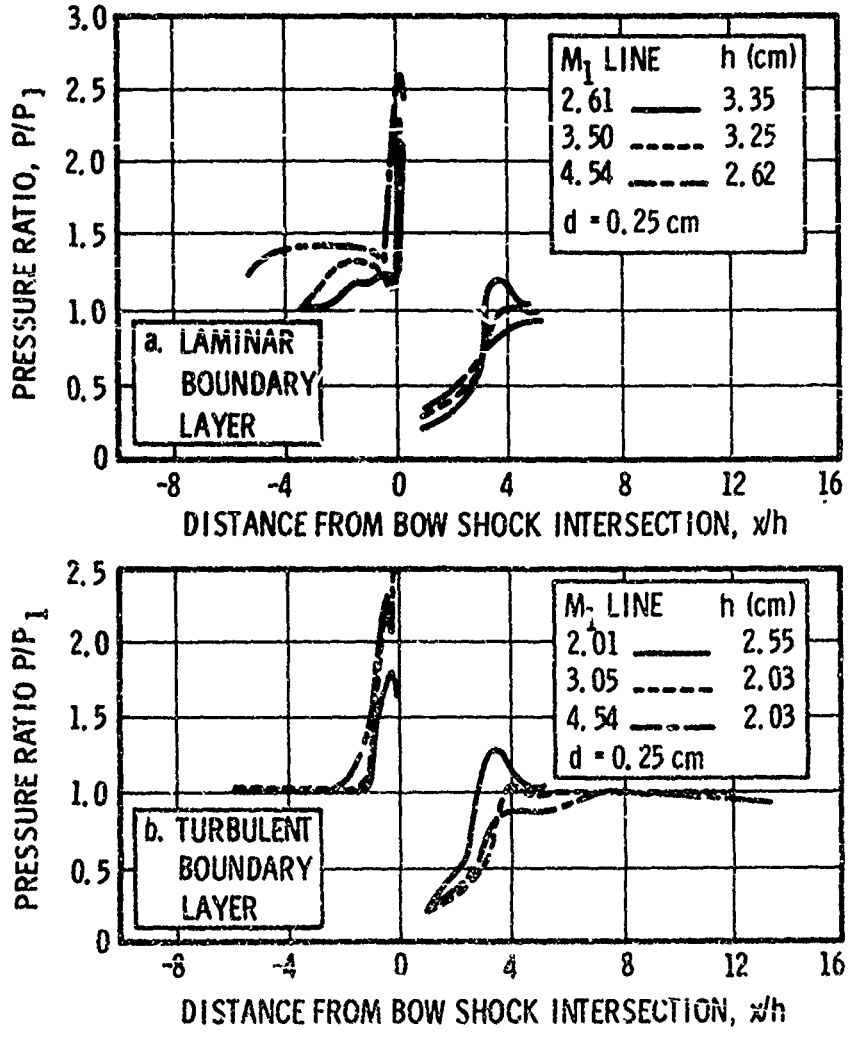

Figure 42. Effect of Mach Number on Centerline Pressure Distribution, Data from Reference 62

present. The data shown are the most complete and self-consistent set known to the authors, however, effects other than that of Mach number are believed present. Other data, to be presented later, indicate that the pressure distributions such as these depend upon h/δ_1. Sources of similar data for pressure distributions on flat plates include References 15, 32, 78, and 79.

A series of tests has been conducted for the purpose of determining the independent effects of pressure ratio, h/d, or h/δ_1, on the details of the static pressure distribution (62). The results of those experiments are summarized by Figures 43 and 44. Figure 43 compares data obtained at nearly the same pressure ratio with different size orifices. Although a reasonable correlation has been

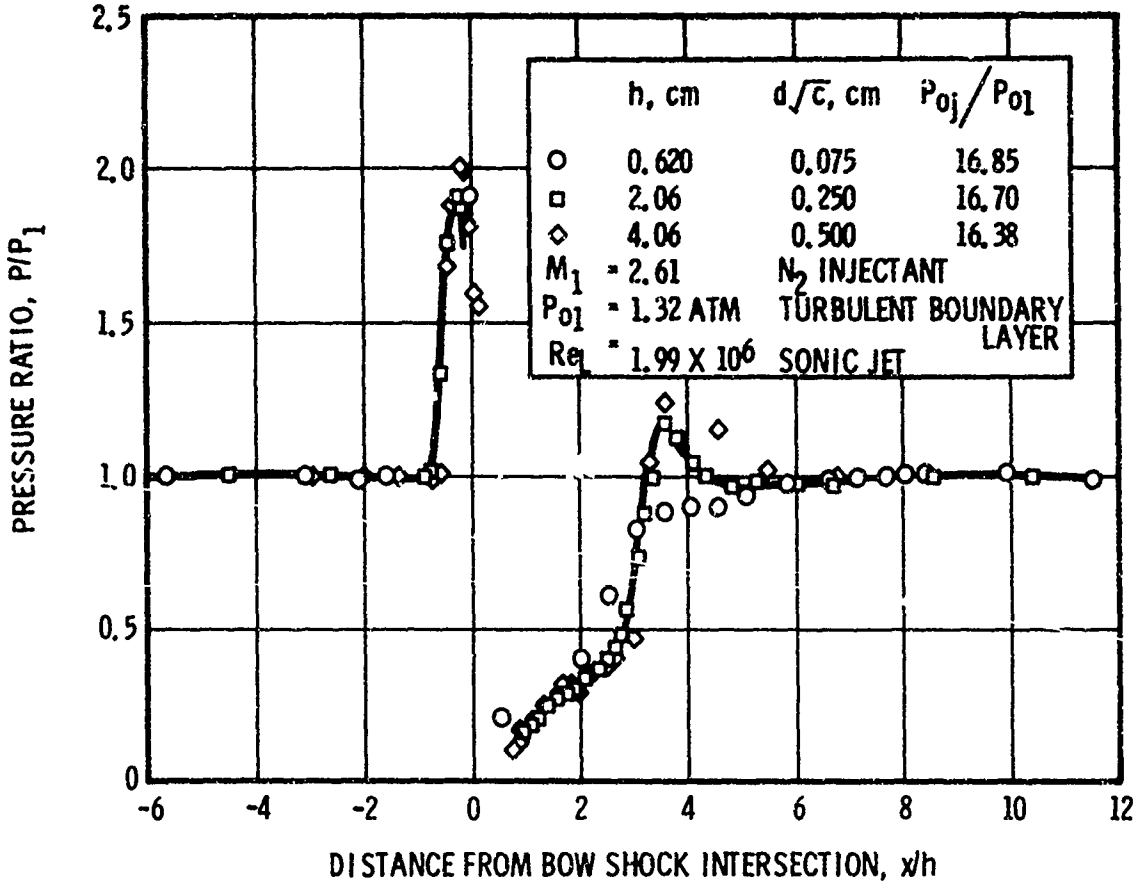

Figure 43. Effect of Changing Nozzle Exit Diameter with Constant Pressure Ratio, Reference 62

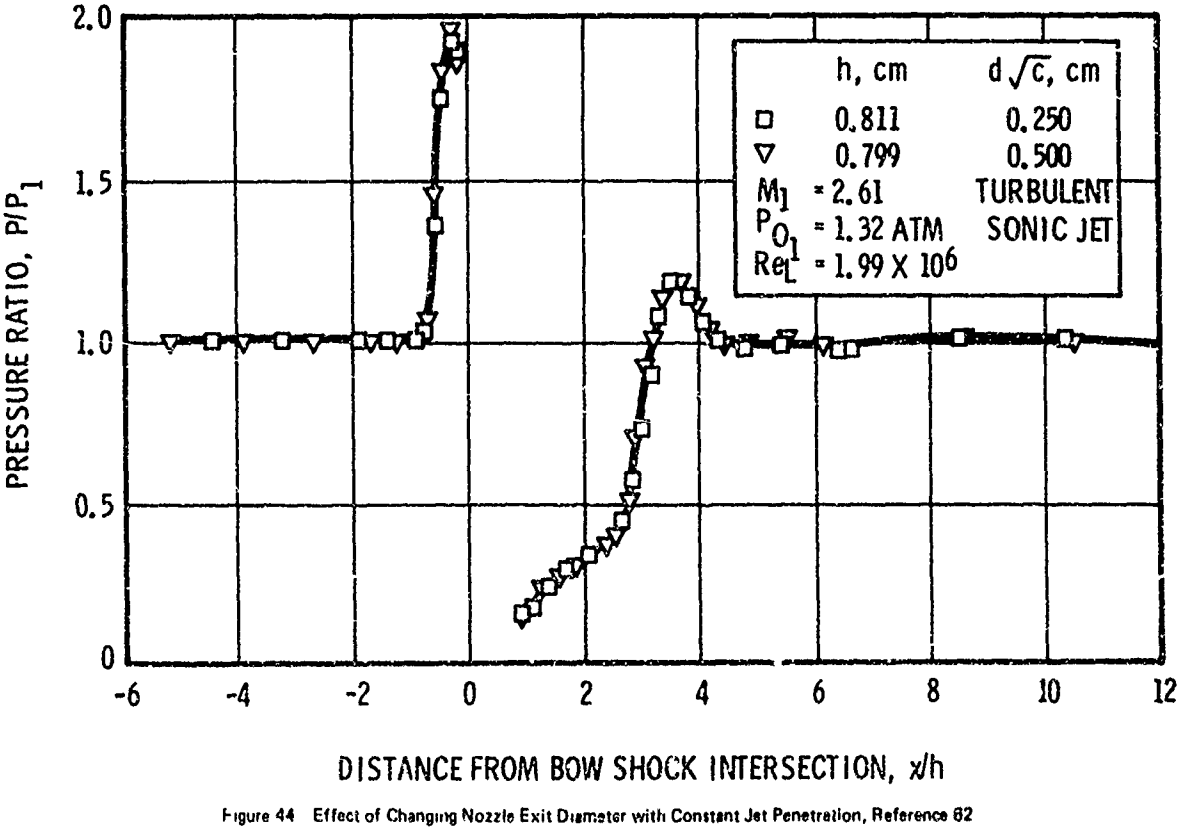

Figure 44 Effect of Changing Nozzle Exit Diameter with Constant Jet Penetration, Reference 62

achieved, the distributions are significantly different in the downstream region, particularly at $3 < x/h < 5$. Similar data in Figure 44 were obtained for the same value of h but different pressure ratios and orifice diameters. Excellent correlation is achieved. Similar results were obtained at other external flow test conditions. It is concluded that h/δ_1 may be an important parameter in determining the pressure distribution in the downstream region and that the pressure ratio or h/d may be relatively unimportant. Additional data indicate that h/d influences the static pressure distribution when $h/\delta_1 \lesssim 1$.

The obstruction produced by a jet from a supersonic nozzle appears to be a different shape from that which results from an underexpanded sonic jet. Shadowgraph photographs of Figure 45 show significant qualitative influence of jet exit Mach number. These are unpublished results of the investigation described in Reference 6 conducted with an external flow at Mach 8. The nozzles have the same throat areas, and values of P_{o_j}/P_1 are approximately the same. The underexpanded sonic jets produce relatively large disturbances near the plate surface, but the supersonic jets, having been expanded within the nozzle, appear to penetrate somewhat more deeply into the external flow at a given axial location. This difference in the shape of the effective disturbance produced by the jet causes the interaction force to decrease somewhat with increasing jet exit Mach number.

These photographs also illustrate the influence of the relative location of transition on the flow field. For test section conditions corresponding to Figures 45a and 45c, the boundary layer on the plate in the absence of the jet appeared to be laminar, and the character of the separated region shown in these figures appears to be primarily laminar. The boundary layer near the jet in Figures 45b and 45d is clearly transitional, resulting in shorter, steeper shear layer angles and a substantially altered wall static pressure distribution.

The difference in jet penetration between sonic and supersonic jets is illustrated in Figure 46 (80). In that illustration, contours of constant injectant concentration are shown at x/h = 10 (h calculated by Equation 20 in each case). This comparison shows that the supersonic jet trajectory penetrates further into the mainstream than that of the sonic jet. Billig, et al, (56), have proposed correlations for the Mach disk location including data for sonic and supersonic jets, as part of a semi-empirical method for computing jet trajectories. For $1.9 \leq M_1 \leq 4.5$ and $1.0 \leq M_e \leq 2.2$ the relation

$$h_s/d = M_e^{1/4}\left(P_j^*/P_{e_b}\right)^{1/2} \tag{22}$$

is proposed, where: h_s is the distance, normal to the plate, from the plate to the center of the Mach disk; d is the nozzle throat diameter; P_j^* is the pressure at the sonic point in the jet nozzle; and P_{e_b} is two-thirds of the stagnation pressure downstream of a normal shock in the external flow. The correlation does not completely account for the influence of M_e, however. Systematic deviations from the correlation, up to approximately 25 percent, are present for $M_e > 1$.

The supersonic jet presents a smaller obstruction to the external flow near the surface of the plate than an underexpanded sonic jet having the same mass flow rate. Therefore, higher exit Mach number jets cause relatively smaller interference forces. This effect is illustrated in Figure 47 by data which were obtained at $M_1 = 8$. In this case, data are presented in the form of amplification factor versus pressure ratio for constant external flow conditions and constant nozzle throat diameter. Note that the decrease in interaction force resulting from the increase in Me is a much larger effect than the increase in jet thrust. Similar results have been presented by Koch and Collins (81).

The effect of inclining the thrust axis of a circular jet relative to the external flow direction, has been investigated in several experiments (80, 81). In general, inclining the nozzle upstream will increase the effective disturbance size and the interaction force. The analysis of Reference 63 was modified to include the effects of forward inclination in Reference 80. The result is that the penetration height, h, given in Equation (20) must be multiplied by the ratio

$$\frac{h}{h_{normal}} = \left(1 + \frac{V_e}{a_j^*}\sin\phi\right)^{1/2} \tag{23}$$

where ϕ is the inclination of the jet thrust axis from normal to the external flow direction (measured positive into the stream) and V_e is the jet exit velocity.

The centerline pressure distributions for inclination forward and aft from normal to a uniform supersonic stream are shown in Figure 48 (80). Also shown (by the solid line) are data for $\phi = 0$. The effect of forward inclination driving the upstream boundary layer separation further forward has been observed in other experiments. The downstream inclination effect on downstream pressure distributions would not necessarily be expected to scale very well with the penetration height calculated by Equations (20) and (23), because of the simplified assumptions from which they were derived.

An aspect of jet nozzle geometry that provides significant control over the aerodynamic interference is the cross-sectional shape of the nozzle or geometry of a cluster of nozzles. There is evidence that multiple circular nozzles in a line transverse to the oncoming mainstream produce an interaction which is similar to that associated with a jet from a finite-span slot (62). This is illustrated in Figure 49. As shown in the figure, the high pressures upstream span the distance between the circular nozzles separated by eight nozzle diameters. Comparing Figure 49 with Figure 39 shows the difference between pressure distributions induced by single and multiple nozzles. The effect of the multiple nozzles is to broaden the region of the disturbance, when the multiple nozzles are spaced sufficiently close together.

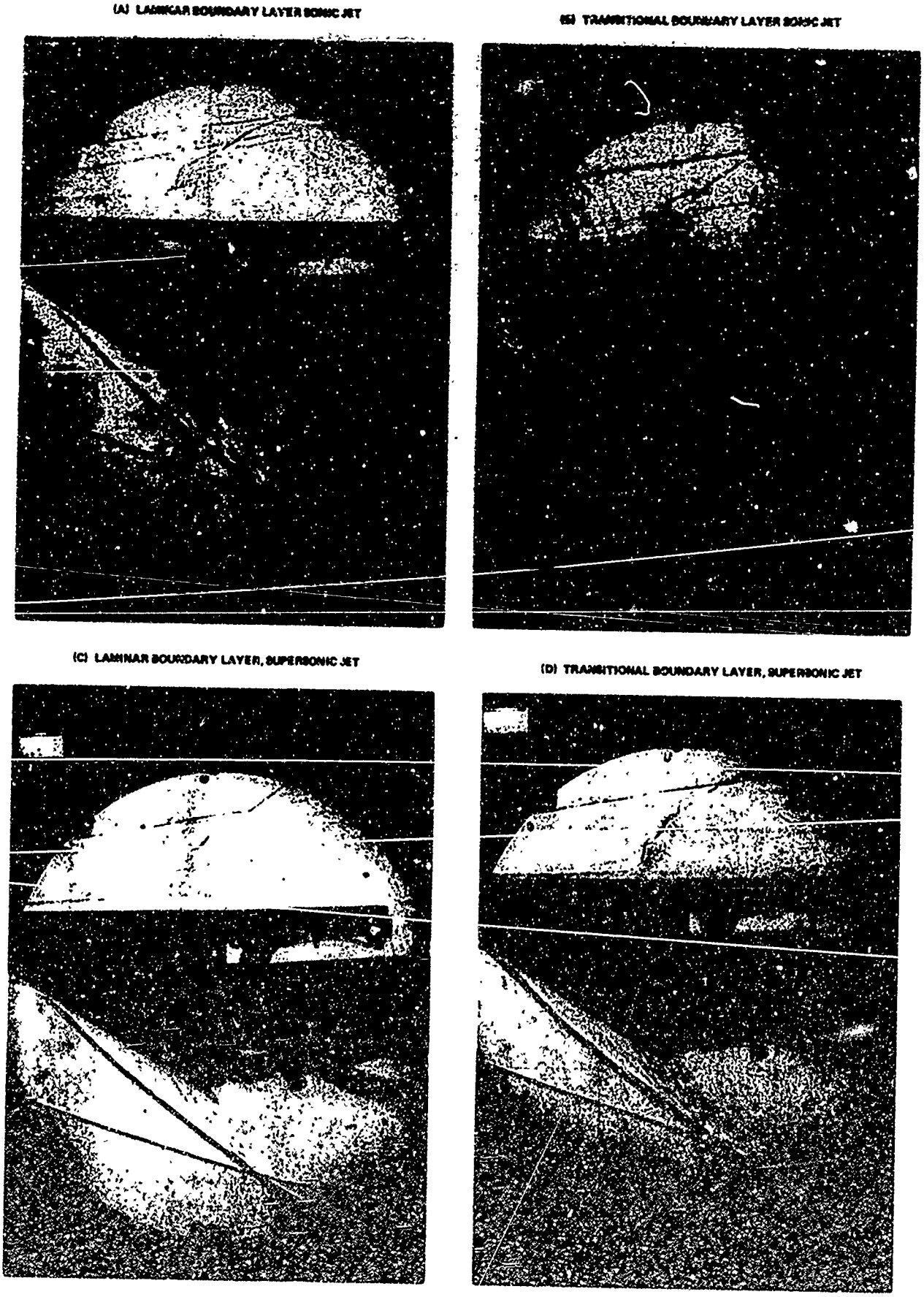

Figure 45. Effect of Jet Exit Mach Number and Transition Location on the Jet Interaction Flowfield at Mach 8

The effect of secondary jet thermodynamic properties on the aerodynamic interference generated by a three-dimensional jet has been the subject of several investigations. The corresponding literature pertaining to jets from transverse slots has already been reviewed. Collins et el (82, 83) have reported work on jet gas property effects. Some data for circular hole jets are shown in Figures 50 and 51 (32, 83). These results are typical of most data concerning the independent effects of jet temperature and molecular weight. Some of the existing data are inconsistent. The data in Figure 50 indicate no discernible effect of jet temperature or molecular weight on amplification factor,

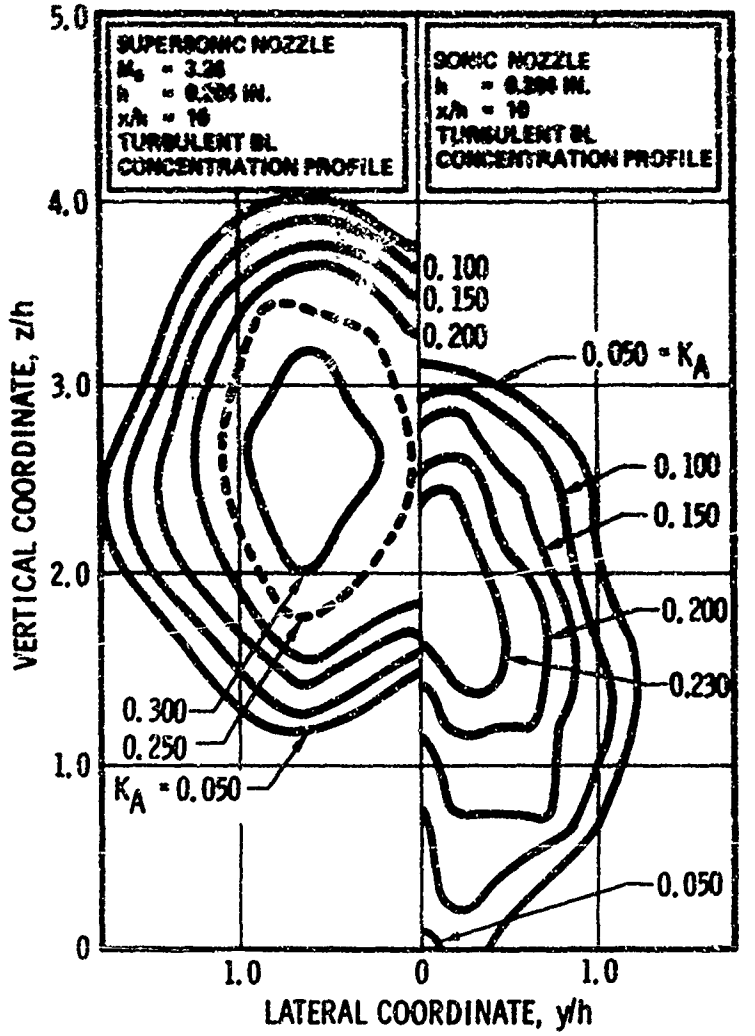

Figure 46. Injectant Concentration Contours in Cross-Sectional Plane Downstream of Sonic and Supersonic Argon Jets

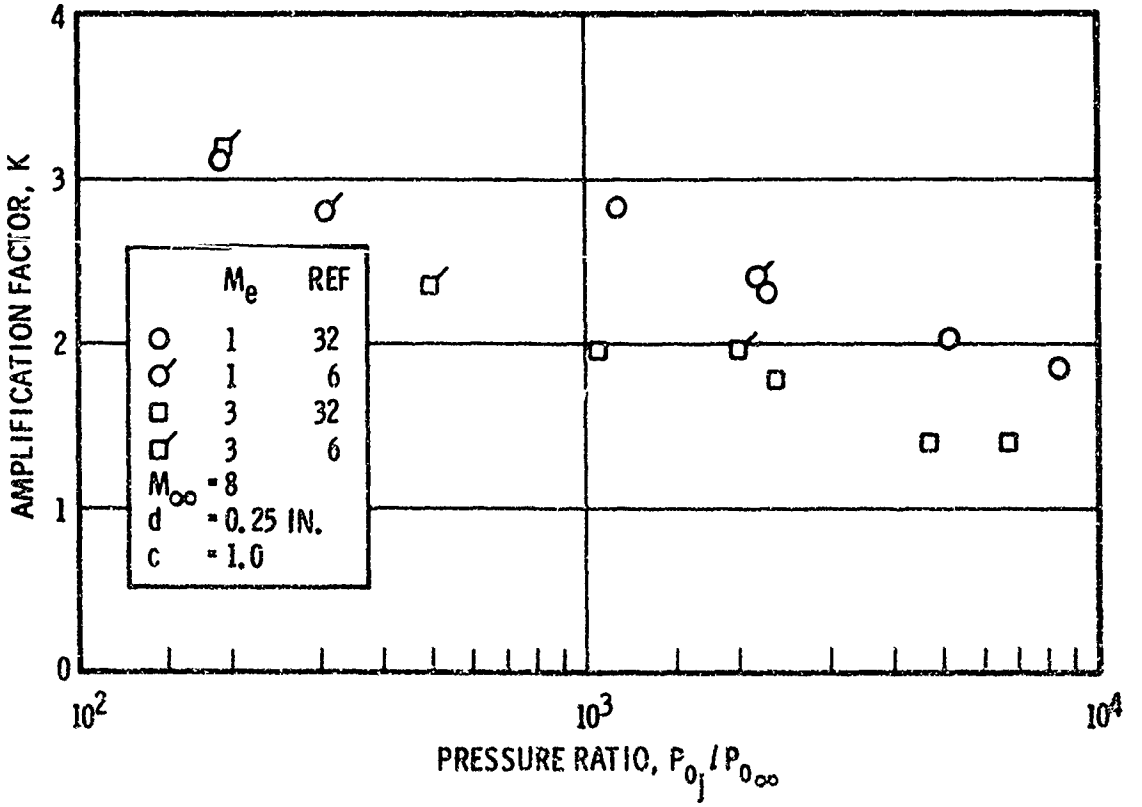

Figure 47 Effect of Exit Mach Number on Amplification Factor for Circular Nozzles and Laminar Boundary Layer

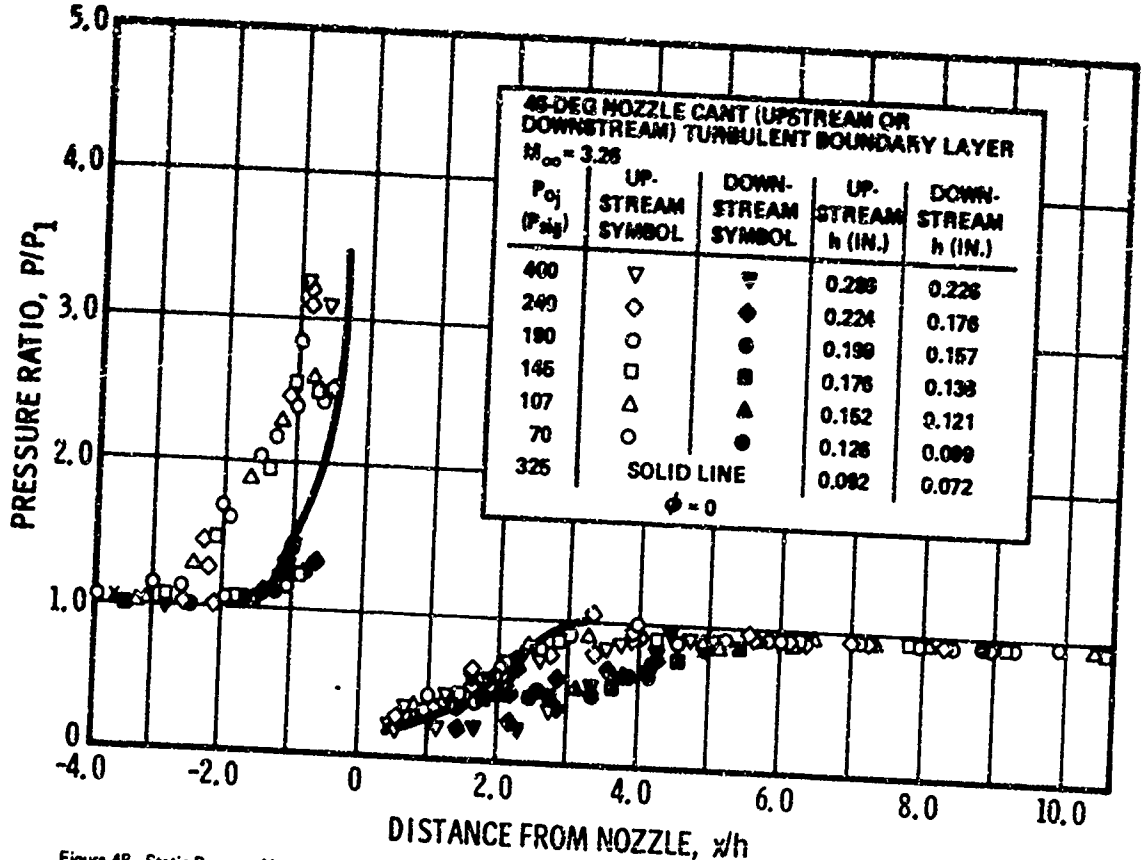

Figure 48. Static Pressure Measurements for Jets Canted Upstream and Downstream from Normal to Plate, Data from Reference 80

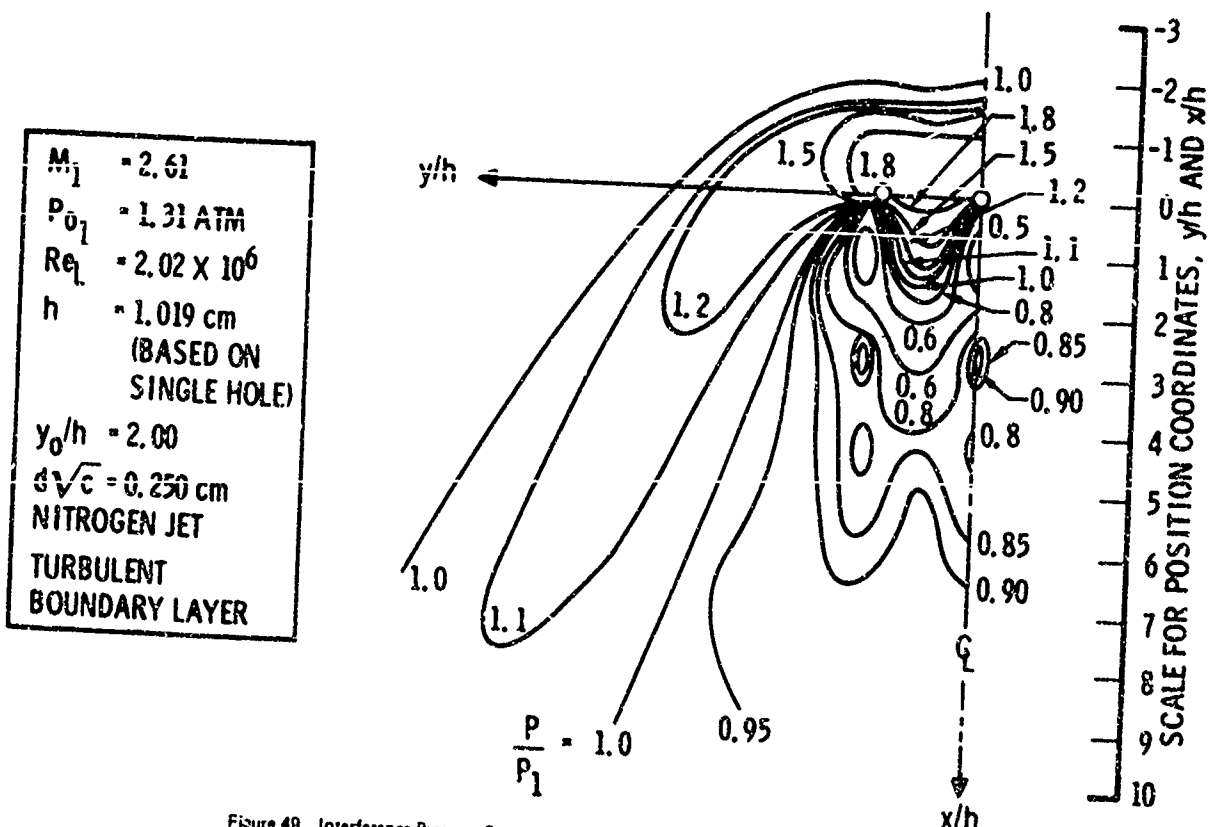

Figure 49. Interference Pressure Contours for Two Adjacent Jets from Flat Plate, Reference 62

while the data in Figure 51 indicate that scaling with a mass flow ratio correlates small effects due to a large change in molecular weight. Since the values of amplification factor shown in Figures 50 and 51 are so nearly constant, the choice of abscisca is relatively unimportant. The significant result is the fact that the interaction force is proportional to jet momentum. Data reported by Peichenau (84, 85) have been correlated using the penetration height calculated by Equation (20), as shown in Figure 52. However, the same method failed to correlate similar data (62) as shown in Figure 53. It is noteworthy that in Figure 52, pressure distributions downstream are correlated while upstream pressures are not. The inverse is the situation in Figure 53.

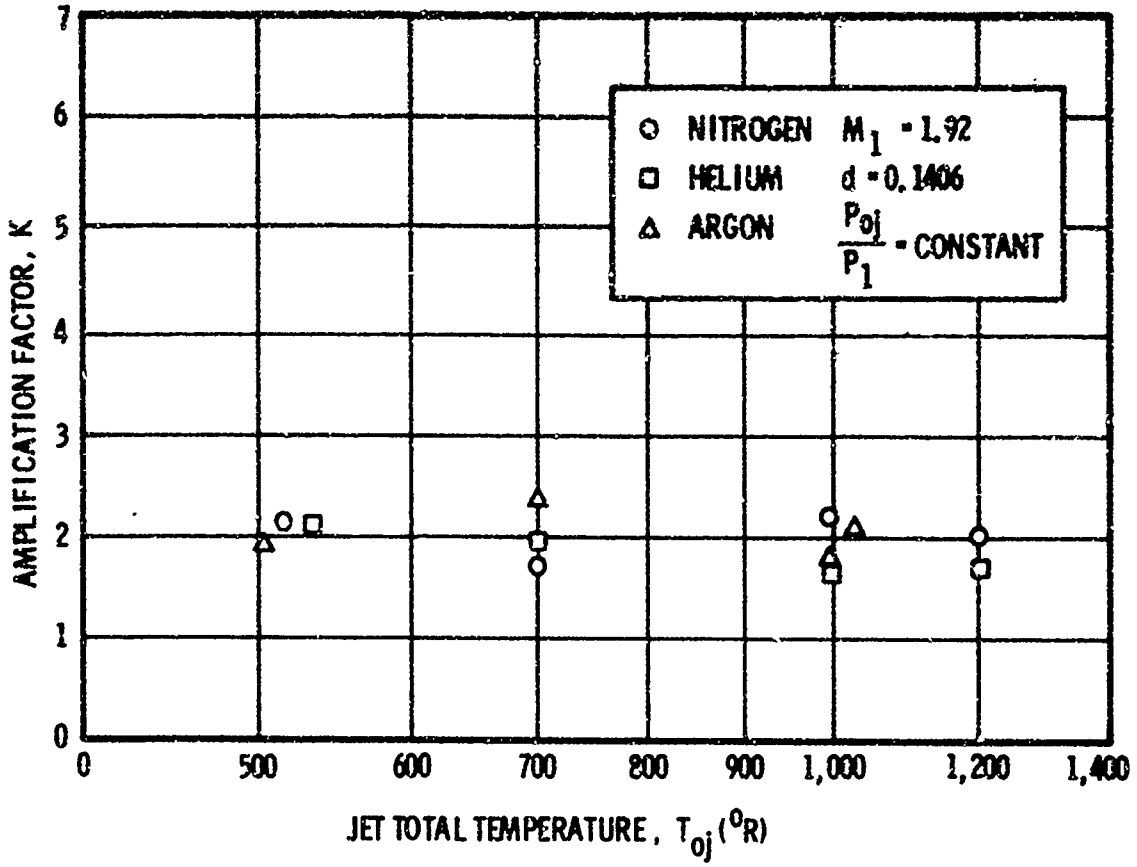

Figure 50. Effect of Jet Stagnation Temperature on Amplification Factor, Reference 83

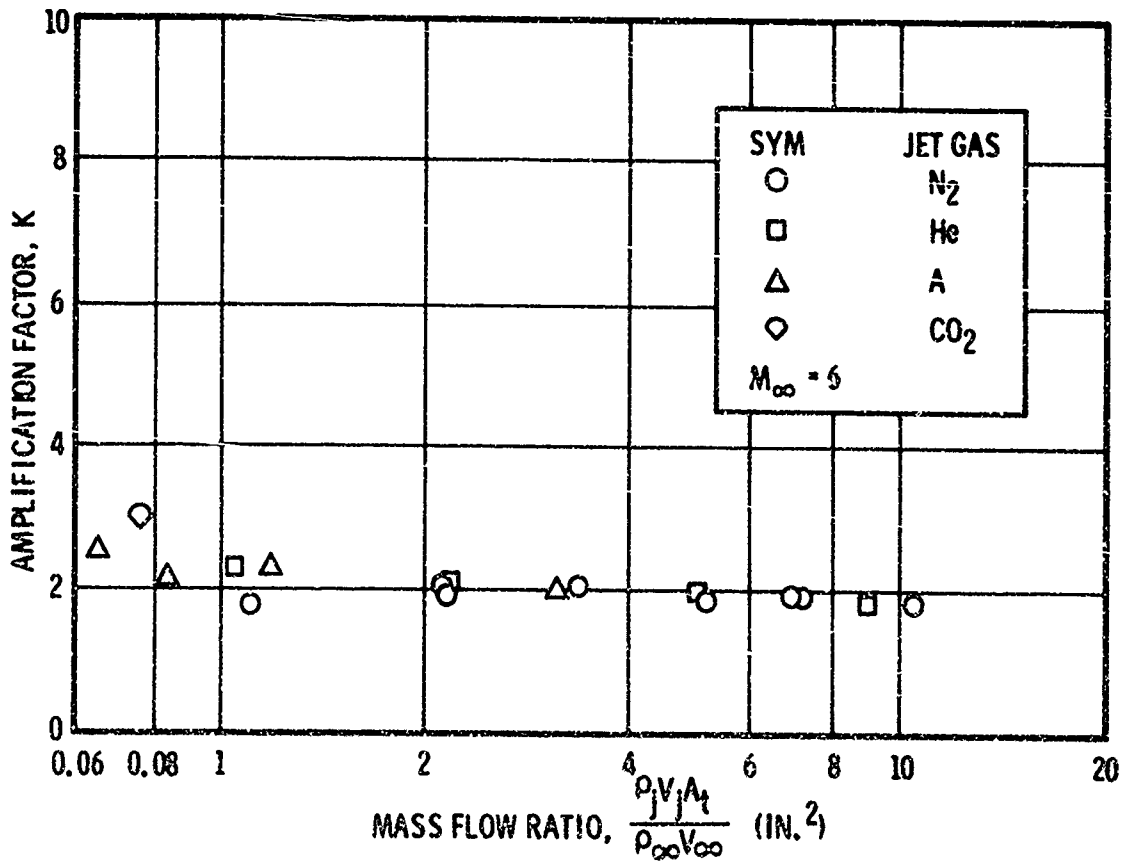

Figure 51. Effect of Jet Molecular Weight Variation on Amplification Factor, Reference 32

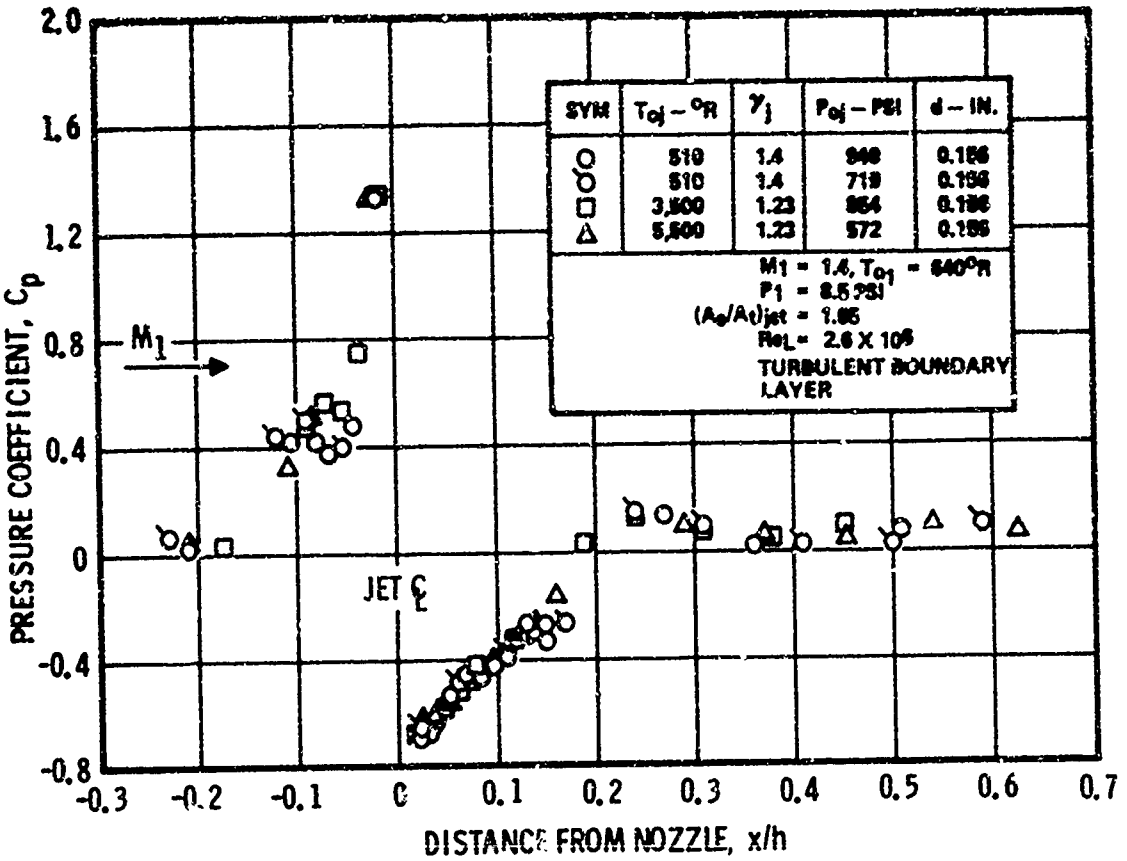

Figure 52. Interference Pressure Distributions for Cold and Hot Jets, Data from References 84 and 86

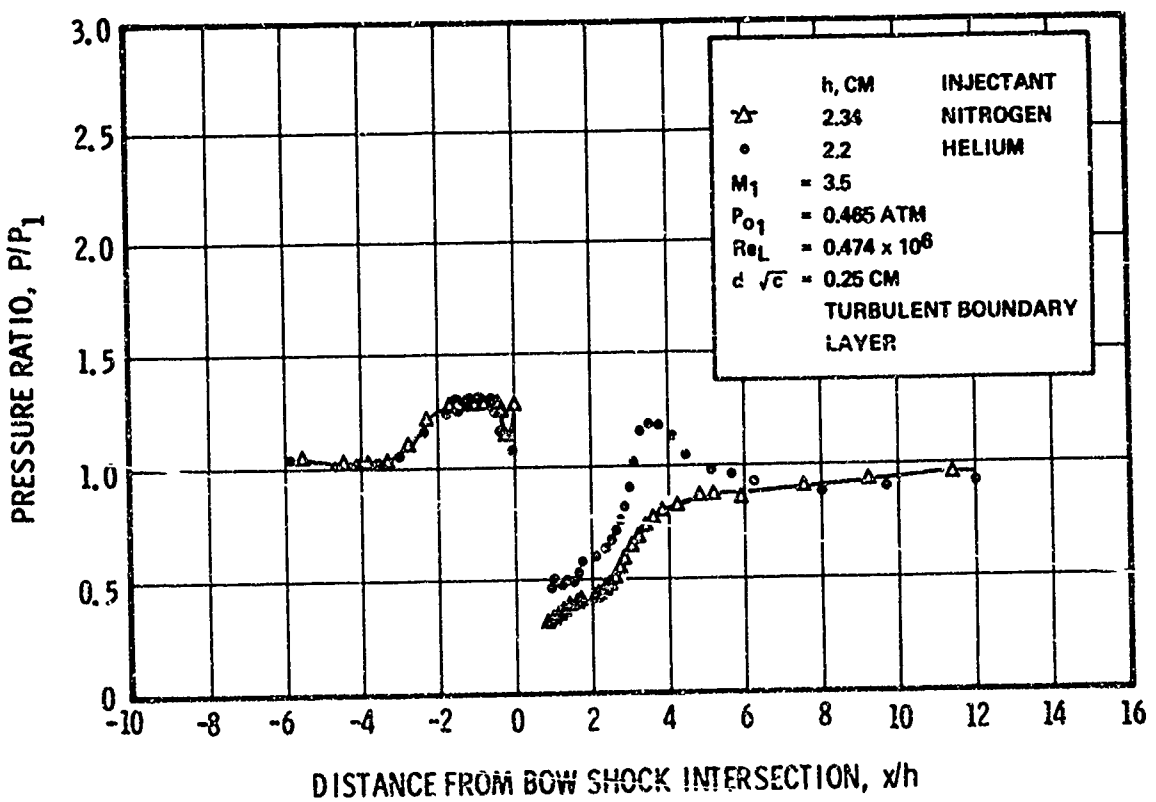

Figure 53. Interference Pressure Distributions for Nitrogen and Helium Jets, Reference 62

In the analysis of jet-induced aerodynamic interference, it is frequently of interest to predict the shape of the shock in the mainstream produced by the jet plume. This shock is the strong bow shock illustrated in Figure 32. Measurements of this shock shape have been used to substantiate the validity of several correlation models (45, 62, 82, 83, 86). A set of shock shape predictions are shown in Figure 54 (45). Here, four different methods of calculating shock shapes were used. Of the four, the method based on the blast wave analogy was found least accurate in the Mach number range considered.

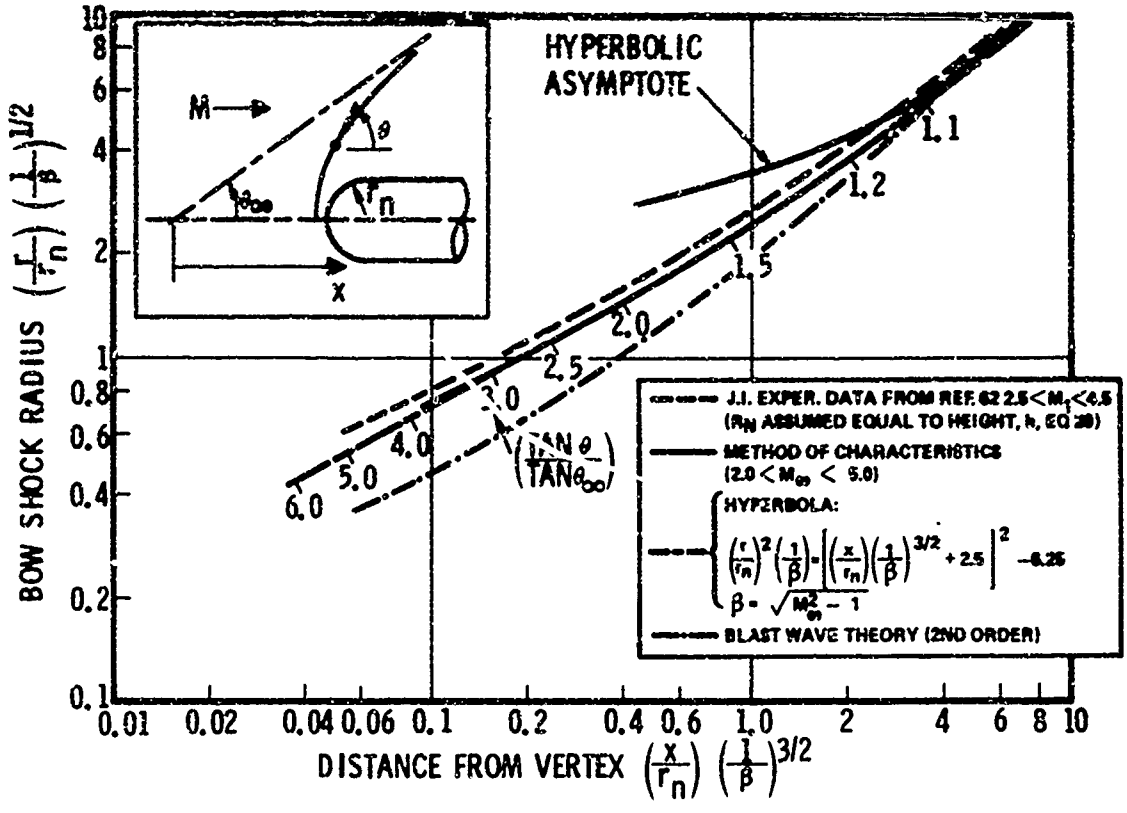

Figure 54. Various Computations of Shock Shapes Compared to Measured Shapes in Meridian Plane, Reference 45

Several sources of experimental data concerning forces induced by circular jets exhausting from flat plates in supersonic flow are available in the literature. The most extensive set of force data is the work of Strike, et al (15, 32, 78). Other data frequently cited are from References 6, 79, and 81. A summary of these data are presented in Figure 55, in the form of amplification factor versus a blockage parameter, $(P_{oj}A_t/q_1)$. Since this parameter is not dimensionless, it is not entirely satisfactory. Data from a given test series show decreasing amplification with increasing jet blowing rate. If the interaction flowfield for external flow conditions were truly self-similar, depending only upon a single length scale proportional to reference value of jet momentum flux, then K would be essentially independent of blowing rate. Data previously cited supports the premise that the observed variations with blowing rate may be an effect of h/δ_1, but probably are not a function of pressure ratio. Although an attempt was made in selecting the data for Figure 55 to include data in which at least most of the interaction region was contained on the plate, effects of plate size cannot be ruled out. Data obtained from experiments with a plate which is not large compared to the extent of the interaction flowfield will always show decreasing amplification with increasing blowing rate. Note that except for the experiments of Amick and Hayes (79), the sizes of plates used to obtain the data of Figure 55 are not greatly different. Data of Figure 55 represent a wide range of external flow conditions, in particular, $3 \leq M_1 \leq 18$. The independent influence of M_1 on K seems to be less than the data scatter or systematic variations resulting from different wind tunnel models, facilities, and instrumentation.

When a jet interaction flowfield occurs in the context of a practical application, the external flow will usually be nonuniform to some degree. If the body is large compared with a characteristic dimension of the interaction region, and if the local radius of curvature of the surface near the nozzle exit is also relatively large, then the degree of nonuniformity of the external flow may be small. Under these conditions, data obtained from experiments with flat plates may provide a good approximation to the actual situation. When the dimensions of the body and of the interaction region are comparable, details of the body geometry can have important effects on the flowfield.

Figure 56 which was taken from a report by Amick, et al (87) shows pressure contours obtained from a wind tunnel test of a body of revolution in which a jet was exhausting from a location near the nose. The model was a sphere-cone-cylinder having an overall length-to-diameter ratio of 7.0, based upon the cylinder diameter. Ambient temperature air was used as the jet gas, and the nominal jet exit Mach number was 3.4, other test conditions are indicated on the figure. A comparison of Figure 56 with Figures 39 and 40 shows considerable qualitative similarity despite the obvious large differences between the two situations. Apparently, results from flat plate experiments can be used to provide at least a qualitative estimate of the flowfield structure in a more complex situation.

An example of force data obtained from the same series of experiments is shown in Figure 57 in the form of amplification factor based on normal force increments versus pressure ratio or jet mass flow rate, for three nozzle locations. Under these conditions, the interaction force always acted in opposition to the jet thrust, almost canceling it at the lowest blowing rates for the jet located nearest the nose. Some insight into this behavior can be gained by re-examining Figure 56. The region of reduced pressure directly downstream of the jet is acting on a portion of the body surface which is roughly parallel to the nozzle exit plane, and provides a large contribution to the interaction force. The high-pressure regions lying downstream and to either side of the nozzle exit are wrapped around the body, so that the contribution of these regions to the interaction force is greatly diminished, relative to a flat plate situation.

SYM	M_∞	Re_L	$\frac{\gamma_{\infty} M_{\infty}}{M_j \gamma_j}$	d	b	A	L	REF NO.
○	3	1.9×10^6	1.0	0.25	8.5	8.0	7.5	16
○	3	1.9×10^6	1.0	0.125	8.5	8.0	7.5	16
□	4	3.5×10^6	1.0	0.125	8.5	8.0	7.5	16
□	4	6.1×10^6	1.0	0.127	5.2	3.82	2.5	79
△	5	2.2×10^6	1.0	0.25	8.5	8.0	7.5	16
△	5	2.2×10^6	1.0	0.125	8.5	8.0	7.5	16
◇	6	5.8×10^6	0.7	0.25	15.0	7.75	10.55	32
◆	8	1.1×10^6	0.4	0.25	15.0	7.75	10.55	32
◆	8	1.6×10^6	0.4	0.25	15.0	7.75	10.55	6
□	10	0.4×10^6	0.1	0.125	24.0	5.7	10.5	76
■	10	0.4×10^6	1.0	0.064	24.0	5.7	10.5	76

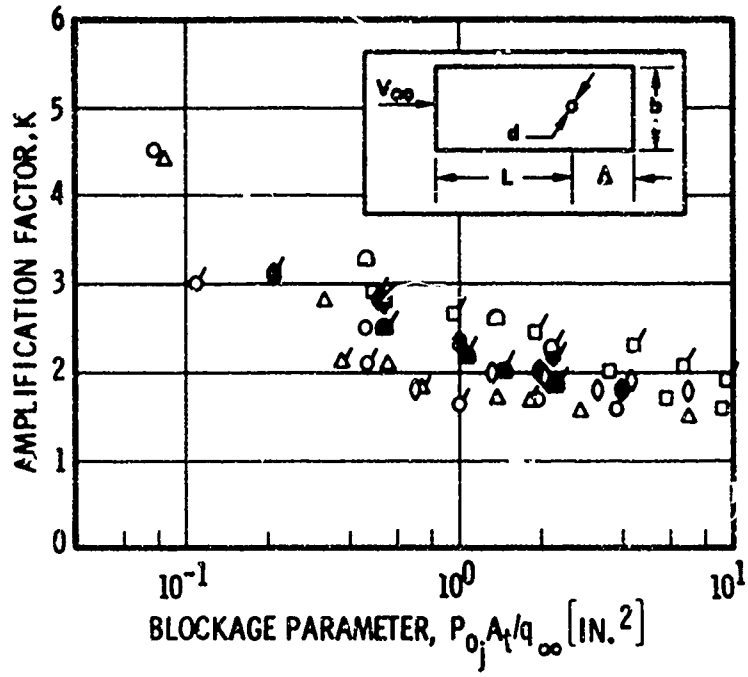

Figure 55. Summary of Amplification Factor Data for Jets from Circular Nozzles

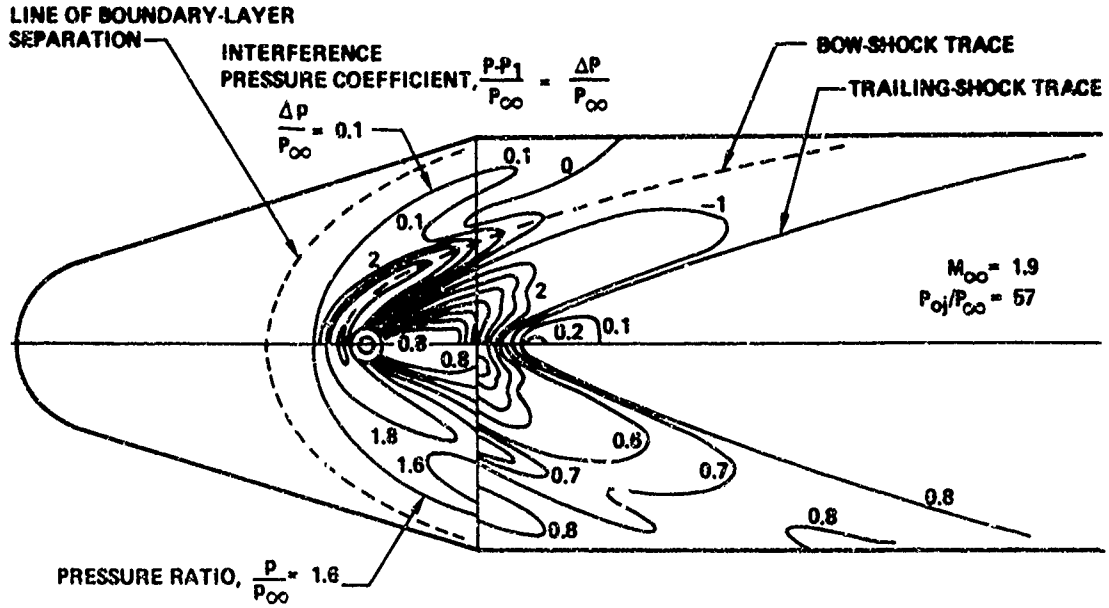

Figure 56. Interference Pressure Contours Near Circular, Sonic Jet Exhausting from Sphere-Cone-Cylinder, Reference 87

Although this review has been restricted almost completely to consideration of jets exhausting normal to the external flow, the introduction of body geometries other than flat plates produces many other possibilities. An extreme example of the influence of body geometry and jet thrust direction on interaction force behavior is illustrated by the data of Figure 58, obtained by Jarvinen, et al (88), from wind tunnel tests of a conical model having a jet exhausting from the nose tip. In this case, the net axial force in the drag direction reached a value of seven times the jet thrust in the direction opposing drag. A large interaction force opposing the drag or jet thrust was observed over a wide range of normalized thrust.

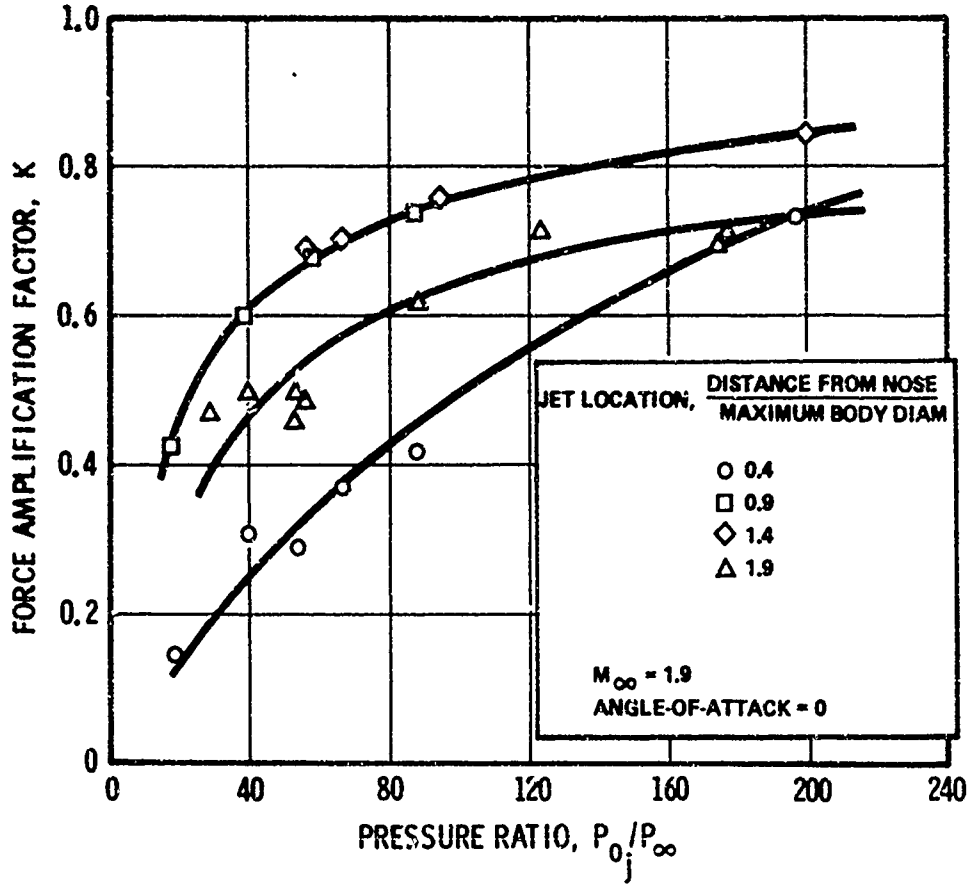

Figure 57. Force Amplification Factor Data for Various Jet Locations in Meridian Plane on Sphere-Cone-Cylinder, Reference 87

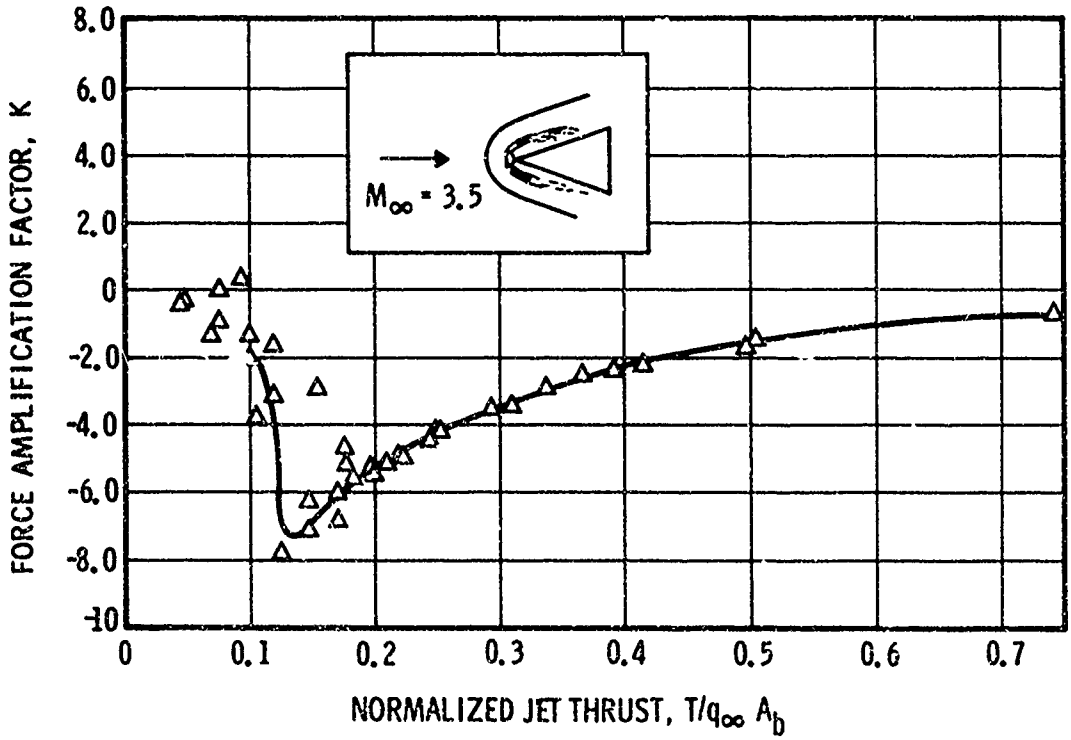

Figure 58. Jet-Flowfield Interference Forces for a Forward-Directed Jet from a Cone, Reference 88

These examples have been chosen to show that there are both similarities and differences between the interactions observed in flat plate experiments and those conducted with other model shapes. A thorough discussion of body configuration effects is beyond the scope of this report. The interested reader will find additional information on this topic in References 9, 45, 46, 55, 60, 74, 76, 79, and 89-94.

4.3 Three-Dimensional Analysis Methods

The three-dimensional jet interaction flowfield may be even more intractable in terms of analytical description than its two-dimensional counterpart, merely because of its three-dimensional nature. On the other hand, because boundary layer separation phenomena seem to play a less prominent role in the three-dimensional case, inviscid three-dimensional flowfield models might offer more promise than inviscid two-dimensional models. At the present time, no attempts have been made to solve the governing conservation equations directly. In discussing the approximate analytical models which have been derived, it is convenient to follow the pattern used in describing the two-dimensional flow models in Section 2 above. Models representing the external flow, and those representing the jet flow will be described separately.

4.3.1 External Flow Models

Broadwell (43) and Dahm (44) have used blast-wave theory to represent the external flow. This approach is subject to the restrictions inherent in the blast-wave approximation mentioned above, namely, large M_1 is required and poor representation is provided for the flow near the nose and near the axis of symmetry. In addition, the intersection of the jet-induced shock with the wall produces a complex three-dimensional separated region which increases the extent of the interaction region and decreases the peak pressures on the wall. Thus, any inviscid approach will be unable to give accurate predictions of static pressure distributions. However, it appears from some comparisons of predictions with data that the effect of separation is to change the static pressure distribution without appreciably altering the total force, so that inviscid calculations may be useful for force predictions. Strike (32) has proposed an analysis in which a contribution to the interaction force from the separated region is estimated and added to the contribution obtained from blast-wave theory.

All other models of the external flow known to the authors replace the jet by an equivalent solid obstacle. This approach can also be used with the blast-wave representation of the external flow, if the drag of the effective solid obstacle is equated to the energy per unit length needed as an input to the blast-wave theory (45). Ferrari (95) has proposed a complex jet interaction analysis in which the jet is treated as an equivalent solid body and the external flow is computed by an approximate, inviscid, three-dimensional blunt body analysis. Cassel, et al (46) have proposed an analysis in which the external flow is computed numerically, using a blunt body solution near the nose of the equivalent body, followed by a method-of-characteristics solution for the supersonic region. At the expense of added complexity, this approach should provide an accurate representation of the assumed physical model. The static pressure distributions on the wall will not be predicted accurately, for the same reasons mentioned earlier, but limited comparisons with experimental force data show reasonable agreement. An analysis by Wu, et al (96) is based on the assumption that the separated boundary layer is tangent to the top of the injectant flow. Flow visualization results indicate that this assumption is realistic only when the scale of the jet penetration is less than the boundary layer thickness.

Other models of the jet interaction flowfield, for example, Zukoski and Spaid (63) and Billig, et al (56) use properties of the external flow only to provide boundary conditions for the jet.

4.3.2 Jet Flow Models

The models of the jet flow proposed by Broadwell and Dahm have already been reviewed in the discussion of the two-dimensional flows. The influence of jet molecular weight and temperature predicted by these methods is not in agreement with most of the data for circular hole jets which indicate that the interaction force is proportional to jet momentum flux. Data presented by Walker, et al (97) were analyzed by Zukoski and Spaid (62, 63). The data are side force measurements obtained from experiments in which various gases were injected into a rocket nozzle. A parameter derived from Broadwell's analysis was shown to provide a much better correlation of these data than a parameter which is proportional to jet momentum flux. This result indicates that the jet flow model of Broadwell or Dahm may be useful when the region far downstream of the jet exit is of primary importance. In a variation of Dahm's analysis, Strike (32) has proposed a model in which the drag or energy per unit length corresponding to the jet flow is simply equal to $\dot{m}_j V_\infty$. This approach predicts that the interaction force will be proportional to jet mass flow rate, for situations in which T_{o_j} or m_j are varied. This prediction is not in agreement with results of numerous experiments.

Most of the remaining models of the jet flow assume that no mixing takes place between the jet and the external stream during the turning process. The remarks from the discussion of two-dimensional flow theories apply here as well, with appropriate modifications for the conversion from two-dimensional to three-dimensional flow. In this case, we find $h/d \sim (P_{o_j}/P_1)^{1/2}$, various predictions concerning the influence of γ_j, and no explicit dependence upon jet temperature or molecular weight.

4.3.3 Matching Between the External Flow and the Jet

As in the two-dimensional case, the matching condition between the jet and the external flow is of primary importance in determining the influence of M_1 predicted by the various analyses. In the control-volume and jet-shock models of the jet flow (corresponding to Categories 2 and 3 in the two-dimensional discussion), it is often assumed that the average pressure acting on the upstream boundary of the jet is proportional to the stagnation point pressure coefficient of the external flow, C_p^*. A similar assumption is made by Billig, et al (56), namely, that the effective back pressure which fixes the Mach disk location in the jet is two-thirds of the stagnation pressure downstream of a normal shock in the external flow. These assumptions seem plausible, based upon observations of Schlieren and shadowgraph photographs. They are also supported somewhat by the correlations of static pressure distributions presented in Figure 42, by the correlation of shock shapes of Figure 54, and the correlation of jet shock locations presented in Reference 56.

Because of the qualitative differences between flows in which $M_e = 1$ and $M_e > 1$, accurate theoretical prediction of the effect of M_e would seem to require an analysis in which the details of the jet expansion and turning process are computed. The physical model of Ferrari (95) might be applicable when $M_e > 1$, although the method does not include the possibility of shock waves in the jet. Probably because of its complexity, few comparisons have been made between Ferrari's theory and experiments. The method of Billig, et al (56) uses empirical correlations to account for variations in M_e, as discussed previously. This analysis provides a prediction of the jet trajectory. Application of the equivalent body concept to determine the influence of M_e on the external flow would require calculation of the flow about a truly three-dimensional body. None of the available equivalent solid obstacle models would warrant the effort required to develop such a calculation technique since they all include assumptions which neglect mixing.

In view of the complexities of the flowfield and the drastic simplification or arbitrary assumptions which are necessary in order to formulate an analysis, detailed predictions of the various theories should probably not be viewed as attempts at exact representations. However, if characteristics of one flowfield are known from experiment, then it should be possible to predict the characteristics of another within some limited range of the independent variables. Based on the preceding discussion, it appears that this can be done by assuming that the boundaries of the two flows are geometrically similar, and that the linear dimensions of each flowfield are proportional to a characteristic length, h, where

$$h \sim \frac{d}{M_1}\left(\frac{P_{o_j}}{C_P^* P_1}\right)^{1/2} \tag{24}$$

Some idea of the limitations of this method can be obtained by referring to the preceding data presentation. The available data indicate that:

1. Effects of variations in M_1 or M_e are not predicted with great precision by this (or any other) technique.

2. The boundary-layer thickness can be an important characteristic length, if it is comparable to other important dimensions of the flowfield.

3. There are qualitative differences between interactions in which the boundary layer is turbulent and those in which it is laminar.

4. Effects of wide variations in injectant molecular weight and stagnation temperature on details of injectant concentration profiles or on forces generated far downstream of the nozzle exit are not well correlated by this method.

5 SONIC AND SUPERSONIC JETS IN SUBSONIC EXTERNAL FLOWS

When the Mach number of the external flow is substantially less than unity, the dynamic pressure of the external flow is much smaller than the static pressure. As a result, the jet flow near the nozzle exit is influenced primarily by P_1. Flow visualization data indicate that, insofar as internal shocks are concerned, jets penetrating in a subsonic cross flow behave as if they were exhausting into still air (66), significant turning of the jet by the external flow does not appear to take place until the jet has become subsonic.

For jets from sonic nozzles exhausting into still air, Christ et al (64) have correlated experimental values of the distance from the nozzle exit to the mach disk, h, for a wide range of pressure ratio. The data fit the empirical equation:

$$h/d = 0.695\,(P_{o_j}/P_1)^{1/2} \tag{25}$$

It has been shown by Durando and Cassel (76, 89) that this characteristic dimension provides satisfactory correlation of the limited body of relevant data. A summary of these results will be presented here. Although this equation does not strictly apply to a diamond shock pattern or a supersonic nozzle, data indicate that the scale of the interference flowfield is proportional to $d\,(P_{o_j}/P_1)^{1/2}$ for a fixed jet Mach number.

In discussing pressure patterns produced by a jet on the surface from which it exhausts, it is common practice to plot the conventional pressure coefficient

$$C_p = \frac{P - P_\infty}{q_\infty}$$

where

$$q_\infty = \frac{\rho_\infty V_\infty^2}{2} = \frac{\gamma}{2} P_\infty M_\infty^2 \text{ is the freestream dynamic pressure.}$$

It has been found, however, that use of this pressure coefficient is very misleading, for the following reason. When the freestream velocity is zero, the jet entrainment effect produces a small interference pressure distribution on the plate. Therefore, as $q_\infty \to 0$, the conventional pressure coefficient becomes singular. For low freestream velocities, interference pressure coefficients are unrealistically high. These extremely large Cp's do not translate into a large interference force, and it would certainly be unreasonable to expect the largest interference effects to occur at zero freestream velocity.

For the present purposes, a more useful method of presenting static pressure data is to plot

$$C_{p_\infty} = \Delta P / P_\infty$$

where ΔP is the difference between the jet-on and jet-off static pressure. In this section, differences between P_∞ and P_1 are very small and these quantities will be used interchangeably.

5. 1 Jets from Flat Plates

The data which provide the most detailed information on interference effects produced by sonic, underexpanded jets exhausting from flat surfaces in subsonic external flows have been reported by Street (98). Results for $M_1 = 0.6$ are presented in Figure 59 through 61, in the form of C_{p_∞} vs the normalized radius

$$\bar{r} = \frac{r}{d(P_{o_j}/P_1)^{1/2}}$$

for three values of the polar angle around the nozzle. A sketch of the polar coordinate system used is shown in the insert of Figure 59. It is evident that the correlation works well, except for a portion of the $\alpha = 180$ degrees ray immediately adjacent to the nozzle (Figure 61). Additional data which have been correlated in this manner are presented in References 76 and 89.

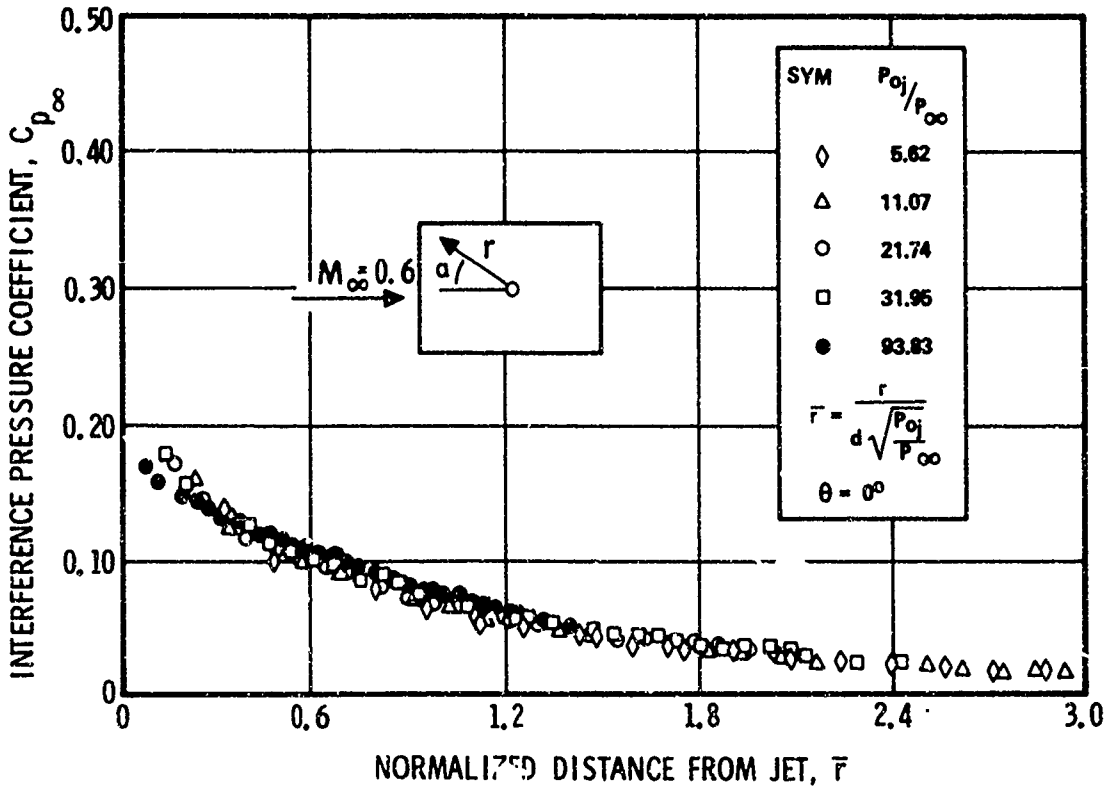

Figure 59. Correlated Pressure Distribution for Circular Nozzle Jet in Subsonic Flow, $\alpha = 0^0$ Ray, Data from Reference 98

Interference pressure contours are presented in Figure 62 and 63 for some of the test conditions of Reference 98. The figures are shown in order of increasing Q, where $Q = q_j^*/q_\infty$, at an approximately constant value of the pressure ratio. It is evident from the figures that the scale of the pressure disturbance is considerably larger than the nozzle diameter. As Q increases, the pattern becomes more symmetric fore and aft The upstream region of positive C_{p_∞} shrinks in size in Figure 62b, and finally disappears in Figure 63 The magnitude of the pressures decreases as Q increases, indicating a reduction of interference effects as the plume becomes straighter. The predominance of regions of negative C_{p_∞} at low external flow Mach numbers is caused by entrainment of freestream flow by the jet, through the turbulent mixing process. The entrained mass must be replaced by a flow from the surroundings toward the jet. This flow is irrotational, outside of the wall boundary layer, so it must be associated with a region of negative C_p on the wall near the jet. As external stream velocity increases, the blockage effect of the jet becomes increasingly important, resulting in positive pressure coefficients in the upstream region. Even though the scale of the interference flowfield under certain conditions depends only on the pressure ratio, the pressure contours of Figures 62 and 63 show that the flowfield itself depends upon the freestream velocity.

5 2 Jets from a Body of Revolution

Reference 76 contains interference pressure data for an underexpanded jet exhausting just forward of the nose juncture from an ogive-cylinder configuration The configuration was tested with one circular nozzle and one slot nozzle, both of which were sonic. Data included forces and moments on the model and the pressure distribution in the neighborhood of the nozzle.

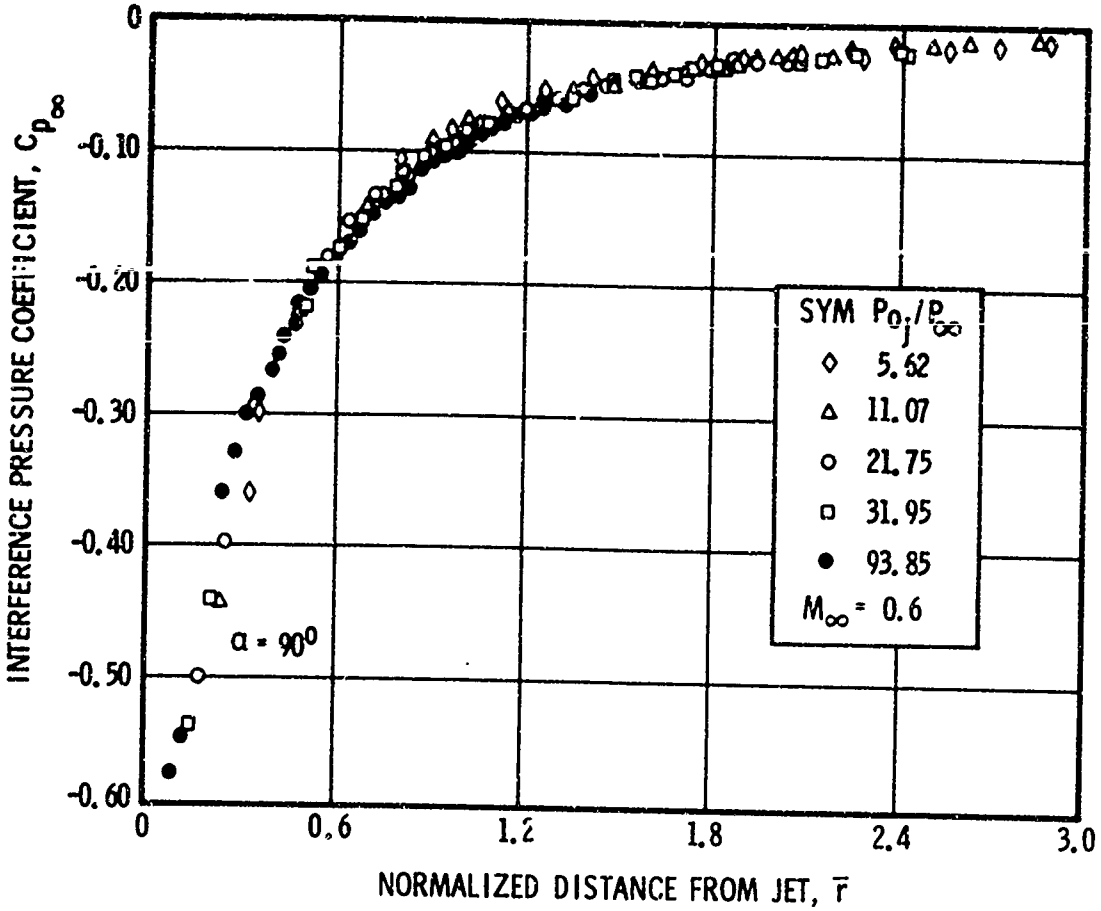

Figure 60. Correlated Pressure Distribution for Circular Nozzle Jet in Subsonic Flow, $\alpha = 90^0$ Ray, Data from Reference 98

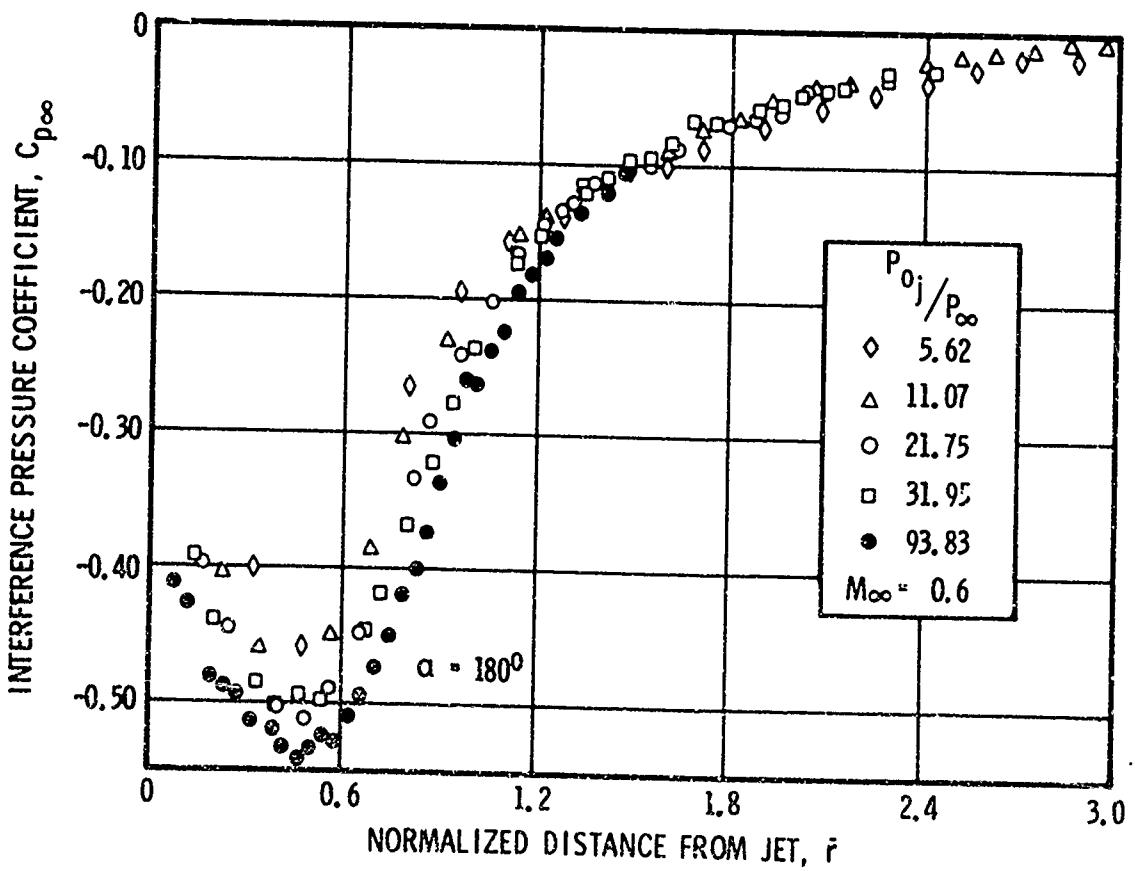

Figure 61. Correlated Pressure Distribution for Circular Nozzle Jet in Subsonic Flow, $\alpha = 180^0$ Ray (Downstream), Data from Reference 98

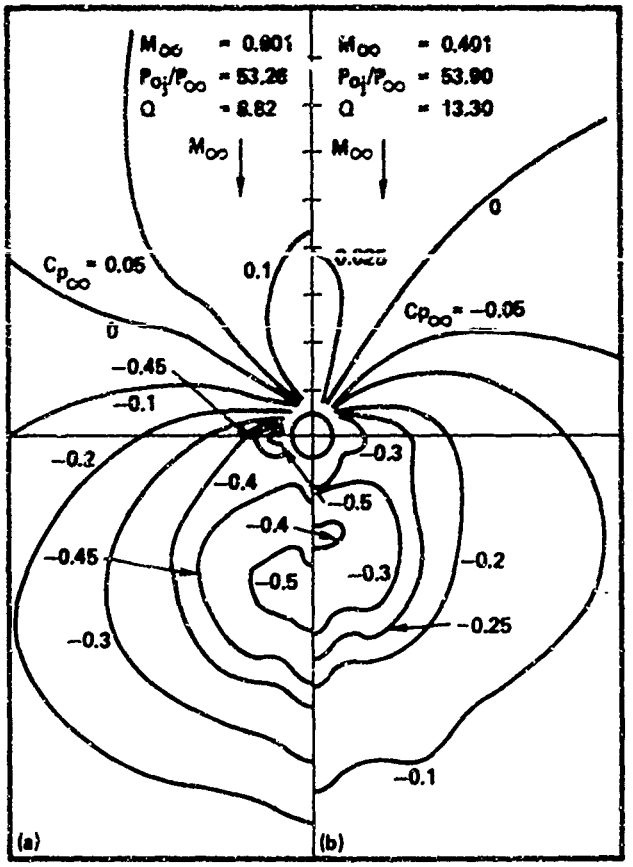

Figure 62. Pressure Coefficient Contours for a Sonic Jet Exhausting from a Flat Plate into Subsonic Flow, Data from Reference 98

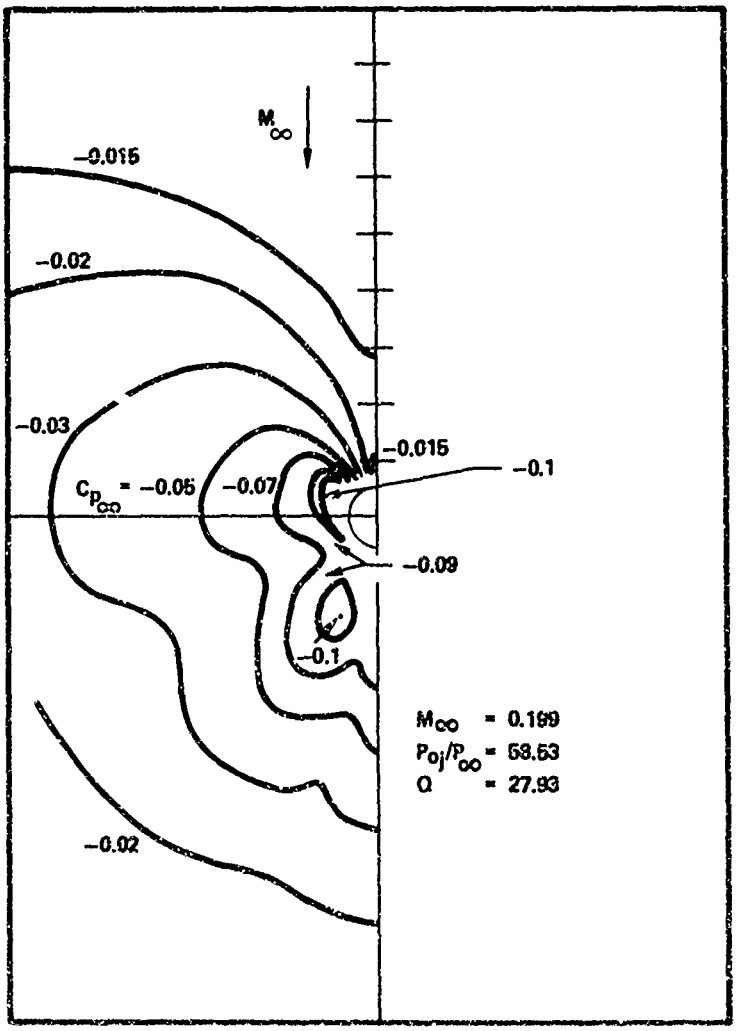

Figure 63 Pressure Coefficient Contours for a Sonic Jet Exhausting into a Low Velocity Stream, Data from Reference 98

Using the coordinate system shown in the insert on Figure 64a, pressure coefficients along the plane of symmetry (S = 0) are plotted in Figure 64 for one value of the freestream Mach number and various pressure ratios. In this case, the pressure coefficient has been defined in the conventional manner:

$$C_P = \frac{P - P_\infty}{q_\infty}$$

Although the nozzle was not quite located on the cylindrical portion of the model, the effects of curvature have been neglected and x has been assumed to be equal to the distance along the model axis. Also, the jet-off pressure distribution has not been subtracted out so that the Cp shown in Figure 64a is not strictly an interference pressure coefficient. The data show that the jet-off Cp is very small and has a negligible effect on the curves of Figure 64a. These curves exhibit the characteristic positive pressure coefficients on the windward ($x < 0$) side, with large negative pressure coefficients on the leeward ($x > 0$) side.

Figure 64b shows the same data as Figure 64a, but with x scaled by the shock intersection height, h, from Equation (25). Evidently, the data for all pressure ratios fall on a single curve. Data for a larger diameter nozzle (d = 0.33 inch) are also included in the figure, and the points correlate well with data for d = 0.22 inches. Figure 65 shows the same data correlation for cases when the freestream Mach number is 0.20. Note that in this case, Cp is negative upstream as well as downstream of the nozzle. The data for $M_\infty = 0.20$ have also been correlated along the line x = 0, in Figure 65. In that correlation, the abscissa represents the arc length $S = R\psi$ normalized by h.

An attempt at correlating pressure distributions obtained with the slot nozzles at the same freestream Mach numbers and different values of the pressure ratio by scaling distances along the ogive cylinder plane of symmetry by h given by Equation (25) is shown in Figure 66. Evidently, the correlation is not successful. The quantity d here represents the throat chord for the transverse slot nozzle. A formula for the Mach disk height should vary directly with P_{o_j}/P_∞. Attempts at using this formula to correlate the slot data described above were also unsuccessful. Indeed, it appears that no power of P_{o_j}/P_∞ between 1 and 1/2 will correlate the pressure distribution. The success of the correlation technique for a circular nozzle and its failure for the slot nozzle lies in the influence of edge effects in the case of the slot nozzle. These effects are described by Durando and Cassel (89).

5.3 Vortices Induced in a Jet

With the exception of truly two-dimensional flow, vortices are produced in the jet when it is turned by the external flow. Durando (75, 77) has proposed an analysis describing this vortex field when the external flow is subsonic. The analysis is semi-empirical, using data on jet vortices reported by Dahlke (91). It utilizes the assumption that the product of vortex strength and separation is a constant. In Durando's analysis, it is also assumed that an underexpanded jet can be related to an equivalent subsonic jet by the relation

$$d\,(\text{equiv}) = A d\,(P_{o_j}/P_\infty)^{1/2}$$

where A is an empirical constant. The predicted influence of downstream distance, pressure ratio, and orifice diameter on the vortex strength, Γ, is given by Durando as

$$\Gamma \sim \frac{d^{1.28}}{x^{0.28}} \left(\frac{P_{o_j}}{P_1}\right)^{0.64} \tag{26}$$

As shown in Reference 76, the relationship is supported by existing data.

6 SUMMARY AND CONCLUSIONS

The jet interaction flowfield is so complex that predictions of induced forces, pressure distributions, concentration distributions, etc., must rely heavily on experimental data. Accurate predictions concerning situations which lie far outside the range of available data will require additional experimentation. The simulation requirements for these experiments have been discussed in Section 2.2. Interpolation or extrapolation of data implies that the appropriate scaling laws are known. It is convenient to discuss two- and three-dimensional flows separately.

The region upstream of a jet in two-dimensional flow is quite similar to the flow upstream of a forward-facing step, except for the immediate vicinity of the jet or step. The equivalent step height is approximately proportional to the ratio of a reference value of jet momentum flux to the external flow dynamic pressure. This scaling law is subject to many restrictions and exceptions; however, many theories contain this basic idea, although it is not always explicitly stated. Two of the proposed methods for estimating the equivalent step height, when the upstream boundary layer is turbulent, are given by Equations (14) and (19). Pressure distributions and forces in this region can be estimated from correlations of data obtained from experiments in which separation was produced by either jets or steps, such as those of Figures 8 and 9, see also Equations (1), (2), and (3). When the upstream boundary layer is turbulent, the wall static pressure distribution is a function primarily of the Mach number of the external flow, the boundary layer thickness, and the effective step height. Static pressure distributions in the downstream region are not as well correlated as in the upstream region, as shown in Figures 10, 11, and 12. The forces induced upstream of two-dimensional jets have been the subject of many investigations. The largest values of upstream amplification factor are associated with low Reynolds number, laminar flow, low blowing rates, and upstream-inclined jets, as shown in Figure 24. Upstream amplification factors produced by underexpanded, normal, sonic jets in turbulent flow lie between approximately 2 and 3 for a wide range of external flow Mach and Reynolds numbers. Many analyses have been

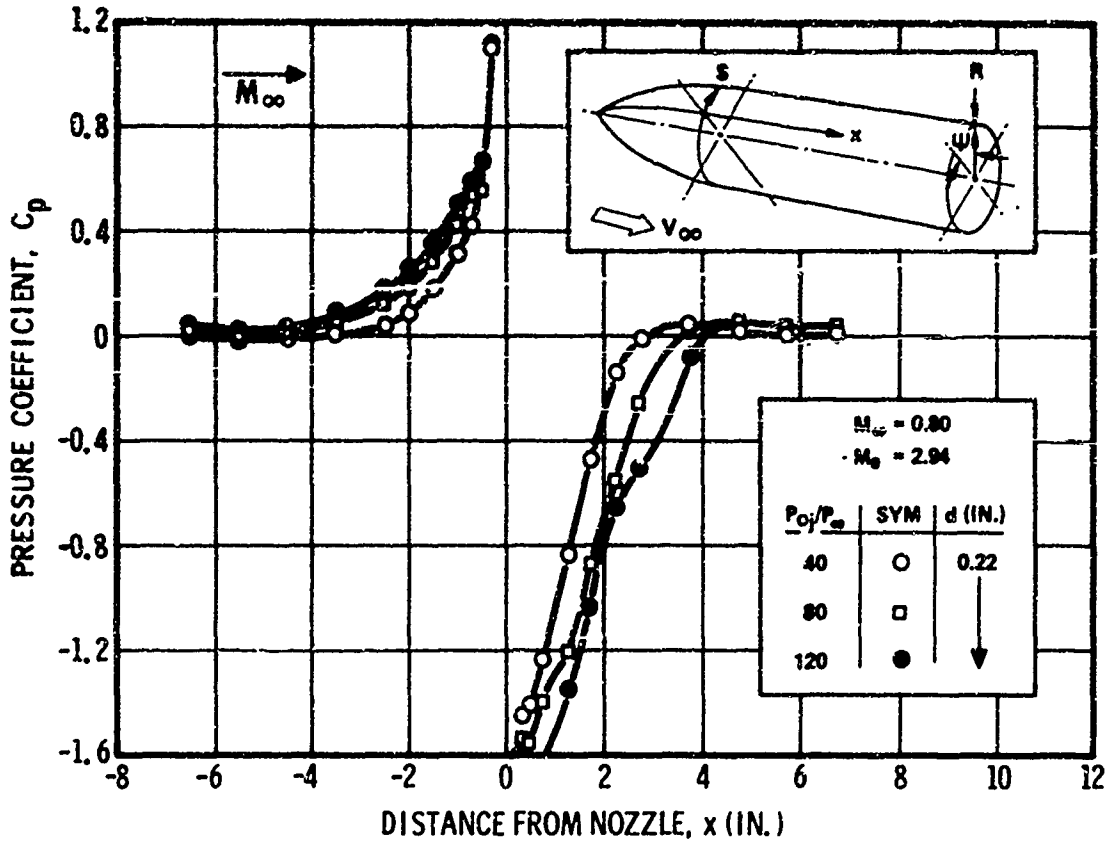

(a) UNCORRELATED MEASUREMENTS

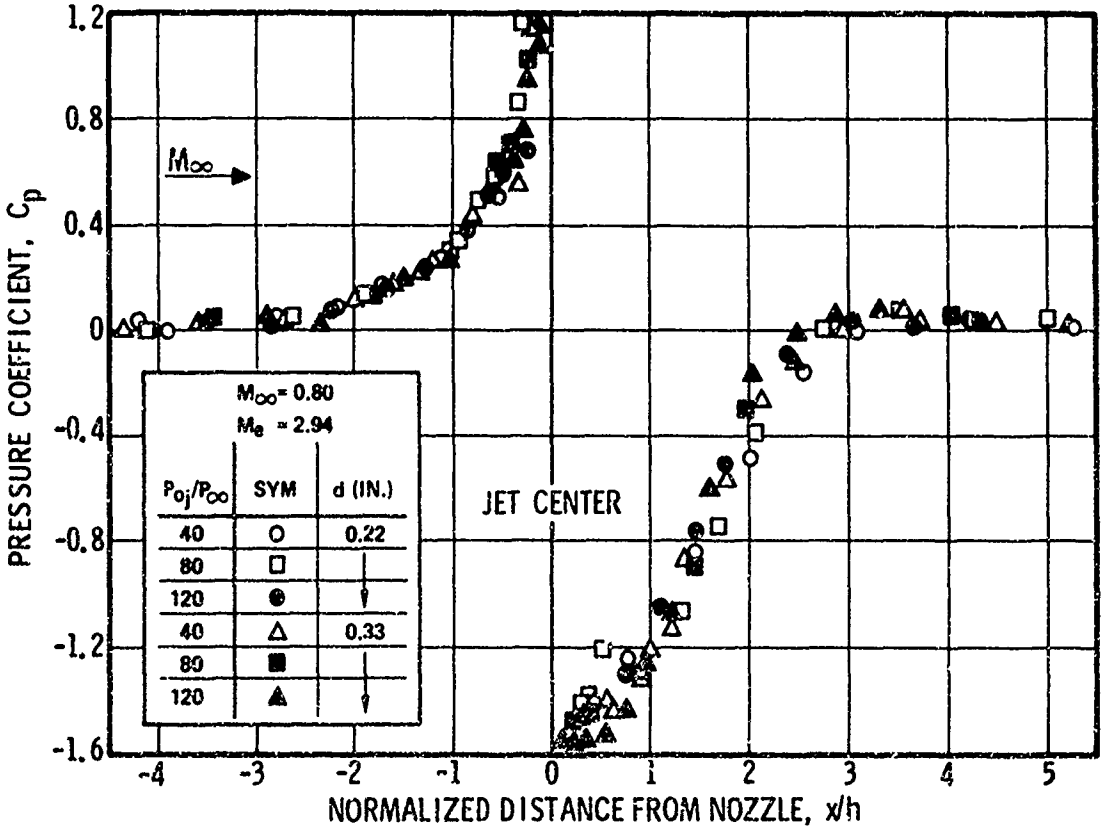

(b) CORRELATION WITH PENETRATION HEIGHT

Figure 64 Interference Pressures in Meridian of Ogive Cylinder with Normal Supersonic Jet in Subsonic Flow, Reference 76

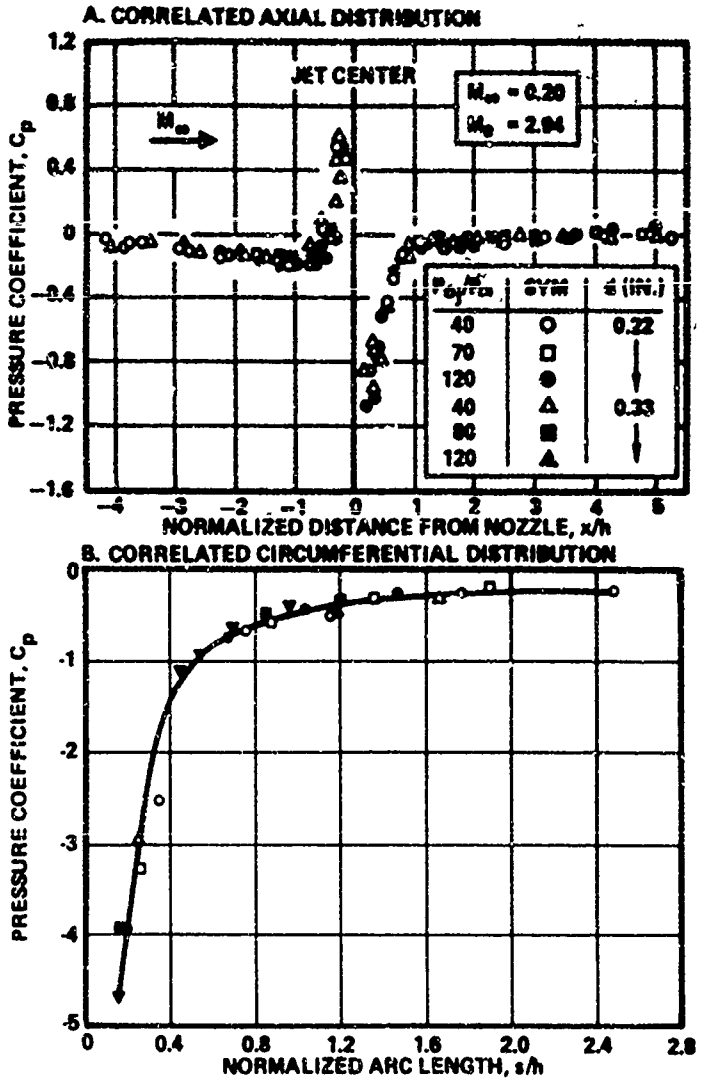

Figure 85. Correlation of Interference Pressures Due to Circular Supersonic Jet from Ogive Cylinder in Low Subsonic Flow

proposed for the prediction of induced forces in this situation, the results of which are compared with data in Figure 27. The inconsistencies to be found among nominally very similar experiments preclude the possibility of recommending a "best" analysis; several of the proposed methods give results which seem consistent with the data.

The contribution to interaction force by pressures downstream of the two-dimensional jet at supersonic Mach numbers less than about 4 or 5 acts in the direction opposite to that of the jet thrust, a situation which is normally regarded as unfavorable interference. At higher Mach numbers, a significant positive contribution to the interaction force can come from the downstream region, as shown in Figure 22 and by the static pressure correlations of Figures 10, 11, and 12.

The flowfield associated with a jet from a finite-span slot is a function of the ratio of effective step height to slot span Situations in which this ratio is small enough that even the central portion is nearly two-dimensional are seldom found in practice because significant lateral flows occur in the upstream recirculation region even at relatively small values. The bow shock wave formed upstream of the jet in this situation wraps around the ends of the jet, and produces regions of increased wall static pressure downstream and to either side of the jet nozzle exit. This effect can provide a significant contribution to the interaction force, and becomes the dominant mechanism in the case of a jet from a circular nozzle.

The interference flow associated with a jet from a circular nozzle in a flat plate has some of the characteristics of the flow past a blunt nosed slender body. The main features of this type of flowfield are controlled to a much smaller extent by separation than in the two-dimensional case. Predictions of flowfield features such as shock shapes, distributions of pressure and injectant concentration and induced forces can best be made by interpolation or extrapolation of data. The first order scaling law for the three-dimensional flowfield is the axisymmetric analog of the two-dimensional one, namely, the effective bluntness dimension associated with the jet is proportional to the square root of the ratio of a reference value of jet momentum flux to the freestream dynamic pressure, see Equation 24. A variation of this technique has been reasonably successful in correlating shock shapes, as shown in Figure 54. Wall static pressure data have been correlated fairly well by this method, see Figures 42 and 44, but variations in Mach number, state and relative thickness of the boundary layer, and injectant molecular weight or temperature also are important. A summary of induced force measurements is given in Figure 55. The most important variable may be the scale of the disturbance produced by the jet relative to the plate size or boundary layer thickness.

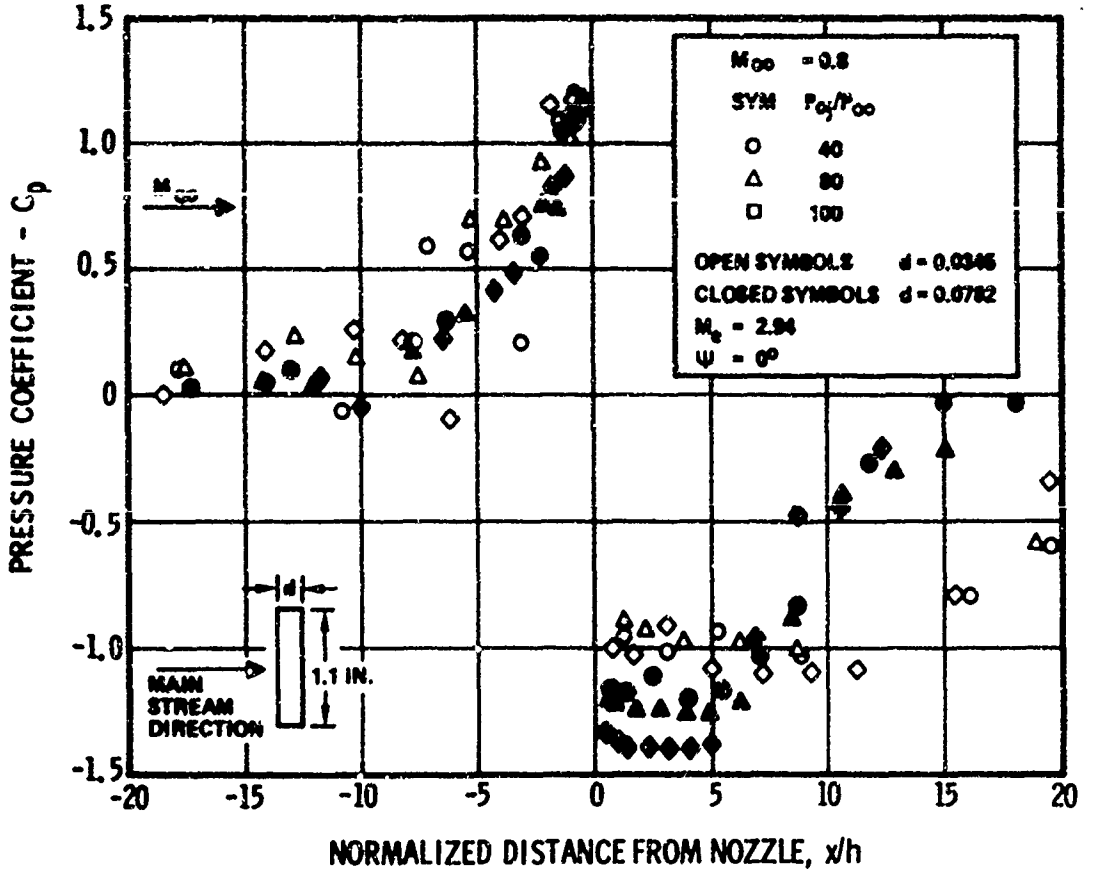

Figure 66. Interference Pressures Due to Rectangular Supersonic Jet Exhausting from Ogive Cylinder in Subsonic Flow, Reference 65

When the external flow is subsonic, entrainment of mass from the external flow by the jet is an important effect, which tends to induce negative pressure coefficients near the nozzle exit when the external flow velocity is low. At subsonic Mach numbers significantly less than unity, the static pressure replaces the dynamic pressure as the most important quantity which characterizes the external flow, and the characteristics dimension of the flow field is proportional to the square root of the pressure ration, as shown in Section 5.0

A few examples of data for jets exhausting from bodies of revolution are also included. It is shown that interference forces can be quite sensitive to the geometry of the body from which the jet exhausts. Even on a simple body of revolution in axisymmetric flow, the interference pressure distribution is quite sensitive to the shape of the jet exit, as shown by comparing Figures 65 and 66.

A phenomena associated with jet interaction which can be quite significant in some practical applications has received little attention. The far wake of the interaction includes a vortex field which can have significant effects when lifting surfaces are located downstream of jet controls. Limited investigations of the phenomena are discussed in Section 5.3.

REFERENCES

1. Mitchell, J. W., "An Analytical Study of a Two-Dimensional Flow Field Associated with Sonic Secondary Injection into a Supersonic Stream," Technical Note 9166-TN-2, Vidya Corp., March 1964.

2. Romeo, D. J., and J. R. Sterrett, "Aerodynamic Interaction Effects ahead of a Sonic Jet Exhausting Perpendicularly from a Flat Plate into a Mach Number 6 Free Stream," TN D-743, April 1961.

3. Spaid, F. W and E. E. Zukoski, "A Study of the Interaction of Gaseous Jets from Transverse Slots with Supersonic External Flows," AIAA Journal, Vol. 6, No. 2, February 1968, pp. 205-212.

4. Kistler, A. L., "Fluctuating Wall Pressure Under A Separated Supersonic Flow," J. Acoust. Soc. Am., Vol. 36, No. 3, March 1964, pp. 543-550.

5. Speaker, W. V., and C. M. Ailman, "Spectra and Space-Time Correlations of the Fluctuating Pressures at a Wall Beneath a Supersonic Turbulent Boundary Layer Perturbated by Steps and Shock Waves," Report SM-49806, November 1965, McDonnell Douglas Corporation, Huntington Beach, California.

6. Barnes, J. W., J. G. Davis, and H. H. Tang, "Control Effectiveness of Transverse Jets Interacting with a High-Speed Free Stream," Vol. I, Design Charts, Theoretical and Experimental Results, AFFDL-TR-67-90, Vol. I, Air Force Flight Dynamics Lab., Wright Patterson Air Force Base, Ohio, July 1967.

7. Driftmyer, R. T., "The Shock Heights of Static Free Jets," NOLTR 72-23, United States Naval Ordnance Laboratory, White Oak, Silver Spring, Maryland, January 1972.

8. Emmons, H. W., Ed., "Fundamentals of Gas Dynamics, Vol. III, High Speed Aerodynamics and Jet Propulsion," Princeton University Press, 1958.

9. Morkovin, M. V., C. A. Pierce, and C. E. Craven, "Interaction of Side Jet with a Supersonic Main Stream," Engineering Research Institute Bulletin, No. 35, University of Michigan, 1952.

10. Thayer, W. J., "The Two-Dimensional Separated Flow Region Upstream of Inert and Chemically Reactive Transverse Jets," DI-82-1066, Boeing Scientific Research Laboratories, Seattle, Washington, March 1971.

11. Shreeve, R. P., "An Investigation of a Supersonic Surface Jet—Hypersonic Flow Interaction with Axial Symmetry," DI-82-0999, Boeing Scientific Research Laboratories, Seattle, Washington, September 1970.

12. Werle, M. J., "A Critical Review of Analytical Methods for Estimating Control Forces Produced by Secondary Injection," NOLTR-68-5, United States Naval Ordnance Laboratory, White Oak, Maryland, January 1968.

13. Driftmyer, R. T., "An Experimental Study of Two-Dimensional, Turbulent Boundary Layer Separation Due to Steps and Interacting Jets," Proceedings of the 9th U. S. Navy Symposium on Aeroballistics, Vol. 1, Paper No. 24, September 1972, Applied Physics Laboratory, The Johns Hopkins University, Silver Spring, Maryland.

14. Spaid, F. W., "Two-Dimensional, Experimental Jet Interaction Studies at High Reynolds Numbers and Low Mach Numbers," McDonnell Douglas Paper, to be published.

15. Strike, W. T., C. J. Schueler, and J. S. Deitering, "Interactions Produced by Sonic Lateral Jets Located on Surfaces in a Supersonic Stream," AEDC-TDR-63-22, Arnold Engineering Development Center, Arnold Air Force Station, Tennessee, April 1963.

16 Spaid, F. W., "Two-Dimensional, Experimental Jet Interaction Studies at High Reynolds Numbers and High Mach Numbers," McDonnell Douglas Paper, to be published.

17. Sterrett, J. R , and J. B. Barber, "A Theoretical and Experimental Investigation of Secondary Jets in a Mach 6 Free Stream with Emphasis on the Structure of the Jet and Separation Ahead of the Jet," Separated Flows, Part II, AGARD Conference Proceedings, No. 4, May 1966.

18. Heyser, A., and F. Maurer, "Experimental Investigations on Solid Spoilers and Jet Spoilers at Mach Numbers of 0.6 to 2.8," Transl. 32, Jet Propulsion Laboratory, California Institute of Technology, February 1964; also Zeitschrift Flur Flugwissenchaften, Vol. 10, 1962, pp. 110-130.

19. Gray, J. D., and R. W. Rhudy, "Investigation of Flat-Plate Aspect Ratio Effects on Ramp-Induced, Adiabatic, Boundary-Layer Separation at Supersonic and Hypersonic Speeds," AEDC-TR-70-235, Arnold Engineering Development Center, Arnold Air Force Station, Tennessee, March 1971.

20. Todisco, A., and Reeves, B. S., "Turbulent Boundary Layer Separation and Reattachment at Supersonic and Hypersonic Speeds," Proceedings of Viscous Interaction Phenomena in Supersonic and Hypersonic Flow, Hypersonic Research Lab., ARL, University of Dayton Press, Dayton, Ohio, 1969.

21. Elfstrom, G. M., "Turbulent Hypersonic Flow at a Wedge-Compression Corner," Journal of Fluid Mechanics, Vol. 53, May 1972, pp. 113-127.

22. Holden, M. S., "Shock Wave-Turbulent Boundary Layer Interaction in Hypersonic Flow," AIAA Paper No. 72-74, San Diego, California, 1972.

23. Zukoski, E. E., "Turbulent Boundary-Layer Separation in Front of A Forward-Facing Step," AIAA Journal, Vol. 5, No. 10, October 1967, pp. 1746-1753.

24. Chapman, D. R., D. M. Kuehn, and H. K. Larson, "Investigation of Separated Flows in Supersonic Streams with Emphasis on the Effect of Transition," Report 1356, NASA, 1958.

25. Werle, M. J., R. T. Driftmyer, and D. G. Shaffer, "Jet-Induced Separation: The Two-Dimensional Problem," AIAA Journal, Vol 10, No. 2, February 1972, pp. 188-193.

26. Reeves, B. L., "Plateau Pressure in Hypersonic Turbulent Boundary-Layer Interactions," AIAA Journal, Vol. 10, No. 11, November 1972, pp. 1546-1548.

27. Hill, W. G., Jr., "Analysis of Experiments on Hypersonic Flow Separation Ahead of Flaps Using a Simple Flow Model," Grumman Aircraft Engineering Corporation, Bethpage, New York, November 1967.

28. Kaufman, L. G., II and F. Koch, II, "High Speed Flows Past Transverse Jets," RE-348, Grumman Aircraft Engineering Corporation, Bethpage, New York, October 1968.

29. Tang, H. H., C. P. Gardiner, and J. W. Barnes, "Jet-Mixing Theory, Extensions, and Applications in Separated Flow Problems," DAC-59181, McDonnell Douglas Astronautics Company, Huntington Beach, California, February 1967.

30. Werle, M. J., R. T. Driftmyer, and D. G. Shaffer, "Supersonic Two-Dimensional Jet Interaction Studies," NOLTR 70-242, United States Naval Ordnance Laboratory, White Oak, Maryland, December 1970.

31. Maurer, F., "Three-Dimensional Effects in Shock-Separated Flow Regions Ahead of Lateral Control Jets Issuing from Slot Nozzles of Finite Length," AGARD Conference Proceedings No. 4, Part II, May 1966.

32. Strike, W. T., Jr., "Analysis of the Aerodynamic Disturbances Generated on a Flat Plate Containing Lateral Jet Nozzles Located in a Hypersonic Stream," AEDC-TR-67-158, Arnold Engineering Development Center, Arnold Air Force Station, Tennessee, January 1968.

33. Kaufman, L G . II, "Hypersonic Flows Past Transverse Jets," Journal of Spacecraft and Rockets, Vol. 4, No. 9, September 1967, pp. 1230-1235.

34 Spaid, F. W., "A Study of Secondary Injection of Gases into a Supersonic Flow," Ph. D Thesis, California Institute of Technology, June 1964

35. Buffum, F. G., Jr., E. W Price, and R. O. Slates, "An Experimental Investigation of the Flow Phenomena Involved in Gaseous Thrust Direction Control Devices," U. S. Naval Ordnance Test Station, China Lake, California. Prepared for the Sixth U. S. Symposium of Aeroballistics, David Taylor Model Basin, Washington, D. C., October 31 through November 1, 1963.

36. Thayer, W. J., and R. C. Corlett, "An Investigation of Gas Dynamic and Transport Phenomena in the Two-Dimensional Jet Interaction Flowfield," AIAA Paper 710561, Palo Alto, California, June 1971.

37. Hawk, N. E. and J L Amick, "Two-Dimensional Secondary Jet Interaction with a Supersonic Stream," AIAA Journal Vol 5, No 4, April 1967, pp. 655-660.

38 Cooper, W R., "Side Forces Resulting from Forward-Facing Steps and Injection through a Slot in a Supersonic Flow," M. E. Thesis, California Institute of Technology, June 1965.

39. Werle, M. J., R. T Driftmyer, and D. G. Shaffer, "Two-Dimensional Jet Interaction with a Mach 4 Mainstream," NOLTR 70-50, United States Naval Ordnance Laboratory, White Oak, Maryland, May 1970.

40. Sterrett, J. R., J B Barber, D. W. Alston, and D. J. Romeo, "Experimental Investigation of Secondary Jets from Two-Dimensional Nozzles with Various Exit Mach Numbers for Hypersonic Control Application," TN-D-3795, NASA, January 1967.

41. Zakkay, V., J. Erdös, and W. Calarese, "An Investigation of the Interaction Between a Transverse Sonic Jet and a Hypersonic Stream," NYU-AA-68-27, New York University, New York, August 1968.

42. Lee, C. G. and B. F. Barfield, "Interaction of Sonic Transverse Jets with Supersonic External Flows," AIAA Journal, Vol. 9, No. 2, February 1971, pp. 304-308.

43. Broadwell, J. E., "Analysis of the Fluid Mechanics of Secondary Injection for Thrust Vector Control," AIAA Journal, Vol. 1, No. 5, May 1963, pp. 1057-1075.

44. Dahm, T. J., "The Development of an Analogy to Blast-Wave Theory for the Prediction of Interaction Forces Associated with Gaseous Secondary Injection into a Supersonic Stream," Tech Note 9166-TN-3, Vidya Division of Itek Corp., May 1964.

45. Cassel, L. A., J. G. Davis, and D. P. Engh, "Lateral Jet Control Effectiveness Prediction for Axisymmetric Missile Configurations," RD-TR-68-5, U. S. Army Missile Command, Redstone Arsenal, Alabama, June 1968.

46. Vinson, P. W., J. L. Amick, and H. P. Liepman, "Interaction Effects Produced by Jet Exhausting Laterally Near Base of Ogive-Cylinder Model in Supersonic Main Stream," Memo 12-5-58W, NASA, February 1959.

47. Dershin, H., "Forces Due to Gaseous Slot Jet Boundary-Layer Interaction," Journal of Spacecraft and Rockets, Vol. 2, No. 4, July-August 1965, pp. 597-599.

48. Vinson, P. W., "Prediction of Reaction Control Effectiveness at Supersonic and Hypersonic Speeds," GR 6487, Martin-Orlando, March 1965.

49. Amick, J. L., "Circular Arc-Jet Flaps at Hypersonic Speeds," AIAA Paper 70-553, Tullahoma, Tennessee, May 1970.

50. Young, C. T., and B. F. Barfield, "Viscous Interaction of Sonic Transverse Jets with Supersonic External Flows," AIAA Journal, Vol. 10, No. 7, July 1972, pp. 853-854.

51. Wu, J. M., and K. Aoyama, "Analysis on Transverse Secondary Injection Penetration into a AIAA Paper No. 69-2, January 1969.

52. Behrens, W., "Separation of a Supersonic Turbulent Boundary Layer by a Forward Facing Step," AIAA Paper 71-127, New York, 1971.

53. Mager, A., "On the Model of the Free, Shock-Separated Turbulent Boundary Layer," Journal of the Aeronautical Sciences, Vol. 23, No. 2, February 1956, pp. 181-184.

54. Korst, H. H., W. L. Chow, and G. W. Zumwalt, "Research on Transonic and Supersonic Flow of a Real Fluid at Abrupt Increases in Cross Section," Final Report, ME-TR-392-5, Engineering Experiment Station, University of Illinois, Urbana, Ill., December 1959.

55. Hefner, J. N., and J. R. Sterrett, "Secondary Jet Interaction with Emphasis on Outflow and Jet Location," Journal of Spacecraft and Rockets, Vol 3, No. 11, November 1966, pp. 1658-1665.

56. Billig, F. S., R. C. Orth, and M. Lasky, "A Unified Analysis of Gaseous Jet Penetration," AIAA Journal, Vol. 9, No. 6, June 1971, pp. 1048-1058.

57. Lewis, J. E., T. Kubota, and L. Lees, "Experimental Investigation of Supersonic Laminar, Two-Dimensional Boundary Layer Separation in a Compression Corner with and without Cooling," AIAA Journal, Vol. 6, No. 1, January 1968.

58. Romeo, D. J., "Aerodynamic Interaction Effects Ahead of Rectangular Sonic Jets Exhausting Perpendicularly from a Flat Plate into a Mach Number 6 Free Stream," TN-D-1800, NASA, May 1963.

59. Whitehead, A. H., J. R. Sterrett, and J. C. Emery, "Effects of Transverse Outflow from a Hypersonic Separated Region," AIAA Journal, Vol. 10, No. 4, April 1972, pp. 553-555.

60. Street, T. A., "An Oil Flow Study of a Sonic Reaction Jet Ejecting from a Body of Revolution into a Free Stream of Mach number Range 1.75 to 4.5," RD-TR-70-7, U. S. Army Missile Command, Redstone Arsenal, Alabama, April 1970.

61. Charwat, A. F. and J. Allegre, "Interaction of A Supersonic Stream and a Transverse Supersonic Jet," AIAA Journal, Vol. 2, No. 11, November 1964, pp. 1965-1972.

62. Spaid, F. W., E. E. Zukoski, and R. Rosen, "A Study of Secondary Injection of Gases into a a Supersonic Flow," TR-32-834, Jet Propulsion Laboratory, Pasadena, California, August 1966.

63. Zukoski, E. E., and F. W. Spaid, "Secondary Injection of Gases into a Supersonic Flow," AIAA Journal, Vol. 2, No. 10, October 1964, pp. 1689-1696.

64. Crist, S., P. M. Sherman, and D. R. Glass, "Study of the Highly Under-expanded Sonic Jet," AIAA Journal, Vol. 4, No. 1, January 1966, pp. 68-71.

65. Orth, R. C., and J. R. Funk, "An Experimental and Comparative Study of Jet Penetration in Supersonic Flow," Journal of Spacecraft and Rockets, Vol. 4, No. 9, September 1967, pp. 1236-1242.

66. Schetz, J. A., F. F. Hawkins, and H. Lehman, "Structure of Highly Underexpanded Transverse Jets in a Supersonic Stream," AIAA Journal, Vol. 5, No. 5, May 1967, pp. 882-884.

67. Schetz, J. A., R. A. Weinraub, R. A Mahaffey, Jr., "Supersonic Transverse Injection into a Supersonic Stream," AIAA Journal, Vol. 6, No. 5, May 1968, pp. 933-934.

68. Broadwell, J. E., "Correlation of Rocket Nozzle Gas Injection Data," AIAA Journal, Vol. 1, No. 8, August 1963, pp. 1911-1913.

69 Torrence, M. G., "Concentration Measurements of an Injected Gas in a Supersonic Stream," TND-3860, NASA, 1967.

70. Torrence, M. G., "Effect of Injectant Molecular Weight on Mixing of a Normal Jet in a Mach 4 Airstream," TN D-6061, NASA, January 1971.

71. Schetz, J. A., and F. S. Billig, "Penetration of Gaseous Jets Injected into a Supersonic Stream," Journal of Spacecraft and Rockets, Vol. 3, No. 11, November 1966, pp. 1658-1665.

72. Povinelli, F. P., L. A. Povinelli and M. Hersch, "Supersonic Jet Penetration (up to Mach 4) into a Mach 2 Airstream," Journal of Spacecraft and Rockets, Vol. 7, No. 8, August 1970, pp. 988-992.

73. Hersch, M., L. A. Povinelli, and F. P. Povinelli, "A Schlieren Technique for Measuring Jet Penetration into a Supersonic Stream," Journal of Spacecraft and Rockets, Vol. 7, No. 6, June 1970, pp. 755-756.

74. Dahlke, C. W., "An Experiment l Investigation of Downstream Flowfield Properties Behind a Forward Located Jet Injected into a Transonic Freestream from a Body of Revolution," TD-TM-68-2, U. S. Army Missile Command, Redstone Arsenal, Alabama, January 1968.

75. Durando, N. A., "On the Vortices Induced In a Jet by a Subsonic Crossflow," McDonnell Douglas Astronautics Company Paper WD-1219, September 1970.

76. Cassel, L. A., N. A. Durando, C. W. Bullard, and J. M. Kelso, "Jet Interaction Control Effectiveness for Subsonic and Supersonic Flight," RD-TR-69-21, U. S. Army Missile Command, Redstone Arsenal, Alabama, September 1969.

77. Durando, N. A., "On the Vortices Induced in a Jet by a Subsonic Crossflow," AIAA Journal, Vol. 9, No. 2, February 1971, pp. 325-327.

78. Strike, W. T., and T. D. Buchanan, "Circular Sonic Lateral Jet Interaction Effects on a Flat Plate at Mach Number 18.5 Using a Small Solid Monopropellant Rocket Motor," AEDC-TR-69-205, Arnold Engineering Development Center, Arnold Air Force Station, Tennessee, January 1970.

79. Amick, J. L., and P. B. Hays, "Interaction Effects of Side Jets Issuing from Flat Plate and Cylinders Aligned with a Supersonic Stream," WADD TR-60-329, Wright Patterson Sir Force Base, Ohio, June 1960.

80. Street, D. R., "Effects of Injection Nozzle Configuration on Secondary Injection into Supersonic Flow," Mechanical Engineer Thesis, California Institute of Technology, 1966.

81. Koch, L. N., and D. J. Collins, "The Effect of Varying Secondary Mach Number and Injection Angle on Secondary Gaseous Injection into a Supersonic Flow," AIAA Paper No. 70-552, May 1970.

82. Chrans, L. J., and D. J. Collins, "Stagnation Temperature and Molecular Weight Effects in Jet Interactions," AIAA Journal, Vol. 8, No. 2, February 1970, pp. 287-293.

83. Chambers, R. A. and D. J. Collins, "Stagnation Temperature and Molecular Weight Effects in Jet Interaction," AIAA Journal, Vol. 8, No. 3, March 1970, pp. 584-585.

84. Reichenau, D. E. A., "Interference Effects Produced by a Cold Jet Issuing Normal to the Airstream from a Flat Plate at Transonic Mach Numbers, AEDC-TR-67-220, Arnold Engineering Development Center, Arnold Air Force Station, Tennessee, October 1967.

85. Reichenau, D. E. A., "Interference Effects of Cold and Hot Rocket Exhaust Issuing Normal to the Airstream from a Flat Plate at Free Stream Mach Numbers from 0.6 to 1.4," AEDC-TR-66-127, Arnold Engineering Development Center, Arnold Air Force Station, Tennessee, June 1966.

86. Hsia, H T., "Equivalence of Secondary Injection to a Blunt Body in Supersonic Flow," AIAA Journal, Vol. 4, No. 10, 1966, pp. 1832-1834.

87. Amick, J L., W. Stubblebine, and P. C. Y. Chen, "Experimental Interaction Effects of Forward-Located Side Jets on a Body of Revolution," WTM-276, University of Michigan, March 1963.

88. Jarvinen, P. O., R. W. Luce, and Wachsler, E., "Propulsive Reentry Aerodynamics," Interim Report MC 68-3001-R1 (BNY), Mithras Division of Sanders Associates, Inc., June 1968.

89. Durando, N. A., and L. A. Cassel, "Viscous Effects in the Interaction Flowfield Near a Jet in a Subsonic Crossflow," RD-TR-70-31, U. S. Army Missile Command, Redstone Arsenal, Alabama, December 1970.

90. Spring, D. J., "An Experimental Investigation of the Interference Effects Due to a Lateral Jet Issuing from a Body of Revolution Over the Mach Number Range 0.8 to 4.5," RD-TR-68-10, U. S. Army Missile Command, Redstone Arsenal, Alabama, August 1968.

91. Dahlke, C. W., "An Experimental Investigation of Downstream Flow-Field Properties Behind a Sonic Jet Injected into Transonic Freestream from a Body of Revolution (Series II)," RD-TM-69-2, U. S Army Missile Command, Redstone Arsenal, Alabama, February 1969.

92. Barber, J. B., and W. F. Staylor, "Investigation of Secondary Jets on a Cone at a Mach Number of 6," Journal of Spacecraft and Rockets, Vol. 3, No. 10, pp. 1544-1555, October 1966.

93 Carvalho, G. F., and P. B. Hays, "Jet Interference Experiments Employing Body-Alone and Body-Fin Configurations at Supersonic Speeds," Technical Report 03942-7-T, GM-979, University of Michigan, December, 1970.

94. Lee, E. E., Jr., and C. M. Willis, "Interaction Effects of a Control Jet Exhausting Radially from the Nose of an Ogive-Cylinder Body at Transonic Speeds," TN D-3752, NASA, January 1967.

95. Ferrari, C., "Interference Between a Jet Issuing Laterally from a Body and the Enveloping Supersonic Stream," Bumblebee Report No. 286, The Johns Hopkins University, Applied Physics Lab., April 1959.

96. Wu, J. M., R. L. Chapkis, and A. Mager, "Approximate Analysis of Thrust Vector Control by Fluid Injection," ARS Journal, Vol. 31, No. 12, December 1961, pp. 1677-1688.

97. Walker, R. E., A. R. Stone, and M. Shandor, "Secondary Gas Injection in a Conical Rocket Nozzle I. Effect of Orifice Diameter and Molecular Weight of Injectant," AIAA Journal, Vol. 1, No. 2, February 1963, pp. 334-338.

98. Street, T. A., "An Experimental Investigation of a Transverse Jet Ejecting from a Flat Plate into a Subsonic Free Stream," RD-TM-70-5, U. S. Army Missile Command, Redstone Arsenal, Alabama, May 1970.